Dissertation

Regulation of tumor growth and immune cell microenvironment by cannabinoid receptor 2 in non-small cell lung cancer

submitted by

Arailym SARSEMBAYEVA, BSc MSc

for the academic degree of

Doctor of Philosophy (PhD)

at the

Medical University of Graz

Otto Loewi Research Center

For Vascular Biology, Immunology, and Inflammation

Division of Pharmacology

under the supervision of

Assoc.-Prof. Dr. Rudolf SCHICHO

2023

STATUTORY DECLARATION

I hereby declare that this thesis is my own original work and I fully acknowledge the name all of individuals and organizations that contributed to the research constituting the thesis, due acknowledgement is made to all other material used for the thesis. Throughout this thesis and associated publication, I followed the “Standards of Good Scientific Practice and Ombuds Committee at the Medical University of Graz”.

Graz, January 02, 2023

Disclosures

This dissertation is based on the following paper:

1. **Arailym Sarsembayeva**[1], Melanie Kienzl[1], Eva Gruden[1], Dusica Ristic[1], Kathrin Maitz[1], Paulina Valadez-Cosmes[1], Ana Santiso[1], Carina Hasenoehrl[1], Luka Brcic[2], Jörg Lindenmann[3], Julia Kargl[1], and Rudolf Schicho[1,4] (2023) Cannabinoid Receptor 2 plays a pro-tumorigenic role in non-small cell lung cancer by limiting anti-tumor activity of $CD8^+$ T and NK cells. *Front. Immunol.* 13:997115. doi: 10.3389/fimmu.2022.997115 (1)

[1]Division of Pharmacology, Otto Loewi Research Center, Medical University of Graz, Graz, Austria

[2]Diagnostic and Research Institute of Pathology, Medical University of Graz, Graz, Austria

[3]Division of Thoracic and Hyperbaric Surgery, Department of Surgery, Medical University of Graz, Graz, Austria

[4]BioTechMed, Graz, Austria

Co-Author contributions:

Melanie Kienzl – helped to carry out *in vitro* and *in vivo* experiments, contributed to data interpretation and manuscript editing.

Eva Gruden - helped to carry out *in vitro* and *in vivo* experiments, contributed to data interpretation and manuscript editing.

Dusica Ristic - helped to carry out *in vivo* experiments, contributed to data interpretation and manuscript editing.

Kathrin Maitz - helped to carry out *in vivo* experiments, contributed to data interpretation and manuscript editing.

Paulina Valadez-Cosmes - helped to carry out *in vivo* experiments, contributed to data interpretation and manuscript editing.

Ana Santiso - helped to carry out *in vivo* experiments, contributed to data interpretation and manuscript editing.

Carina Hasenoehrl - conducted preliminary experiments, contributed to data interpretation and manuscript editing.

Luka Brcic - provided human NSCLC samples, contributed to data interpretation and manuscript editing.

Jörg Lindenmann - provided human NSCLC samples, contributed to data interpretation and manuscript editing.

Julia Kargl – planned and co-supervised the project, contributed to data interpretation and manuscript editing.

Rudolf Schicho – designed, planned and supervised the project and co-wrote the manuscript.

All co-authors have consented to the inclusion of their published data in the dissertation and permission from publisher and the copyright holders for reproduction have been obtained.

During my PhD studies, I additionally contributed to the following publications:

- Melanie Kienzl, Carina Hasenoehrl, Paulina Valadez-Cosmes, Kathrin Maitz, **Arailym Sarsembayeva**, Eva Sturm, Akos Heinemann, Julia Kargl & Rudolf Schicho (2020) IL-33 reduces tumor growth in models of colorectal cancer with the help of eosinophils, *OncoImmunology*, 9:1, DOI: 10.1080/2162402X.2020.1776059.
- Melanie Kienzl, Carina Hasenoehrl, Kathrin Maitz, **Arailym Sarsembayeva**, Ulrike Taschler, Paulina Valadez-Cosmes, Oliver Kindler, Dusica Ristic, Sofia Raftopoulou, Ana Santiso, Thomas Baernthaler, Luka Brcic, Lisa Hahnefeld, Robert Gurke, Dominique Thomas, Gerd Geisslinger, Julia Kargl & Rudolf Schicho (2021) Monoacylglycerol lipase deficiency in the tumor microenvironment slows tumor growth in non-small cell lung cancer. *OncoImmunology*, 10:1, DOI: 10.1080/2162402X.2021.1965319.

Acknowledgements

I would like to express my deepest gratitude to **Prof. Rudolf Schicho** for giving me an opportunity to do research in his lab. I am extremely grateful for helping me to grow as a scientist and expand my horizons by giving intangible support, guidance, and expertise throughout my PhD studies.

I would like to extend my sincere thanks to the head of the Institute of Experimental and Clinical Pharmacology, **Prof. Akos Heinemann**, for providing such an enjoyable and friendly working environment where the knowledge or expertise is shared among research groups.

Moreover, I would like to thank my thesis committee, **Dr. Eva Sturm**, **Dr. Julia Kargl** and **Dr. Andreas Reinisch**, for their invaluable advice, generously provided knowledge and expertise.

Additionally, this endeavor would not have been possible without the **Austrian Science Fund (FWF; grants P33325 and KLI887)** and **the Medical University of Graz** for funding my research through the **PhD program Molecular Medicine (MolMed).**

Special thanks to **Melanie Kienzl** for being a great listener and advisor throughout my PhD studies.

I am also grateful to **Veronika Pommer, Eva Gruden** and **Dusica Ristic** for their help with different experiments.

I had the pleasure of working with the colleagues from **Pharmacology Department**, particularly with **Claudia, Sabine Kern, Sabine Donner, Paulina, Ana, Kathi, Zala, Oliver, Ilse, Wolfgang, Eva**, **Aitak, Florian** and **Giulia**.

I am also grateful for my friends for supporting and creating happy memories throughout my PhD studies. Many thanks to **Manu Kanti, Sharmaine, Meekha, Amit, Anantha, Chris**, and **Himanshi**.

Lastly, I would like to say many thanks to **my parents, Aliya Smagulova** and **Amankeldy Sarsembayev** and **my lovely sister**, **Aigerim Sarsembayeva** for always being there for me through my ups and downs. Their belief in me and unconditional support has kept my spirits, enthusiasms and motivation high during this process.

Table of contents

Abbreviations

Abbreviation	Explanation
2-AG	2-arachidonoylglycerol
ADCC	Antibody-dependent cell-mediated cytotoxicity
AEA	Anandamide
ALK	Anaplastic Lymphoma Kinase
ANOVA	Analysis of variance
APCs	Antigen-presenting cells
ATR	Ataxia telangiectasia and Rad3-related
BrdU	Bromodeoxyuridine
BTLA	B- and T-lymphocyte attenuator
CB	Cannabinoid
CB_1	Cannabinoid receptor 1
$CB_1^{-/-}$	CB_1 knockout
CB_2	Cannabinoid receptor 2
$CB_2^{-/-}$	CB_2 knockout
CCL19	C-C motif chemokine ligand 19
CCL21	C-C motif chemokine ligand 21
CCR7	C-C chemokine receptor type 7
cDC1	Type 1 conventional dendritic cells
CEACAM1	Carcinoembryonic AG-related cell adhesion molecule 1
CK	Cytokeratin
CTLA-4	Cytotoxic T-lymphocyte antigen-4
CXCL10	C-X-C motif chemokine ligand 10
CXCL11	C-X-C motif chemokine ligand 11
CXCL9	C-X-C motif chemokine ligand 9
CXCR3	C-X-C motif chemokine receptor 3
CXCR6	C-X-C motif chemokine receptor 6
DC	Dendritic cells
DMEM	Dulbecco's Modified Eagle Medium
EC	Endothelial cells
ECS	Endocannabinoid system
EGF	Epidermal growth factor
EGFR	Epidermal growth factor receptor
EPCAM	Epithelial cell adhesion molecule
ERK	Extracellular signal-regulated kinase

FAAH	Fatty acid amide hydrolase
FASL	FAS/FAS ligand
FBS	Fetal bovine serum
FDA	Food and Drug administration
FGL1	Fibrinogen-like protein 1
FMO	Fluorescence minus-one
FREP1	Fibrinogen-associated protein 1
FVD	Fixable Viability Dye
GM-CSF	Granulocyte-macrophage colony-stimulating factor
GPCR	G-protein-coupled receptor
GPR55 and GPR18	G protein-coupled receptors 55 and 18
HMGB1	High mobility group box 1
HVEM	Herpes virus entry mediator
i.p.	Intraperitoneal
ICAM-1/2	Intercellular adhesion molecule-1/2
ICI	Immune checkpoint inhibitor
IDO	Indoleamine-2,3-dioxygenase
IFN-γ	Interferon-gamma
IL-10	Interleukin-10
IL-2	Interleukin-2
ILCs	Innate lymphoid cells
iNKT	Invariant natural killer T
ISH-IF	In situ hybridization and immunofluorescence
JNK	Jun NH_2-terminal kinase
KIR	Killer-cell immunoglobulin-like receptors
KRAS	Kirsten rat sarcoma viral oncogene
LAG-3	Lymphocyte activation gene-3
LAMP-1/2	Lysosomal-associated membrane protein-1/2
LLC1	Lewis lung carcinoma
LSECtin	Lymph node sinusoidal endothelial cell C-type lectin
M1	M1 macrophages
M2	M2 macrophages
MAIT	Mucosal-associated invariant T
MAPK	Mitogen-activated protein kinase
MDSCs	Myeloid-derived suppressor cells
MEK	Mitogen-activated protein kinase kinase

MFI	Median fluorescence intensity
MGL	Monoacylglycerol lipase
MHC	Major histocompatibility complex
MTOC	Microtubule-organizing center
NAPE-PLD	N-acylphosphatidyl-ethanolamine phospholipase D
NCR1	Natural cytotoxicity receptor 1
NF-κB	Nuclear factor-κB
NK	Natural killer
NKT	Natural killer T
NS	Non-stimulated
NSCLC	Non-small cell lung cancer
OEA and PEA	Oleoyl- and palmitoyl-ethanolamide
P/S	Penicillin/ streptomycin
PBMCs	Peripheral blood mononuclear cells
PBS	Phosphate Buffered Saline
PD-1	Programmed death-1
pDC	Plasmacytoid dendritic cells
PD-L1	Programmed death-ligand 1
PI	Propidium Iodide
PI3K	Phosphoinositide 3-kinase
PMA/Iono	Phorbol myristate acetate/Ionomycin
PPARs	Peroxisome proliferator-activated receptors
PtdSer	Phosphatidylserine
PTPN22	Protein tyrosine phosphatase non-receptor type 22
PVDF	Polyvinylidene difluoride
RT-qPCR	Real time- quantitative polymerase chain reaction
Rb	Retinoblastoma protein
RBC	Red blood cell
RPMI	Roswell Park memorial Institute
s.c.	Subcutaneous
SB	Staining buffer
SCLC	Small-cell lung cancer
SD	Standard deviation
SEM	Standard error of mean
TAMs	Tumor-associated macrophages
TBST	Tris-buffered saline with 0.1% Tween® 20 Detergent

TCR	T-cell receptor
TGF	Transforming growth factor
TGF-β	Transforming growth factor-beta
Th_1	T helper 1
Th_{17}	T helper 17
Th_2	T helper 2
THC	Delta-9-tetrahydrocannabinol
TIGIT	T cell immunoglobulin and ITIM domain
TIM-3	T cell immunoglobulin and mucin domain-containing protein-3
TMB	Tumor mutational burden
TME	Tumor microenvironment
TNF-α	Tumor necrosis factor-alpha
Trp53	Transformation-related protein 53
TRAIL	Tumor necrosis factor related apoptosis inducing ligand
Tregs	Regulatory T cells
TRPV1	Transient receptor potential cation channel subfamily V member 1
VCAM-1	Vascular cell adhesion molecule-1
WB	Western blotting
WHO	World Health Organization
WT	Wild type

List of Figures:

List of Tables:

ZUSAMMENFASSUNG

Der Lungenkrebs gehört zu den am häufigsten diagnostizierten Neoplasien und ist nach wie vor weltweit eine der Hauptursachen für Krebs-assoziierte Todesfälle. Das Nicht-kleinzellige Lungenkarzinom (NSCLC) ist die häufigste Form von Lungenkrebs und macht 85% aller Lungenkrebsfälle aus. Cannabinoid (CB)-Rezeptoren (CB_1 und CB_2) sind Teil des sogenannten Endocannabinoid-Systems. Sie werden in Tumorzellen verschiedener Krebsarten, einschließlich dem Lungenkrebs, exprimiert und können das Tumorwachstum beeinflussen. Darüber hinaus exprimieren auch Zellen, die in der unmittelbaren Umgebung der Tumorzellen liegen (in der sogenannten Tumor Mikroumgebung [Tumor microenvironment; TME]), CB_1 und CB_2 Rezeptoren. Seit langem ist bekannt, dass Immunzellen des TME das Tumorwachstum wesentlich beeinflussen können. Die Rolle von CB_1 und CB_2 Rezeptoren des TME in der Tumorentwicklung ist jedoch unklar. Wir untersuchten daher den Einfluss von CB_1 und CB_2 Rezeptoren des TME auf das Tumorwachstum in einem NSCLC-Modell.

Um Tumore zu generieren, die keine CB Rezeptoren im TME exprimieren, verwendeten wir ein NSCLC-Modell der Maus. Dazu wurden CB_1- ($CB_1^{-/-}$) und CB_2-knockout ($CB_2^{-/-}$) Mäusen oder ihren Wildtyp (WT)-Littermates subkutan KP Adenokarzinomzellen (mit einer Kras-Mutation und einem ausgeknockten p53 Gen) aus einem Lungenkrebs der Maus verabreicht. Wir verwendeten In-situ-Hybridisierung und Immunfluoreszenz, um die Expression von CB_1- und CB_2-Transkripten in Tumor- und Immunzellen zu bestimmen. Das Immunzell-Profil des TME wurde mittels Durchflusszytometrie analysiert.

Beide CB-Rezeptoren werden im NSCLC Modell und in menschlichem NSCLC Gewebe sowohl in Tumorzellen als auch in Immunzellen des TME exprimiert. Die Expression von CB_2-mRNA in Tumor-infiltrierten Immunzellen war stärker als die von CB_1 Rezeptoren. Ferner beobachteten wir, dass nur der Gen-Knockout oder die pharmakologische Blockade von CB_2, aber nicht von CB_1, zu einem signifikanten Rückgang des Tumorwachstums führte. Der CB_2 knockout in der Maus (d. h. die Deletion von *Cnr2*, dem codierenden Gen für den CB_2 Rezeptor) führte zu einer erhöhten Infiltration und antitumorigenen Aktivität von $CD8^+$ T- und natürlichen Killerzellen (NK) im Tumor. Darüber hinaus erhöhte das Fehlen des CB_2 auf den Wirtszellen der CB_2-knockout Maus die Menge an CCL21 Chemokin (C-C motif ligand 21) im Tumor. Des Weiteren war die Expression von PD-1 (programmed cell death protein 1) auf lymphoiden und des PD-1 Liganden PD-L1 (programmed death-ligand 1) auf myeloiden Zellen erhöht. Die Expression des CCL21 Rezeptors, CCR7, war auf den $CD8^+$ T- und NK-Zellen von $CB_2^{-/-}$ - im Vergleich zu den WT-Mäusen - signifikant reduziert. Eine wichtige Entdeckung war,

dass die CB_2-knockout Mäuse deutlich besser auf eine Anti-PD-1-Antikörpertherapie ansprachen als die WT-Mäuse. Diese Art von Immuntherapie mit Anti-PD-1-Antikörpern verstärkte die Infiltration von $CD8^+$ T- und NK-Zellen in das TME von $CB_2^{-/-}$ Mäusen.

Insgesamt lassen die in dieser Arbeit präsentierten Ergebnisse den Schluss zu, dass CB_2 Rezeptoren des TME eine immunsuppressive und Tumorwachstum-fördernde Rolle im NSCLC Modell spielen, indem sie die Infiltration und zytotoxische Aktivität von $CD8^+$ T- und NK-Zellen, die nachweislich Tumorwachstum inhibieren können, begrenzen. Ein Knockout von CB_2 Rezeptoren in Zellen des TME könnte einen zusätzlichen klinischen Nutzen für eine Anti-PD-1/PD-L1-Therapie des NSCLC bieten.

ABSTRACT

Lung cancer is the most frequently diagnosed type of cancer, and it remains a leading cause of cancer-associated deaths worldwide. Non-small cell lung cancer (NSCLC) is the most common type of lung cancer, accounting for 85% of all lung cancer cases. Cannabinoid receptors 1 and 2 (CB_1 and CB_2) are part of the endocannabinoid system that are expressed in tumor cells of various cancer entities, including lung cancer, and they are well-known to influence tumor growth. Additionally, cells of the tumor surrounding niche, called tumor microenvironment (TME) also express CB_1 and CB_2, however, their role in tumor development has not been elucidated yet. As a consequence, we investigated the influence of TME-derived CB_1 and CB_2 on tumor growth in a model of NSCLC.

To create a TME deficient in CB receptors, we used a murine NSCLC model in which CB_1-($CB_1^{-/-}$) and CB_2-knockout ($CB_2^{-/-}$) mice or their wild type (WT) littermates subcutaneously received KP (Kras mutant, Trp53-null) lung adenocarcinoma cells. In situ hybridization and immunofluorescence were performed to determine expression of CB_1 and CB_2 transcripts in tumor and immune cells. Using flow cytometry, the profile of immune cells of the TME was analyzed.

Tumor cells and tumor-infiltrated immune cells of murine and human NSCLC both express CB receptors. The expression of CB_2 mRNA in tumor-infiltrated immune cells was higher than of CB_1. We observed that gene knockout or pharmacological blockade of CB_2, but not of CB_1 resulted in a significant reduction of tumor growth. Deletion of *Cnr2* (the gene encoding CB_2) on host cells induced increased infiltration and local anti-tumorigenic activity of $CD8^+$ T and natural killer (NK) cells. Moreover, it increased the expression of C-C motif chemokine ligand 21 (CCL21), and the expression of programmed death-1 (PD-1) and its ligand (PD-L1) on lymphoid and myeloid cells, respectively. In addition, expression of CCR7 (CCL21 receptor) was significantly reduced on $CD8^+$ T and NK cells from $CB_2^{-/-}$ vs. WT mice. Importantly, mice lacking the *Cnr2* gene responded significantly better to anti-PD-1 blocking therapy than WT mice. The immunotherapy with anti-PD-1 antibodies further increased infiltration of $CD8^+$ T and NK cells into the TME of $CB_2^{-/-}$ mice.

Altogether, the findings presented in this thesis suggest that TME-derived CB_2 plays a pro-tumorigenic and immunosuppressive role in murine NSCLC tumors by limiting cytotoxic activity of $CD8^+$ T and NK cells. Knockout of CB_2 in TME cells of NSCLC could provide additional clinical benefit to anti-PD-1/PD-L1 therapy.

1 Introduction

1.1 Lung cancer

Based on the World Health Organization (WHO) statistics for 2019, cancer results nowadays in more deaths than all types of coronary heart disease and stroke in 112 of 183 countries, ranking as the first or second main cause of death prior to the age of 70 years (1).

Lung cancer is the most frequently diagnosed type of cancer (11.4% of the total diagnosed cancer cases), and it is one of the main causes of cancer-associated morbidity (18% of the total cancer-associated deaths) worldwide (1). Non-small cell lung cancer (NSCLC) accounts for approximately 85% of all newly diagnosed lung cancer cases, which comprises adenocarcinoma (gland forming and most common subtype), squamous cell carcinoma and large-cell carcinoma histological subcategories. The remaining 15% represents small-cell lung cancer (SCLC) (2; 3). Prolonged exposure to tobacco smoke results in a well-defined change in the morphology of the bronchial epithelium, proceeding from basal cell hyperplasia to metaplasia, severe dysplasia, carcinoma *in situ* and, eventually, to total carcinoma (4). These alterations are correlated mainly with the squamous subtype of NSCLC. In contrast, adenocarcinomas are often considered to be a prevailing subtype in never smokers that had reduced carcinogen exposure. However, adenocarcinomas can still occur in smokers with a high carcinogen exposure (5). To differentiate between inactive and surgically removable SCLCs and highly malignant, metastatic NSCLCs, it is pivotal to understand and identify the oncogenic driver mutations in a subgroup of tumors (4). In NSCLC, *Kirsten rat sarcoma viral oncogene (KRAS)*, *epidermal growth factor receptor (EGFR)* and *anaplastic lymphoma kinase (ALK)* are the most widely known transformed oncogenes that act as genomic tumor drivers (6). Furthermore, aberrations in tumor suppressor genes such as *transformation-related protein 53 (Trp53)* and *retinoblastoma protein* (*Rb)* are commonly present in all lung cancer subtypes (4). To escape immune surveillance, tumors have developed different strategic approaches, including modifications in oncogenic signaling, cellular metabolism, and epigenetics that subsequently protect them from an effective immune response (4; 7). Furthermore, Busch et al. demonstrated that the immune cell profile within lung tumor subtypes is dictated by the genomic tumor drivers. For instance, *EGFR*-mutant tumors showed an enhanced myeloid cell infiltration but little response of lymphoid cells; on the other hand, *KRAS*-mutant cancers revealed a wide range of different immune cells (8), suggesting complex mechanisms and interactions that regulate the immune cell composition in tumors of lung cancer.

1.2 Tumor microenvironment (TME)

Carcinogenesis is driven not only by mutations, but it is tightly controlled by the surrounding niche, named tumor microenvironment (TME) (9; 10). The TME is composed of cells of the immune system, cells of the tumor-associated vasculature and lymphatics, fibroblasts, pericytes, and occasionally of adipocytes (10). Additionally, abiotic elements of the TME include a hypoxic milieu, an altered buildup of metabolites, acidic pH, together with a selection of immunosuppressive cytokines, chemokines and growth factors. These rough conditions not only influence the tumor cell response to the surrounding cells, but additionally affect the status and function of tissue resident and tumor-infiltrating immune cell populations (11). The TME can modulate differentiation of regulatory immune cells, prevent activation of immune cells, as well as promote apoptosis, or terminate proliferation of immune cells (12–16).

1.2.1 Immune cell composition of the TME: 'cold' versus 'hot'

Tumors can be categorized into one of the three following immunophenotypes: immune-desert, immune-excluded, and immune-inflamed, based on the spatial distribution of cytotoxic immune cells in the TME (17). Immune-desert and immune-excluded tumors fall under category of 'cold' tumors. Immune-desert tumors are lacking $CD8^+$ T cells. In immune-excluded tumors, $CD8^+$ T cells are more localized at tumor margins, and are not present within the tumor (18). In conjunction with low T-cell infiltration, 'cold' tumors are defined by a low tumor mutational burden (TMB), and a reduced expression of major histocompatibility complex (MHC) class I and programmed death-ligand 1 (PD-L1) (19). Additionally, the immune cell population of 'cold' tumors mainly consists of immunosuppressive cells, such as tumor-associated macrophages (TAMs), regulatory T cells (Tregs), and myeloid-derived suppressor cells (MDSCs). Furthermore, 'cold' tumors seldomly respond to immune checkpoint inhibitor (ICI) monotherapy. In contrast, immune-inflamed tumors, also known as 'hot' tumors, are portrayed by increased T-cell infiltration, enhanced interferon-gamma (IFN-γ) and cytolytic T-cell signature, increased expression of PD-L1, and a high TMB (19). 'Hot' tumors are efficiently responsive to ICI-based immunotherapy or a combination therapy (20; 21).

1.2.1.1 $CD8^+$ T cells – tumor cell-killing immune cells of the adaptive immune system

The presence of tumor antigen-specific cytotoxic T cells in the TME is one of the key indicators of a positive response to immunotherapy. However, to conduct its anti-tumor functions, $CD8^+$ T cells greatly rely on the capacity to infiltrate the tumor site, which is accomplished by chemoattraction of $CD8^+$ T cells into the TME. In a nutshell, the field of cancer immunology

and immunotherapy focuses on identifying the total number, type, and cytotoxic activity of tumor antigen-specific cytotoxic T cells in the TME (reviewed in (22; 23)).

$CD8^+$ T cells are cytotoxic cells of the adaptive immune system. Their stages of differentiation have been comprehensively described by Zhang and Bevan, 2011 (24). Briefly, once naïve $CD8^+$ T ($CD44^{low}CD62L^{hi}$) cells are exposed to foreign antigens presented by MHC I complex, they get activated, and start to expand profoundly within the first 1-2 weeks after the exposure. Afterwards, T cells develop into effector $CD8^+$ T ($CD44^{hi}CD62L^{low}$) cells with distinct powers to eliminate target cells via the production of effector cytokines (such as IFN-γ and tumor necrosis factor-alpha (TNF-α)) and the development of two independent mechanisms including the granzyme/perforin-mediated cytotoxicity and FAS/FAS ligand (FASL) pathways to directly kill targeted cells without leading to auto-injury (24; 25). Once T cells reach their maximum level of proliferation, about 90-95% of effector $CD8^+$ T cells die through programmed cell death. The rest of $CD8^+$ T cells differentiate into memory $CD8^+$ T ($CD44^{hi}CD62L^{hi}$) cells and remain in the resting state till re-exposure to the same or similar antigen (reviewed in (25)). Of note, tumor antigens are poorly immunogenic, and the majority of tumor-specific T cells have low precursor frequencies. Additionally, the affinity of T-cell receptors is low, because high avidity tumor-specific T cells are deleted in the thymus during the selection process (26). Moreover, antigen processing and presentation are deteriorated in a chronic inflammatory environment, like the TME. Even though effector T cells infiltrate the TME, a heterogenous immunosuppressive network that includes tumor cells, inflammatory cells, stromal cells and cytokines, hinders a differential and functional role of T cells, resulting in a wide range of T cell subsets as well as activation of inhibitory checkpoint pathways (reviewed in (27)).

1.2.1.1.1 Infiltration state of $CD8^+$ T cells

Increased infiltration of $CD8^+$ T cells into tumor sites contributes to an advanced ‘immunoscore’ that usually associates with a good prognosis for patients with different types of cancers, including skin (28), breast (29), colorectal (30), ovarian (31), bladder (32), lung (33–36) and pancreatic (37) cancers. Additionally, an enhanced $CD8^+$ T cell infiltration may determine the response rate to chemotherapy (38–40) and immunotherapy with checkpoint-blocking antibodies against CTLA-4 (cytotoxic T-lymphocyte antigen-4; CD152) (41) or PD-1 (programmed death-1) (42; 43). As a consequence, it is vital to understand the underlying mechanisms that regulate infiltration of $CD8^+$ T cells into the TME.

The process of migration of T cells requires multiple links between T cells and endothelial cells (EC). This process starts with an initial temporary binding to the endothelium, continued by rolling, solid adhesion, and T cell activation on the surface of ECs, and eventually T cell

extravasation via the vasculature to the site of infection or the tumor (44). In order for these steps to occur, the interplay of selectins, integrins, and chemokine receptors and their ligands secreted from tumor or host immune cells, are essential. Miscommunication in any of the mentioned steps interfere with the infiltration of $CD8^+$ T cells into the TME (45). Tumor cells can alter the adhesion and chemotactic signals in the blood vessels to promote infiltration of suppressive cells, and to eliminate anti-tumorigenic T cells (46). Expression of adhesion molecules, such as intercellular adhesion molecule (ICAM)-1/2, vascular cell adhesion molecule-1 (VCAM-1) and CD34 on endothelium is inhibited in several cancers, influencing a key step in T cell migration (45). In ovarian cancer, the endothelin B receptor is upregulated on endothelial cells of tumor vasculature, and it reduces T cell infiltration via clustering of ICAM-1 (47).

The chemoattraction of immune cells, including cytotoxic T cells to the tumor site is tightly regulated by chemokine-chemokine receptor interactions (45). C-X-C motif chemokine receptor 3 (CXCR3) is expressed by activated $CD8^+$ T cells in various tumor entities such as colorectal (48), breast (49), skin (50) cancers, to promote migration to the TME. In addition, a number of studies showed that C-X-C motif chemokine ligand 9 (CXCL9), C-X-C motif chemokine ligand 10 (CXCL10) and C-X-C motif chemokine ligand 11 (CXCL11) released by cancer or host cells can attract $CXCR3^+$ tumor-infiltrating immune cells, including $CD4^+$ T cells, $CD8^+$ T cells and natural killer (NK) cells to the tumor site (50–55). On the other hand, cancer cells may express insufficient levels of the ligands for CXCR3, which may compromise infiltration of effector and memory $CD8^+$ T cells to the tumor site (49; 50). Interestingly, expression of all three ligands for CXCR3 are induced by IFN-γ (56). As a consequence, IFN-γ release into the TME by cytotoxic T cells may further contribute to the T cell infiltration via CXCR3 (45). Another chemokine receptor is C-X-C motif chemokine receptor 6 (CXCR6) that is expressed at low levels on naïve T cells, and its expression is enhanced upon stimulation. Mice deficient of CXCR6 displayed low infiltration of T cells and enhanced tumor progression in breast cancer (57) and hepatocellular carcinoma (58). Wang et al. demonstrated that $CD8^+$ T cells positive for CXCR6 had higher cytotoxic activity, and they better responded to anti-PD-1 immunotherapy (59). C-C chemokine receptor type 7 (CCR7) is another G-protein-coupled (GPCR) chemokine receptor that is found on dendritic cells (DCs), naïve T, NK, natural killer T (NKT) and B cells. CCR7 may be temporarily expressed on activated T cells (60), but its expression is generally reduced upon differentiation towards effector cells (61). On the other hand, CCR7 expression on the surface of DCs is stimulated upon maturation (62–64). Ligands for CCR7, such as C-C motif chemokine ligand 19 (CCL19)/C-C motif chemokine ligand 21 (CCL21, also known as 6Ckine, SLC, TCA4, Exodus-2), are abundantly expressed on high

endothelial venules of lymph nodes and Peyer's patches, lymphatic endothelial cells, T cell zones of the spleen and lymph node, and on stromal cells of the spleen and the appendix (60), (65). Ligand-binding to CCR7 promotes activation of G-protein, and induces the extracellular signal-regulated kinase (ERK) 1/2 signaling pathway, calcium release, and migration of cells (66). Mice deficient of CCR7 demonstrate a delay in antibody production, develop type IV hypersensitivity reactions, and show morphological aberrations in secondary lymphoid organs due to impaired homing of DCs and lymphocytes (67; 68). Therefore, the expression of chemokine receptors and its ligands may not only influence infiltration of immune cells into the TME, but they can also dictate the differentiation stage as well as activation status of immune cells.

1.2.1.1.2 Functional state of $CD8^+$ T cells

During $CD8^+$ T cell activation, tumor-specific $CD8^+$ T cells start expressing immune checkpoint proteins as an early sign of activity, however a continual, enhanced expression or co-expression of these checkpoints may lead to exhaustion of $CD8^+$ T cells, and subsequently to an inhibition of the cell's killing capacity (reviewed in (69)). In general, $CD8^+$ T cells infiltrating the TME can become dysfunctional either because of insufficiency of cytolytic factors, or because of enhanced expression levels of immune checkpoint proteins, including CTLA-4, PD-1, TIGIT (T cell immunoglobulin and ITIM domain), TIM-3 (T-cell immunoglobulin and mucin-domain containing 3), LAG-3 (lymphocyte-activation gene 3), and BTLA (B- and T-lymphocyte attenuator) (70). A list of immune checkpoint molecules, cells positive for these molecules and their ligands is given in **Table 1**.

In addition to the mentioned immune checkpoints, exhausted T cells express and co-express an array of other cell surface inhibitory proteins. Moreover, co-expression of multiple inhibitory receptors is a main indicative point of exhaustion (reviewed in (71)). For instance, tumor-infiltrated $CD8^+$ T cells that are double-negative for TIM-3 and PD-1 have a good effector function, whereas $TIM\text{-}3^-$ $PD\text{-}1^+$ single positive $CD8^+$ T cells possess a milder exhaustion/dysfunctional state, but $TIM\text{-}3^+$ $PD\text{-}1^+$ double-positive $CD8^+$ T cells exhibit the late terminal or dysfunctional phenotype of $CD8^+$ T cell exhaustion (72–74).

Table 1. *Immune checkpoints and ligands.*

Immune checkpoint molecules	***Cells expressing immune checkpoints***	***Ligands***	**References**
CTLA-4	conventional $CD4^+$ and $CD8^+$ T, Tregs, NK cells, B cell subsets and DCs	CD80 (B7.1), CD86 (B7.2)	(75–83)
PD-1	activated T cells, NK, B cells, Tregs, T follicular helper, and myeloid cells	PD-L1 (B7-H1), PD-L2 (B7-DC)	(75; 84–88)
TIGIT	activated $CD8^+$ T and $CD4^+$ T cells, NK cells, Tregs, and follicular $CD4^+$ T cells	CD155 (Necl-5), CD112 (Nectin2), CD113 (Nectin3), Nectin4	(89–98)
TIM-3	$CD4^+$ Th_1 cells, $CD8^+$ cytotoxic T cells, Tregs, NK/NKT cells, DCs, monocytes, and macrophages	Galectin-9, PtdSer, HMGB1, CEACAM1	(99–104)
LAG-3	T cells, Tregs, γδT, MAIT, iNKT cells, NK, B cells, plasmacytoid DCs, and neurons	MHC II complex, galectin-3, LSECtin, α-synuclein, fibrinogen-like protein 1, FGL2	(105–114)
BTLA	T, B, NK/NKT cells, DCs, and macrophages	Herpes virus entry mediator (HVEM)	(115–118)

1.2.1.2 NK cells –cytotoxic cells of the innate immune system

NK cells are specialized members of group 1 innate lymphoid cells (ILCs) that are larger and much shorter lived than the typical lymphocytes. They have specialized granules in the cytoplasm (119) and are assigned to group 1 ILCs, because after stimulation, both group 1 ILCs and NK cells release IFN-γ and TNF-α (120). However, different to group 1 ILCs, NK cells have cytolytic functions that are similar to $CD8^+$ T cells (120). Human NK cells are recognized as $CD3^-CD56^+CD16^+$ cells whereas murine NK cells are recognized based on the surface

expression of NK1.1 (NKR-P1C), natural cytotoxicity receptor 1 (NCR1; NKp46/CD335), and CD49b (DX5, Integrin VLA-2α) markers. NK cells are recognized as $CD3^{-}NK1.1^{+}$ or $CD3^{-}NKp46^{+}$ cells in C57BL/6, FVB/N, and NZB mouse strains. The NK1.1 receptor is not expressed in some strains such as in BALB/c, CBA/J, AKR, C3H, DBA/1, NOD, SJL, and 129 strains, therefore, NK cells in these strains can be distinguished as $CD3^{-}CD49b^{+}$ cells. In humans, NK cells represent 5-20% of peripheral blood mononuclear cells (PBMCs). In inbred mouse strains, NK cells account for 2-7% of lymphocytes in peripheral blood (121). The main place for NK cell development is the bone marrow, although NK cells can also develop and mature in liver and thymus (122; 123). Analogous to B and T cells, NK cells originate from common lymphoid progenitor cells (124). NK cell distribution within the body is relatively widespread. They are found in lymphoid organs and non-lymphoid organs, such as in skin, intestines, liver, lungs, uterus, kidneys, pancreas, brain, adipose tissue, bladder, joints, and breast (125; 126). Throughout the maturation process, NK cells acquire a set of different activating and inhibitory receptors that give them the capacity to interact with damaged, infected, and pre-malignant cells. Two classes of inhibitory receptors, i.e., killer-cell immunoglobulin-like receptors (KIR) and CD94-NKG2A are expressed by mature NK cells (127; 128). A number of activating receptors have been determined on NK cells, including NKGs, such as NKG2C and NKG2D as well as various NCRs, such as NKp30, NKp44, and NKp46 (129). The cytotoxicity levels of NK cells correlate with its activation status (130). The whole process of cytotoxic immune response of NK cells represents a degranulation mechanism, during which cytotoxic molecules such as perforin and granzyme are released into the target cell to activate apoptotic pathways and subsequently kill the target cell. Lysosomal-associated membrane protein-1 (LAMP-1 or CD107a) and -2 (LAMP-2 or CD107b) are degranulation proteins that temporarily surface on NK cells during the NK cell degranulation (131). In general, NK cells have been demonstrated to regulate the cells of the innate and adaptive immune system via cytokines. Human NK cells respond to monokines, such as IL-12, IL-15, and IL-18 cytokines, which result in enhanced proliferation and production of an array of cytokines, including IFN-γ, IL-10, IL-13, TNF-β, and granulocyte-macrophage colony-stimulating factor (GM-CSF) (132–135). Interestingly, APCs affect the phenotypical and cellular functions of NK cells (136). On the other hand, NK cells influence APCs via “DC editing” and stimulate monocytes to release TNF-α (137–139).

1.3 Lung cancer and immunotherapy

A decade ago, Chen and Mellman described the view of the „cancer-immunity cycle”, in which they mapped out the series of steps that must occur to generate an immune response to tumors (140). Management of lung cancer has been expanded for the last ten years from the

use of standard platinum-based chemotherapy or/and radiotherapy to a more personalized way of treating patients that was based on the presence/absence of molecular and immunological markers (141). In 2015, two anti-PD-1 inhibitors, nivolumab and pembrolizumab were the first immunomodulatory agents approved by the US Food and Drug administration (FDA) to treat advanced NSCLC (142; 143). Since then, a number of immune checkpoint inhibitors directed against PD-L1, CTLA-4 have been introduced to treat solid tumors, including NSCLC, and they have demonstrated a response rate of around 40%. In addition, targeting immune checkpoint axes, including LAG-3, TIM-3, TIGIT, and others, are under investigation (reviewed in (144)). The introduction of ICIs to treat patients with NSCLC has become a phenomenon, however, this breakthrough had no lasting effect. Tumor resistance is one of the challenges to fully benefit from ICIs. Throughout the course of immunotherapy, particularly during treatment with ICIs, patients were segregated into three groups, based on the response rate to ICIs: long-term responders (initial and continuous response), primary resistance (no initial response), and acquired resistance (initial response with a consecutive late relapse). Approximately 40-50% of lung cancer patients manifest rapid progression and even hyper-progressive disease during first cycles of ICIs. Different mechanisms of resistance to ICIs have been characterized including alterations in the TME and acquired genetic changes in cancer cells (145; 146). In lung cancer, mechanisms of ICI resistance include abnormalities in the TMB, immune cell composition, specifically, in the infiltration of effector $CD8^+$ T cells into the TME, epigenetics, mRNA signature, signaling pathways, microbiome, and in T-cell dysfunction and exhaustion (reviewed in (147)). Approved predictive markers to initiate ICI therapy for NSCLC patients are components of the PD-1/PD-L1 axis, the TMB, and microsatellite instability. However, these predictive factors are not ideal (148). Even if PD-L1 is present in half of the tumor cell population, the overall response rate remains 44.8% (149). In addition, TMB does not cover synonymous changes, such as copy number alterations, small insertions, and deletions. These alterations can also lead to heterogenous tumors that influence the sensitivity to ICIs (147; 150–152). In spite of moving forward with ICIs in cancer therapy by improving the response rate, some questions remain open. Therefore, it is crucial to identify new biomarkers and targets to predict the response rate and treat cancer patients without acquiring resistance during ICI therapy (153).

1.4 Cannabinoid receptors as part of the endocannabinoid system

The endocannabinoid system (ECS) is a complex multifunctional system that consists of endogenous ligands known as endocannabinoids, such as anandamide (AEA) and 2-arachidonoylglycerol (2-AG), cannabinoid receptors 1 and 2 (CB_1 and CB_2; class A GPCRs), the enzymes involved in the endocannabinoids' synthesis (diacylglycerol lipase-α and -β, *N*-

acylphosphatidyl-ethanolamine phospholipase D (NAPE-PLD), protein tyrosine phosphatase non-receptor type 22 (PTPN22)) and degradation (fatty acid amide hydrolase (FAAH) and monoacylglycerol lipase (MGL)), as well as protein transporters for endocannabinoids (154; 155). The ECS can be found in the major systems of the body, however, its most prominent expression is in the nervous and the immune system (156). The ECS has a number of physiological roles within the body, but is also implicated in diseases, such as neurodegenerative disorders, cardiovascular disease, inflammation, obesity and cancer (157; 158). An 'expanded' ECS (known as 'endocannabinoidome') also includes endocannabinoid-like lipids, for instance, oleoyl- and palmitoyl-ethanolamide (OEA and PEA), putative cannabinoid receptors that are responsive to endocannabinoids and synthetic/plant-derived cannabinoids (but phylogenetically unrelated to CB_1 and CB_2), such as G protein-coupled receptors 55 and 18 (GPR55 and GPR18), peroxisome proliferator-activated receptors (PPARs), transient receptor potential cation channel subfamily V member 1 (TRPV1), 5-HT3 receptors, and potassium channels (159; 160). **Figure 1** depicts the main components of the ECS and the 'expanded' ECS.

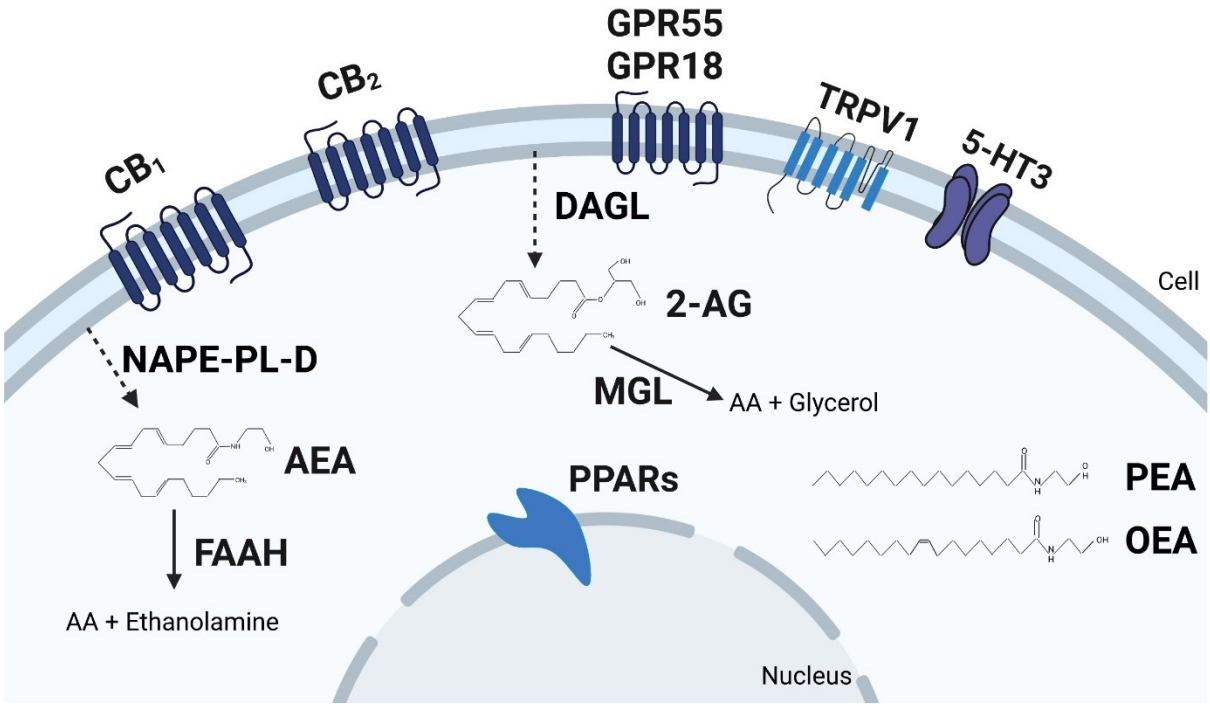

Figure 1. *Main components of the endocannabinoid system and 'endocannabinoidome'.*

Created with BioRender.com.

1.4.1 Cannabinoid receptors and the immune system

CB_1 is abundantly expressed in the central nervous system, but to a much lesser extent in peripheral organs, including the adrenal gland, heart, lung, prostate, uterus, ovary, testis, bone

marrow, thymus, tonsils, liver, adipose tissue, skin, and also cells of the immune system (154; 156). In the immune system, the highest expression of the *Cnr1* gene (encoding CB_1) is found on B cells, followed by NK cells, monocytes, neutrophils, $CD8^+$ T and $CD4^+$ T cells. The expression of CB_1 (at transcriptional and translational levels) on immune cells relies on the activation status of the cells, cell type, immune stimulus and presence of endocannabinoids (156; 161). CB_2 is mainly expressed in lymphoid organs and cells of the immune system. In peripheral organs, levels of CB_2 transcripts are 10-100-times higher than those of CB_1. The CB_2 receptor is found in almost all immune cells, but, similar to the CB_1 receptor, the expression of CB_2 receptors in these cells depends on the cell type and activation status. Due to a lack of specific antibodies against CB_2 receptor, the amount of CB_2 protein content is unclear (162). In human blood, highest levels of *Cnr2* mRNA (encoding CB_2) are seen in B cells and eosinophils, followed by NK cells, macrophages, polymorphonuclear cells (neutrophils and eosinophils), $CD4^+$ T and $CD8^+$ T cells (163; 164).

The ECS has an important role in keeping balance in the immune system via the stimulation of classical and putative CB receptors (165). CB_1 and CB_2 are mostly known to initiate signaling pathways via heterotrimeric $G_{i/o}$-proteins that induce inhibition of adenylyl cyclase upon binding to their endogenous and exogenous ligands. Signaling pathways of CB_1 and CB_2 have been compared in cell systems, and differences between the two receptors have been found (166). CB_1, upon binding to its ligand, regulates a set of signaling pathways that modulates ion channels and stimulates several downstream signaling steps, including p38, p42/44 mitogen-activated protein kinase (MAPK, ERK-1/2), and phosphoinositide 3-kinase (PI3K) pathways. Furthermore, CB_1 activation affects intracellular Ca^{2+} content, the arachidonic acid pathway, and nitric oxide production (167). CB_2 activation modulates three major MAPKs: extracellular signal-regulated protein kinase (ERK), p38 MAPK, and c-Jun NH_2-terminal kinase (JNK), and it also regulates intracellular Ca^{2+} content (reviewed in (166)). Adenylate cyclase and MAPK signaling pathways are major pathways to be involved in both immune cell development and immune cell reactions to extracellular stimuli. These stimuli include mitogens, heat, osmotic stress, and cytokines that control immune cell functions, such as cytokine production, proliferation, migration and apoptosis. All these functions are vital in maintaining homeostasis of the immune response, and in combating infections and abnormal growth (163). The influence of CB receptors on immune functions, such as migration, proliferation/differentiation, apoptosis, cytokine production, and Ab production has been assessed *in vitro* and *in vivo* (reviewed in (161; 163).

1.4.1.1 Cannabinoid receptors and migration

Jourdan and co-workers demonstrated that in a model for diabetes, rats treated with the CB_1 antagonist JDS037, showed reduced macrophage infiltration into pancreatic islets, a shift in macrophage polarization (from M1 to M2), and a subsequent delay in the disease onset (168). Furthermore, Mai et al. demonstrated that mouse models of liver injury treated with the CB_1 antagonist AM281 had reduced infiltration of bone marrow-derived monocytes/macrophages into injured liver, and that this effect was mediated via the $G_{(\alpha)i/o}$/RhoA/ROCK signaling pathway. However, blockade of CB_1 showed no influence on the migration behavior of T cells and DCs in a model of liver injury and inflammation (169). On the other hand, a number of immune cells, including human peripheral blood monocytes, neutrophils, eosinophils, NK cells, and murine DCs, B cells and microglial cells migrate toward the endocannabinoid 2-AG in a CB_2-dependent manner (described in (160; 163)).

1.4.1.2 Cannabinoid receptors: immune cell proliferation/differentiation and cytokine production

Several studies have demonstrated that inhibition of T cell functions like proliferation, migration, and cytokine production by exo- and endo-cannabinoids either relied on CB_2 or non-cannabinoid receptors (163; 170; 171). For instance, CB_2 agonist JWH-133 significantly reduced proliferation of antigen-specific mouse $CD4^+$ T cells *in vitro* as well as expression of IL-2 and IFN-γ transcripts after antigen stimulation (172). Regarding CB_1, a series of publications by Borner et al. identified increased expression of CB_1 in T cells in the presence of cannabinoid agonists and cytokines, such as IL-4, indicating the involvement of CB_1 also in T cell function (173–176). Two synthetic cannabinoids, CP55,940 and WIN55212-2, and the psychoactive component of marijuana, delta-9-tetrahydrocannabinol (THC), caused an increase in B-cell proliferation in a dose-dependent manner, however, a definitive mechanism behind this effect was not elucidated (177). In addition, it has been reported that activation of CB_2 results in immunoglobulin class switching from IgM to IgE in anti-CD40- and IL-4-stimulated B cells of the mouse (178). Furthermore, Newton et al. demonstrated that CB receptors mediated THC-induced Th_1 and Th_2 polarization after infection with *L. pneumophila*, with CB_1 reducing Th_1, and CB_2 enhancing Th_2 responses. Moreover, both CB receptors inhibited the release of IL-12 by DCs (179). Activation of CB_2 on LPS/IFN-γ- stimulated murine microglial cells potentiated the reduction of the release of pro-inflammatory cytokines, such as IL-12 and IL-23, and enhanced increase of IL-10 production. Analogous findings were demonstrated with human microglial cells (180; 181). Finally, *in vivo* administration of THC reduced the cytolytic activity of NK cells in the spleens of mice. Antagonists for CB_1 and CB_2

reversed this effect, suggesting the involvement of CB receptors in regulating the cytolytic activity of NK cells (182).

1.4.1.3 Cannabinoid receptors and apoptosis

It has been demonstrated that murine bone marrow-derived DCs treated with exogenous cannabinoids like THC undergo apoptosis through the involvement of death-receptor and mitochondrial pathways. Treatment with either CB_1 antagonist SR141716A or CB_2 antagonist SR144528 dose-dependently reduced the THC-mediated apoptosis. Furthermore, combined use of the CB antagonists was more efficacious in inhibiting the THC-induced apoptosis than their separate use, suggesting simultaneous stimulation of both CB_1 and CB_2 receptors may be needed to promote apoptosis (183). Lombard et al. showed that the single use of CB_2 agonist JWH-015 limited proliferation of splenocytes and lymphocytes, and also increased apoptosis rates in thymocytes. In addition, the group showed that immune cells treated with JWH-015 *in vitro* underwent apoptosis via both the intrinsic and extrinsic pathways. Furthermore, they reported that mice treated with JWH-015 developed thymic involution that was associated with reduced proliferation of peripheral T cells as well as enhanced levels of apoptosis. The effect was partly reversed by CB_2 antagonist SR144528 (184).

1.5 Cannabinoid receptors - either pro- or anti-tumorigenic in lung cancer

CB_1 and CB_2 expression may be increased or reduced under pathological conditions, such as cancer, and expression levels of CB receptors are well-known to affect tumor cell growth (185). Nevertheless, it is still unclear whether they are pro- or anti-tumorigenic in cancer and whether CB receptor-expressing tumor cells or/and immune cells of the TME are involved in tumor progression.

Since the mid-1980s, the effect of marijuana smoking on lung physiology and immune cell composition has become an interesting area for researchers to investigate (186). Both CB_1 and CB_2 transcripts are found in the lungs and bronchial tissue, revealing that the expression of CB_1 transcripts significantly exceed that of CB_2 (156; 186). On the cellular level, however, human lung-resident macrophages express higher amounts of CB_2 than CB_1. Activation of these receptors stimulates ERK1/2 phosphorylation and production of reactive oxygen species (187). Furthermore, NSCLC tissues demonstrated highly expressed levels of CB_1 (24%) and CB_2 (55%) in comparison to adjacent or non-neoplastic lung tissue (188). Human NSCLC cell lines, such as A549, H1299, H358 and H838 revealed high CB_1 expression, accompanied by low CB_2 content while H1975 and SW-1573 cell lines lacked detectable expression of CB_1 (189). Another group found that A549 and SW-1573 cells expressed high levels of CB_2 protein but low levels of CB_1 (190). Several studies described expression levels of CB receptors

correlating with patient survival in NSCLC, and the role of THC and CB_1/CB_2 agonists on proliferation, invasiveness, and metastasis in NSCLC cells (190–195). Vidinsky et at. demonstrated that CB_2 agonist JWH133 had anti-proliferative and -angiogenic effects on A549 lung cancer cells (191). Furthermore, Preet et al. reported that NSCLC cells treated with THC had reduced EGF-mediated growth, migration, and invasion. Moreover, THC significantly inhibited subcutaneous tumor growth and lung metastasis of NSCLC cells in severe combined immunodeficient mice, suggesting that CB receptors have anti-tumorigenic and -metastatic properties in NSCLC (190). Interestingly, the use of CB_1 and CB_2 agonists revealed equivalent findings, showing that either use of THC ligand or CB receptor agonists lead to the same effects (192). In addition, NSCLC tumor-bearing mice treated with CB_2 agonist JWH-015 showed reduced tumor growth, accompanied by inhibited macrophage infiltration and epithelial to mesenchymal progression (193). Milian and co-workers reported that NSCLC patients with increased expression levels of both CB_1 and CB_2, or only CB_1, had significantly increased survival rates, suggesting the expression levels of CBs can be potentially used to predict survival of patients with NSCLC (194). In contrast to these findings, Xu et al. showed that upregulation of CB_2 in NSCLC tissue was associated with overall poor survival, increased tumor size and advanced pathological grading, indicating that blockade of CB_2 may reduce tumor growth and proliferation of lung cancer cells (195).

1.6 Hypothesis and aims of the thesis

The importance of CB receptors in controling lung cancer growth has been demonstrated by several studies (193–195). However, the available studies report discrepant results on the role of CB receptors in lung cancer tissues, and data on the role of CB receptors in immune cells of the TME in NSCLC are missing, indicating that more studies are needed to unravel the role of CB_1 and CB_2 receptors in lung cancer development.

The aim of this thesis was to identify the role of CB receptors expressed in the TME and how the presence of these receptors affected immune cell behavior and tumor burden in a model of lung cancer. To investigate this research question, we used a mouse model of NSCLC, in which immunocompetent wild type (WT) and CB_1- ($CB_1^{-/-}$) or CB_2-knockout ($CB_2^{-/-}$) mice received a subcutaneous injection of syngeneic mouse lung adenocarcinoma cells (KP cells (196)), thus creating a tumor model in which TME cells would either express or lack CB receptors.

The obtained knowledge should help to elucidate the role of CB receptors in lung cancer development and to improve response rates to ICI therapy.

2 Materials and Methods

As parts of this dissertation have previously been published as an original research article in Frontiers in Immunology (197), the Materials and Methods section has been partially adapted from the article and any resemblances in regards to content and phrasing are to be expected.

2.1 Ethical issues

All *in vivo* experiments were granted by the Austrian Federal Ministry of Science and Research (protocol number: BMBWF-66.010/0041-V/3b/2018).

2.2 Mouse models

All animals were bred and maintained in the animal facilities of the Medical University of Graz. Wild type C57BL/6J (B6) mice were purchased from Charles River, Germany. Mouse strains deficient for CB_1 ($CB_1^{-/-}$) on B6 background were kindly donated by Dr Andreas Zimmer, University of Bonn, Germany. $CB_2^{-/-}$ mice (B6.129P2-Cnr2^{tm1Dgen}/J on B6 background) were obtained from Jackson Laboratories (Bar Harbor, ME, USA). Mice from both sexes and 6-14 weeks of age were used for *in vitro* and *in vivo* experiments.

2.3 Cancer cell lines

The mouse KP cell line was a generous gift by Dr McGarry Houghton from the Fred Hutchinson Cancer Center, Seattle, USA. The cell line was isolated from a lung adenocarcinoma, grown in a Kras mutant/Trp53-null (Kras$^{LSL\text{-}G12D}$/p53$^{fl/fl}$) mouse after intratracheal administration of adenoviral Cre recombinase, as described before (198). Briefly, pieces of mechanically disaggregated lung tumors were cultured in Dulbecco's Modified Eagle Medium (DMEM) supplemented with 10% fetal bovine serum (FBS, Life Technologies), penicillin (100units/mL) and streptomycin (100µg/mL) until tumor cells were free of stromal contaminants (198). Lewis lung carcinoma (LLC1) cell line was purchased from the ATCC (Rockville, Maryland, USA). Both lung cancer cell lines were maintained in DMEM medium supplemented with 10% FBS and 1% penicillin/ streptomycin (P/S, PAA Laboratories) and kept in a humidified incubator (5% CO_2) at 37°C and passaged every 48 hrs. The cell lines were routinely tested and identified to be mycoplasma free.

2.4 Subcutaneous tumor models

To generate subcutaneous (s.c.) tumors, KP or LLC1 cell lines (5×10^5) suspended in 450 µL Dulbecco's Phosphate Buffered Saline (PBS, Gibco) were injected s.c. into the lower right flanks of mice on day 0. The injections were performed under inhaled isoflurane anaesthesia. The end of the experiment in the KP and LLC1 tumor model was on day 15 and 21,

respectively, when tumors were collected, weighted, measured with a digital caliper *ex vivo,* and used for subsequent downstream experiments. Tumor volume was calculated based on the following formula: v = length x width x height x π/6 (199).

2.5 Pharmacology

For pharmacological blockade of CB_1 receptors, tumor-bearing C57BL/6J WT mice were intraperitoneally (i.p.) injected with 1 mg/kg/d CB_1 antagonist SR141716 (200; 201) (Cayman Chemical, Ann Arbor, MI). Tumor-bearing $CB_2^{-/-}$ mice were i.p. injected with 20 mg/kg/d CB_2 agonist JWH-133 (202) (Axon Medchem, Groningen, NL). For pharmacological blockade of CB_2 receptors, tumor-bearing $CB_2^{-/-}$ mice and C57BL/6J WT mice were i.p. treated with 10 mg/kg/d CB_2 antagonist SR144528 (201; 203) (Cayman Chemical, Ann Arbor, MI) or vehicle (ethanol). The treatment duration for upstream interventions was ten days, initiating from day 5 (when tumors reached palpable size) until day 14. To inhibit PD-1, tumor-bearing $CB_2^{-/-}$ mice and WT littermates were injected i.p. with 250 µg of rat monoclonal anti-mouse PD-1 antibody (204) (clone 29F.1A12, BioXCell, Lebanon, NH) or rat IgG2a isotype control (clone 2A3, BioXCell, Lebanon, NH) on days 6, 9, and 12.

2.6 Single-cell suspensions of murine tissues

KP cell tumors

Tumors were mechanically dissociated into small parts using a surgical scissor and digested in Roswell Park memorial Institute (RPMI) medium containing DNase I (160 U/ml; Worthington) and collagenase (4.5 U/ml; Worthington) for 30 minutes at 37°C, while rotating at 800-1000 rpm. The tumor tissue was then passed through a 40 µm strainer, suspended in staining buffer (SB, PBS+2% FBS), washed in cold PBS, counted, and subsequently used for surface, intracellular and nuclear antigen staining.

Spleen tissues

Spleens were harvested from healthy age and sex-matched $CB_2^{-/-}$ mice and WT littermates, and processed for flow cytometry to identify immune cell composition. Briefly, whole spleens were minced with a syringe plunger and passed through a 40 µm cell strainer, suspended in SB, and centrifuged at 4°C for 5 min at 500 g. Afterwards, the supernatant was removed and the pellet was treated with 5 mL of 1x RBC lysis buffer (BioLegend, # 420301) and incubated for 5 min on ice with occasional shaking. To neutralize lysis of the cells, four volumes of PBS were added and centrifuged at 4°C for 5 min at 500 g. Then, cells were washed twice in PBS, resuspended in PBS, counted, and used for surface antigen staining.

Lung tissues

Lungs of healthy age and sex-matched $CB_2^{-/-}$ mice and WT littermates were perfused with PBS and processed for flow cytometry. Briefly, tissues were cut into small pieces using a surgical scissor, and digested in RPMI medium with DNase I (40 U/ml; Worthington) and collagenase (150 U/ml; Worthington) for 30 min at 37°C, while rotating at 800-1000 rpm. After incubation, tissue was passed through a 40 µm cell strainer, suspended in SB, and centrifuged for 5 min at 500 g (4°C). The pellet was then incubated in 5 mL of 1x RBC lysis buffer (BioLegend, # 420301) for 5 min on ice with occasional shaking. To terminate the process of lysis, four volumes of PBS were added and centrifuged at 4°C for 5 min at 500 g. Then, cells were washed, resuspended in PBS, counted, and used for surface antigen staining.

2.6.1 Flow cytometry

To exclude dead cells, single cell suspensions of the s.c. tumors were pre-stained with eBioscience™ Fixable Viability Dye (FVD) eFluor™ 780 (1:2000, ThermoFisher Scientific, # 65-0865-14) for 20 minutes at 4°C (protected from light). Prior to staining with surface and intracellular antibodies, single cell suspensions were incubated in 1 µg TruStain FcX™ (BioLegend, # 101320) for 10 min at 4°C. Staining of immune cells was performed for 30 min at 4°C (protected from light) with a pre-mixed panel of antibodies (**Table 3**). Cells were then washed and fixed in eBioscience™ IC Fixation Buffer (ThermoFisher Scientific, # 00-8222-49) for 10 min at 4°C. To identify FoxP3 nuclear antigen within the cells, surface-stained cells were permeabilized and fixed in Transcription Factor Buffer Set (BD Biosciences, # 562574) and then stained with FoxP3 antibody (**Table 3**). To detect expression of IFN-γ and CD107a, single-cell suspensions (2×10^6 cells) were suspended in 100 µL RPMI medium containing 10% FBS, 1% P/S, and GolgiStop (1.5 µl/ml, BD Biosciences), seeded into 96- well U-bottomed plates and incubated for 4 hrs at 37°C (5% CO_2). During incubation time, a CD107a antibody was added, and cells were stimulated with phorbol myristate acetate (PMA) (100 ng/ml, Sigma Aldrich) and ionomycin (Iono) (1 µg/ml, Sigma Aldrich), or they were used unstimulated (205; 206). Then, surface and intracellular staining (BD Cytofix/Cytoperm™ Kit) was performed with the pre-mixed antibody panel (**Table 3**). To determine the TME cells positive for CCL21, cells were stained based on the protocol described by Eberlein et al. (207) with several modifications. Briefly, cells (2×10^6 cells per well) were suspended in 100 µL RPMI medium containing 10% FBS, 1% P/S, and GolgiStop (1.5 µl/ml, BD Biosciences) and seeded into 96-well U-bottomed plates. During incubation time, cells were stimulated with PMA (100 ng/ml, Sigma Aldrich) and Iono (1 µg/ml, Sigma Aldrich). Then they were pre-stained with FVD eFluor™ 780 for 20 minutes at 4°C (protected from light). After that, surface staining was

performed with a pre-mixed antibody cocktail (**Table 3**). Then, intracellular indirect staining (BD Cytofix/Cytoperm™ Kit) was performed with CCL21 as a primary (1:20, R&D systems, # AF457) and Alexa Fluor® 488 bovine anti-goat IgG as a secondary antibody (1:500, Jackson Immuno Research, # 805-545-180). Fixed cells were then washed and suspended in SB. Fixed cells were either acquired on a BD LSR Fortessa™ or a BD Canto™ flow cytometer with FACSDiva software (BD Biosciences). FlowJo software (Treestar) was used to perform data analysis and compensation. To define gates, fluorescence minus-one (FMO) controls were used (**Figure 21 A-F**).

2.6.2 Proliferation of tumor cells and tumor-infiltrated immune cells *in vivo*

To identify proliferation within the KP cell tumor, tumor-bearing $CB_2^{-/-}$ and WT mice received 1.5 mg/kg of bromodeoxyuridine (BrdU) solution intraperitoneally on experimental day 14. On day 15, tumors were collected to proceed with proliferation analysis (**Figure 2**). Next, single cell suspensions of tumors were processed for flow cytometry based on the aforementioned description. Cells were then stained for surface antigens for 30 min at 4°C (protected from light) (**Table 3**). After that, cells were washed and fixed in eBioscience™ IC Fixation Buffer (ThermoFisher Scientific, # 00-8222-49) for 10 min at 4°C, they were measured on a BD Canto™ flow cytometer with FACSDiva software (BD Biosciences). FlowJo software (Treestar) was used for analysis and compensation. To define gates, FMO controls were used (**Figure 21 G**).

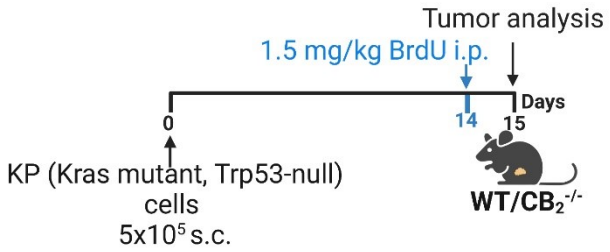

***Figure 2**. Schematic diagram for proliferation assessment in vivo.*

2.6.3 Apoptosis of tumor and immune cells

KP cell tumors were processed for flow cytometry analysis as described in 2.6. and 2.6.1. Single cells suspensions of dissected mice tumors were pre-stained with CD45-APC (BioLegend, # 103112) antibody for 30 min at 4°C (**Table 3**). Then, cells were processed for apoptosis analysis using FITC Annexin V Apoptosis Detection Kit (BD Pharmingen™, # 556547), according to the manufacturer's instruction. Stained cells were acquired on a BD Canto™ flow cytometer with FACSDiva software (BD Biosciences). FlowJo software (Treestar)

was used for analysis and compensation. Fluorescence minus-one-samples were used to define gates (**Figure 21 H**).

2.7 Flow cytometry of human NSCLC tissues

2.7.1 Study design and approval

Patients with NSCLC stages IA-IIIB were recruited from the Department of Internal Medicine, Department of Oncology and Department of Surgery (Division of Thoracic Surgery) at the Medical University of Graz (Graz, Austria). Informed consent was obtained from all participants. The study complied with the Declaration of Helsinki and was approved by the Ethics Committee of the Medical University of Graz (protocol number: 30-105 ex17/18).

2.7.2 Single cell suspension

Lung tumor tissue was cut into small pieces using surgical scissors, and digested in RPMI medium containing DNase I (40 U/ml; Worthington) and collagenase (150 U/ml; Worthington) for 30 min at 37°C. Tissue was then passed through a 100 µm cell strainer, suspended in SB, and centrifuged for 5 min at 500 g (4°C). The pellet was resuspended in 1x RBC lysis buffer (BioLegend, # 420301) and incubated for 3 min at 4°C with occasional shaking. The process of lysis was neutralized by adding four volumes of cold PBS. Then, cells were passed through a 40 µm cell strainer and washed in SB. Cells were then washed and resuspended in cold PBS. $2x10^6$ cells per 96-well plate were used for surface antigen staining.

2.7.3 Flow cytometry

Cells were first incubated with FVD eFluor™ 780 (1:2000, ThermoFisher Scientific, # 65-0865-14) for 20 min at 4°C (protected from light) to exclude dead cells. Then they were stained with anti-CB_2 antibody (1:50, Abcam, # ab3561) for 45 min at 4°C. Cells were further stained with a goat anti-rabbit IgG H&L (Alexa Fuor® 488) secondary antibody (1:500, Abcam, # ab150077) for 45 min at 4°C followed by pre-incubation with human TruStain FcX™ (BioLegend, # 422302) for 10 min at 4°C to block Fc receptor. Then, cells were again stained with a pre-mixed panel of antibodies for 20 min at 4°C (protected from light) (**Table 3**). After each staining step, cells were washed twice in SB. Subsequently, cells were fixed in eBioscience™ IC Fixation Buffer (ThermoFisher Scientific, # 00-8222-49) for 10 min at 4°C. Fixed cells were measured on a BD LSR Fortessa™ equipped with FACSDiva software (BD Biosciences). FlowJo software (Treestar) was used to perform data analysis and compensation. To define gates, FMO controls were used (see **Figure 21 I**).

2.8 RNA extraction and RT-qPCR

RNA was isolated from tissue using Trizol (Life Technologies), and from cultured cells using RNeasy Kit (Qiagen), according to manufacturer's recommendations. RNA samples were

treated with either a DNA-*free*™ DNA Removal Kit (Invitrogen) or an RNase-Free DNase set (Qiagen) for removal of genomic DNA or DNase after treatment, respectively. Following RNA isolation, the quality and concentration of RNA were evaluated by a NanoDrop ND-1000 spectrophotometer (Thermo Fisher Scientific). A High-Capacity cDNA Reverse Transcription Kit (Applied Biosystems™) was used to reversely transcribe 1 µg of total RNA into single-stranded cDNA. Thermal-cycling conditions were specified according to the manufacturer's protocol and were as follows: 25°C for 10 min, 37°C for 120 min, 85°C for 5 min, and 4°C for 5 min. Quantification of gene expression was performed by real time PCR (CFX Connect Real-Time System, Bio-Rad) using SsoAdvanced Universal SYBR Green Supermix (Bio-Rad). Primers were obtained from Bio-Rad (*Hprt;* mouse, ID: qMmuCED0045738) and from Eurofins (**Table 2**). Relative gene expression was calculated using ΔCq- and ΔΔCq-methods (208).

Table 2. *Primers from Eurofins used for RT-qPCR.*

Target	Species	Sequence	Direction
***Cnr2* PrimerBank ID: 31981837a1**	mouse	ACGGTGGCTTGGAGTTCAAC	forward
		GCCGGGAGGACAGGATAAT	reverse

2.9 In situ hybridization (ISH) and immunofluorescence (IF)

Murine and human NSCLC tissue samples

Tumor tissue from mice were fixed in acid-free phosphate-buffered 10% formaldehyde solution (Roti®- Histofix 10%, pH7) for 24-48 hrs at room temperature with gentle shaking. Human NSCLC tissue samples (formalin-fixed and paraffin-embedded) were obtained from the Biobank of the Medical University of Graz. Ethical approval was acquired from the Institutional Review Board of the Medical University of Graz (EK-numbers: 30-105ex17/18). All procedures involving clinical samples followed the ethical standards of the institutional and/or national research committee and the 1964 Helsinki Declaration and its later amendments or comparable ethical standards. Written informed consent was given by all participants. Following fixation, tissue was dehydrated and processed for paraffin embedding, according to standard protocols. Then, tissue was cut in sections (5 µm thickness), baked in 60°C oven for 1 hr, de-waxed, and rehydrated. Detection of CB_1 and CB_2 transcripts in murine tumor tissue and human NSCLC tissue was conducted using RNAscope® probes from Advanced Cell Diagnostics (ACD, Newark, USA) (**Table 4**). ISH was performed using RNAscope® 2.5 HD red kit based on manufacturer's guidelines. Briefly, sections of tumor tissue were first covered with RNAscope® hydrogen peroxide for 10 min at room temperature followed by antigen target retrieval in the Brown FS3000 food steamer at 95°C for 15 min. Then, the sections were

digested with protease IV in HybEZ™ II oven (ACD, Newark, USA) at 40°C for 20 min, washed in distilled water, followed by incubation with the corresponding probes at 40°C for 2 hrs. Lastly, the signal was detected using Fast Red stain. Tissue sections from tumors of $CB_1^{-/-}$ or $CB_2^{-/-}$ and WT mice were placed on a single slide. Earlier, our group confirmed the specificity of the mouse CB_1 and CB_2 probes in $CB_1^{-/-}$ and $CB_2^{-/-}$ mice (162).

After the detection of ISH signals, tissues were incubated overnight at 4°C in PBS and further processed by immunofluorescence. First, tissues were blocked in blocking buffer (0.1 M PBS, 1% of goat serum, and 0.3% Triton X in PBS) for 3 hrs at room temperature. Then, tissues were incubated overnight at 4°C with primary antibodies in blocking buffer. A list of primary antibodies and their sources (**Table 5**). Tissues were then washed three times with PBS, incubated with fluorophore-conjugated secondary antibodies, such as Alexa Fluor® 488-labeled goat anti-rabbit IgG (1:500, Jackson Immuno Research, #111-546-144) and Alexa Fluor® 488-labelled bovine anti-goat IgG (H+L) (1:500, Jackson Immuno Research, # 805-545-180) for 3 hrs at room temperature. Simultaneously, tissues were stained only with secondary antibody as a negative control. Nuclear staining was performed by mounting in Vectashield® (containing DAPI to stain nuclei; Vector Laboratories). Images were taken using an Olympus IX73 fluorescence microscope (Olympus) connected with a Hamamatsu ORCA-ER digital camera (Hamamatsu Photonics K.K., Japan). Images were studied with an Olympus CellSens® 1.17 imaging software containing a deconvolution program (Olympus). To enumerate CB receptor expression in, and co-localization with tumor cells and tumor-infiltrated immune cells, ImageJ software was used.

2.10 Immunofluorescence (IF)

Murine tissue samples

To perform antigen retrieval, tissue sections (5 µm thickness) were boiled in sodium citrate for 10 min in a microwave, and then incubated in 0.3% hydrogen peroxide in PBS for 30 min at room temperature to block endogenous peroxidase activity. After that, tissue was treated with blocking buffer for 3 hrs at room temperature and incubated with Ki-67 rabbit monoclonal antibody (1:400, Cell Signaling Technology, # 12202) at 4°C, overnight. Tissue was then washed in PBS (three times for 20 min each) and stained with Alexa Fluor® 488-labeled goat anti-rabbit IgG (1:500, Jackson Immuno Research, #111-546- 144) secondary antibody for 3 hrs at room temperature. After staining procedures and washings, tissue sections mounted with Vectashield® (containing DAPI to stain nuclei; Vector Laboratories). Images were visualized by an Olympus IX73 fluorescence microscope (Olympus) connected with a Hamamatsu ORCA-ER digital camera (Hamamatsu Photonics K.K., Japan). Images were

analysed with an Olympus CellSens® 1.17 imaging software (Olympus). ImageJ software was used to count cells positive for Ki-67 marker.

2.11 Cytokine array and ELISA

To collect supernatants from KP cell tumors of $CB_2^{-/-}$ and WT mice, tumor tissue was cut into small pieces using sterile surgical scissors and then placed into a 24-well plate containing DMEM medium with 1% P/S for 24 hrs in a humidified incubator (5% CO_2) at 37°C. After incubation, tumor supernatants were aliquoted, snap-frozen in liquid nitrogen and stored at –80°C. Content of 111 cytokines, chemokines and growth factors in tumor supernatants was quantified using a Proteome Profiler Mouse XL Cytokine Array Kit (R&D systems, # ARY028), according to the manufacturer's instruction. Analysis was performed using Image Lab 5.2 software (Bio-Rad). The CCL21 ELISA (ThermoFisher Scientific; EMCCL21a) was performed with tumor supernatants and serum of healthy $CB_2^{-/-}$ and WT mice, according to the manufacturer's instruction.

2.12 Isolation of lymphocytes from spleen

$CD8^+$ T cells and NK cells were isolated from spleens of tumor-bearing $CB_2^{-/-}$ and WT mice using EasySep™ mouse $CD8^+$ T cell (STEMCELL™ Technologies, # 19853A) and NK cell (STEMCELL™ Technologies, #19855) isolation kits, according to the manufacturer's instruction. Isolated cells were subsequently used for *in vitro* experiments.

2.12.1 $CD8^+$ T and NK cell migration assay

$CD8^+$ T and NK cell migration assays were conducted using transwell 96-well plate (Corning; # CLS3387-8EA). Briefly, isolated $CD8^+$ T and NK cells were suspended in RPMI medium supplemented with 0.2% FBS (Life Technologies). The lower wells of the transwell plate were filled with RPMI medium supplemented with 0.2% FBS (100 µL/well), also containing different concentrations of mouse recombinant CCL21 chemokine protein (0.5-5 µg/mL; BioLegend; # 586406). $CD8^+$ T cells or NK cells (1 $x10^5$ cells/well) were added to the upper compartments of the transwell system and incubated for 4 hrs in a humidified incubator (5% CO_2) at 37°C. Media was used as a negative control. Recombinant CCL19 chemokine protein (0.5 µg/mL BioLegend; # 587802) was used as a positive control. Following incubation, cells from the lower wells were collected and fixed. Fixed cells were acquired for 60 seconds at a higher rate on a BD Canto™ flow cytometer with FACSDiva software (BD Biosciences) and analyzed on a FlowJo software (Treestar).

2.13 Western Blotting

Using Western blot (WB) analysis, the quantification of caspase protein in KP cell tumors was identified. Briefly, 30 µg of total protein was separated by 5-12% Bis Tris gradient gel, and transferred onto polyvinylidene difluoride (PVDF) membranes. The membrane was blocked in Tris-buffered saline with 0.1% Tween® 20 Detergent (TBST) buffer containing 5% skimmed dry milk for 1 hr, and then incubated with primary antibodies against caspase-3 (1:1000, Cell Signaling Technology, # 9662; antibody detects full-length caspase-3 (35 kDa) and the large fragment of caspase-3 resulting from cleavage (17 kDa)) and β-actin (1:5000, Sigma, # A5316, 42kDa) at 4°C overnight under gentle shaking. After four washes with a wash buffer (15 min each wash), the membrane was incubated with horseradish peroxidase-conjugated secondary antibody (goat anti-rabbit, 1:5000, Jackson Immuno Research, # 111-035-045) for 1 hr at room temperature. Clarity™ Western ECL substrate (Bio-Rad, # 170-5061) was added onto the membrane and then the image was developed with a ChemiDoc™ MP Imaging System. Size of bands were measured using Image Lab 5.2 software (Bio-Rad). Caspase-3/cleaved caspase-3 bands were normalized to β-actin before a ratio was calculated (209).

2.14 Statistical analysis

Data were analyzed using Prism v.9.3.1 (GraphPad Software, La Jolla, CA, USA) and presented as means ± standard deviation (SD) or standard error of means (SEM). Differences between experimental groups were assessed by unpaired student's *t*-tests, multiple *t*-tests or two-way analysis of variance (ANOVA) with the indicated *post hoc* test for corrections of multiple comparisons. For multiple comparisons with three or more experimental groups, a one-way ANOVA was applied with the indicated *post hoc* test for corrections of multiple comparisons. Shapiro-Wilk and Kolmogorov-Smirnov tests were applied to test a normal distribution. Correlations between tumor weight and infiltration of $CD8^+$ T and NK cells in the TME was determined using Pearson's correlation coefficient (r_p) and Spearman's correlation coefficient *rho* (r_s).

In all cases, a p-value <0.05 was considered significant and represented with one, two or three asterisks when lower than 0.05, 0.01, or 0.001, respectively.

3 Results

As parts of this dissertation have previously been published as an original research article in Frontiers in Immunology (197), the Results section has been partially adapted from the article and any resemblances in regards to content and phrasing are to be expected.

3.1 Only CB_2 but not CB_1, regulates tumor growth in a mouse model of NSCLC

3.1.1 Genetic deletion of CB_2 reduces lung tumor burden

To investigate the role of TME-derived CB receptors on tumor growth in a lung adenocarcinoma model, we used $CB_1^{-/-}$ and $CB_2^{-/-}$ knockout mice, and their WT littermates. To induce tumor growth, mice were subcutaneously injected with KP tumor cells. We observed that there were no significant differences in tumor burden between $CB_1^{-/-}$ mice and WT littermates (**Figure 3 A**), whereas mice lacking CB_2 demonstrated a 50% reduction in tumor growth (assessed by tumor weight and volume) in comparison to WT mice (**Figure 3 B**).

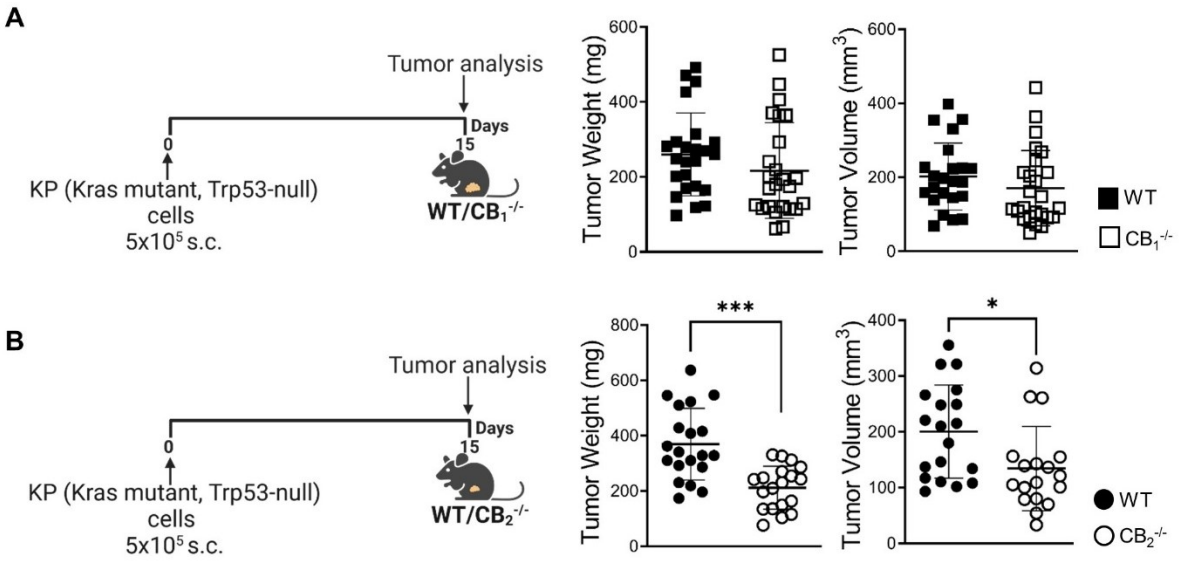

Figure 3. *Only knockout of CB_2 but not CB_1 causes tumor growth reduction.*

(A) Experimental scheme: on day 0, $5x10^5$ KP (Kras mutant, Trp53-null) lung adenocarcinoma cells were subcutaneously (s.c.) injected into the flanks of $CB_1^{-/-}$ mice and wild type (WT) littermates. KP tumors were measured *ex vivo* on day 15 and collected for analysis. Graphical results are presented as means ± SD from three pooled independent experiments. n= 23-25. **(B)** Experimental scheme: on day 0, $5x10^5$ KP (Kras mutant, Trp53-null) lung adenocarcinoma cells were s.c. injected into $CB_2^{-/-}$ mice and WT littermates. KP tumors were measured *ex vivo* on day 15 and harvested for analysis. Data presented as mean values ± SD from two pooled independent experiments. n= 18-20. *p<.05; ***p<.001, analyzed by unpaired student`s *t*-test. This figure has been adapted from (197).

3.1.2 Pharmacological blockade of CB_2 reduces lung tumor burden

Using previously published doses of the CB_1 antagonist SR141716 (200; 201) and the CB_2 antagonist SR144528 (201; 203), we pharmacologically blocked CB_1 or CB_2 receptors in tumor-bearing C57BL/6J WT mice and demonstrated findings that were concordant with those in knockout mice. Thus, both tumor weight and volume did not change after injections with the CB_1 antagonist SR141716 (**Figure 4 A**). In contrast, treatment with the CB_2 antagonist SR144528 resulted in a significant reduction in tumor weight and volume when compared to C57BL/6J WT mice treated with vehicle (**Figure 4 B**).

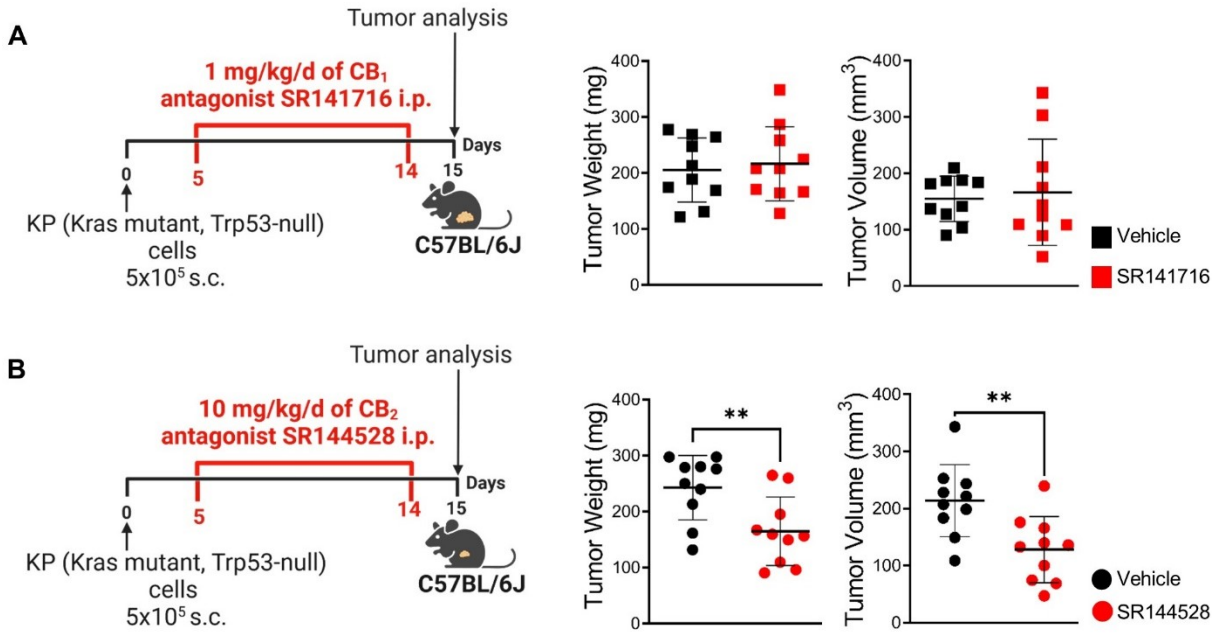

Figure 4. *Pharmacological blockade of CB_2 but not CB_1 reduces tumor burden.*

(A-B) Experimental scheme: on day 0, $5x10^5$ KP lung adenocarcinoma cells were subcutaneously (s.c.) injected into the flanks of C57BL/6J wild type mice. For 10 days, tumor-bearing mice received intraperitoneal (i.p.) injections of either **(A)** 1 mg/kg/d of the CB_1 antagonist SR141716 or **(B)** 10 mg/kg/d of the CB_2 antagonist SR144528 (or vehicle). *Ex vivo* measurement of tumor weight and volume was performed on day 15. Representative results from one independent experiment are shown. Data are presented as means ± SD. n= 9-10. **p<.01, analyzed by unpaired student`s *t*-test. This figure has been adapted from (197).

3.1.3 Expression of CB receptors in murine and human tumor cells and tumor-infiltrated immune cells

To further identify the role of CB receptors in the TME, we aimed to detect transcripts of CB_1 and CB_2 in KP cell tumors and tumor-infiltrating immune cells using dual ISH-IF. Tumor cells as well as immune cells, including $CD3^+$ T cells, $CD8^+$ T cells, NKp46/$NCR1^+$ cells, $CD163^+$ or $F4/80^+$ macrophages, and $CD11b^+$ myeloid cells, expressed CB_1 (**Figure 5 A**). Co-localization

of CB_1 with respective immune cell markers was low and accounted for less than 10% (**Figure 5 A**). Regarding CB_2 mRNA expression, approximately 25% of tumor cells (identified as cytokeratin positive) co-localized with CB_2 mRNA (**Figure 5 B**). However, we identified higher expression of CB_2 transcripts in tumor-infiltrated immune cells than of CB_1, ranging between 20 and 40% co-localization (**Figure 5 B**). According to a number of studies, CB_1 and CB_2 receptors are expressed in tumor tissues of patients with NSCLC (190; 194; 195). By applying ISH-IF in human lung cancer tissue sections and flow cytometry in NSCLC tissues, we identified expression of CB receptors in tumor cells as well as infiltrated immune cells. In accordance with our data in the mouse, less than 10% of $CD3^+$ T, $CD8^+$ T cells, NKp46/$NCR1^+$ NK cells, and $CD163^+$ macrophages expressed CB_1 (**Figure 6 A**), on the other hand, expression of CB_2 was higher than of CB_1 in immune cells and ranged between 20 and 60% (**Figure 6 B-C**).

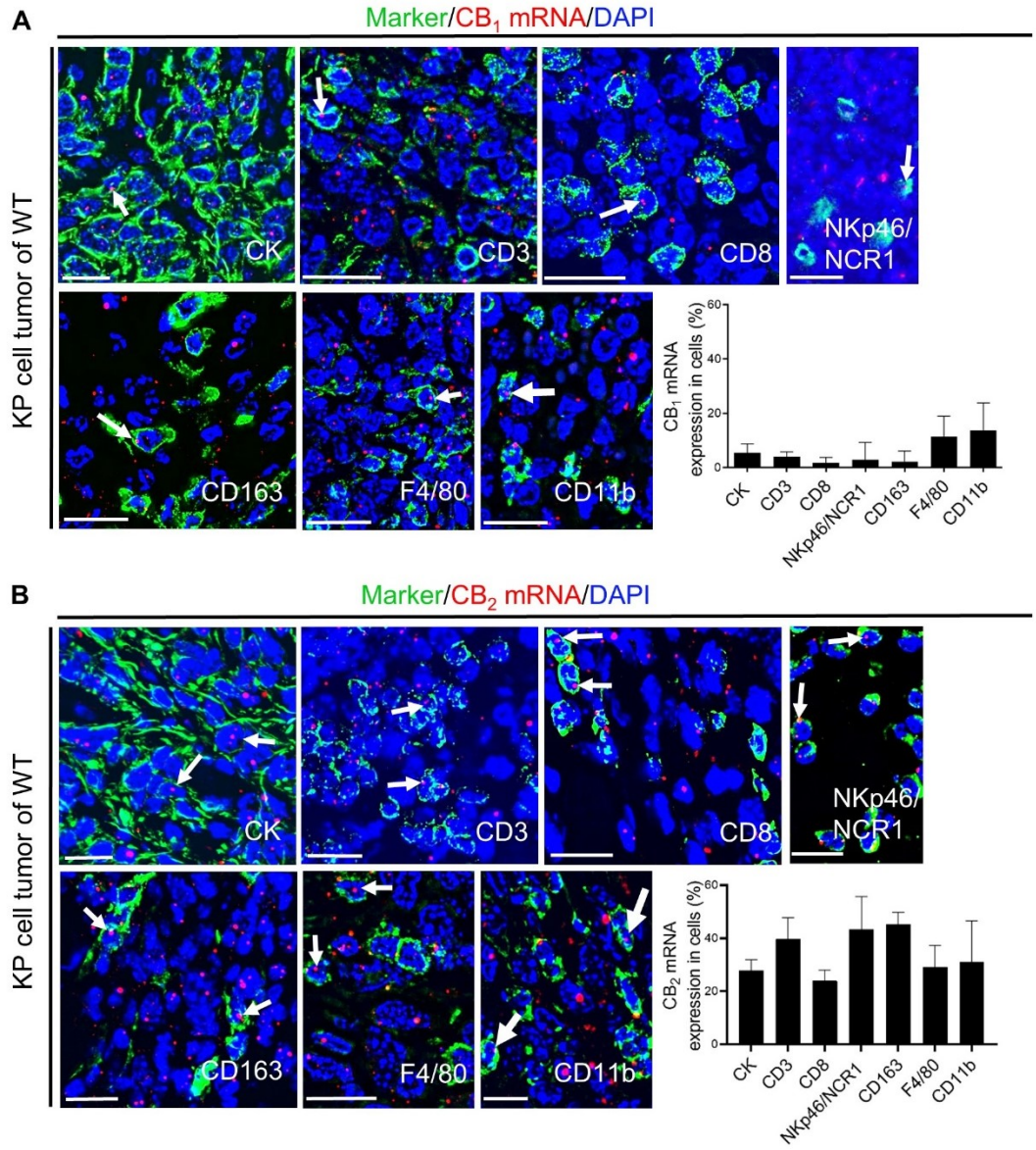

Figure 5. *Expression of CB_2 but not CB_1 was higher in tumor and immune cells of the TME.*

(A-B) Using in situ hybridization (ISH) and immunofluorescence (IF), tumor cells and tumor-infiltrated immune cells in KP cell tumor sections of WT mice were analyzed for CB receptors expression. **(A)** The graph shows the percentages of tumor cells (cytokeratin-stained, CK^+ cells; ~ 5%) and immune cells of the TME, such as $CD3^+$ T cells (~ 4%), $CD8^+$ T cells (~ 3%), NKp46/$NCR1^+$ cells (natural killer, NK cells; ~ 14%), $CD163^+$ M2 macrophages (~ 7%), $F4/80^+$ M1 and M2 macrophages (~ 11%), and $CD11b^+$ myeloid cells (~ 14%) co-localizing with CB_1 transcripts. **(B)** The graph represents the percentages of CB_2-expressing tumor cells (~ 25%), and of TME-infiltrated/CB_2-expressing leukocytes, including $CD3^+$ T cells (~ 39%), $CD8^+$ T cells (~ 24%), NKp46/$NCR1^+$ NK cells (~ 43%), $CD163^+$ M2 macrophages (~ 43%), $F4/80^+$ M1 and M2 macrophages (~ 29%), and $CD11b^+$ myeloid cells (~ 29%). Arrows indicate CB_1 or CB_2 mRNA signals within tumor and immune cells. Calibration bars = 20 µm. Data presented as mean values +SD. n=3 (sections from three different tumors, 30-150 cells counted/section). *WT*, wild type; *TME*, tumor microenvironment. This figure has been adapted from (197).

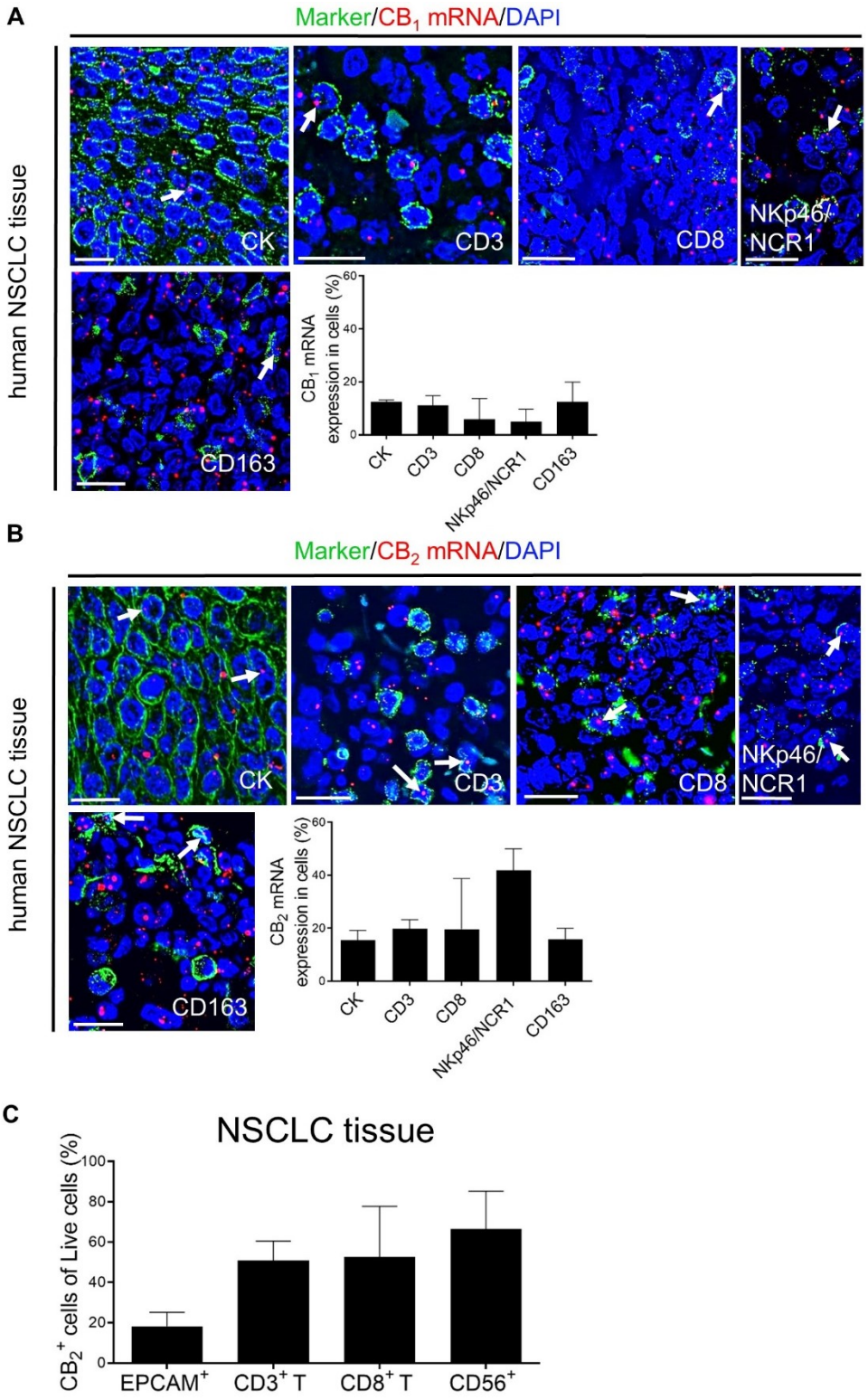

***Figure 6**.CB₁ and CB₂ expression in human NSCLC tissues.*

(A-B) Illustrative ISH-IF images of human NSCLC tissue sections. The graphs depict the percentages of tumor cells (cytokeratin-positive, CK^+ cells) and tumor-infiltrating leukocytes ($CD3^+$ T cells, $CD8^+$ T cells, NKp46/$NCR1^+$ NK cells, and $CD163^+$ M2 macrophages) co-localizing with CB_1 and CB_2 transcripts. Arrows point at positively-stained tumor and immune

cells that express CB_1 or CB_2. Calibration bars = 20 µm. Data are presented as mean values +SD. n=3 (tissue sections from three different patients with NSCLC were stained for quantification, 30-150 cells counted/section). **(C)** The graph shows CB_2 expression in cancer cells ($EPCAM^+$) and tumor-infiltrating immune cells, such as $CD3^+$ T, $CD8^+$ T, and $CD56^+$ NK cells (out of live cells). Results are depicted as mean values +SD. n=4 (tissues from four different patients with NSCLC were used for flow cytometry analysis). *ISH-IF*, in situ hybridization and immunofluorescence; *NSCLC*, non-small cell lung cancer; *NK*, natural killer cells; *TME*, tumor microenvironment; *EPCAM*, epithelial cell adhesion molecule. This figure has been adapted from (197).

Taken together, these findings demonstrate that tumor cells and TME-located immune cells express CB_1 and CB_2 receptors. However, only knockout of CB_2 on host cells or pharmacological blockade of CB_2, but not CB_1, leads to a reduction of tumor growth.

To confirm our findings from the KP cell tumor model, $CB_2^{-/-}$ mice and WT littermates were also subcutaneously injected with LLC1 lung tumor cells (**Figure 7 A**). The results showed that tumors of $CB_2^{-/-}$ mice were significantly smaller than of WT mice, corroborating the KP cell lung tumor model (**Figure 7 A-B**). Similar results were also demonstrated in a recently published study (210).

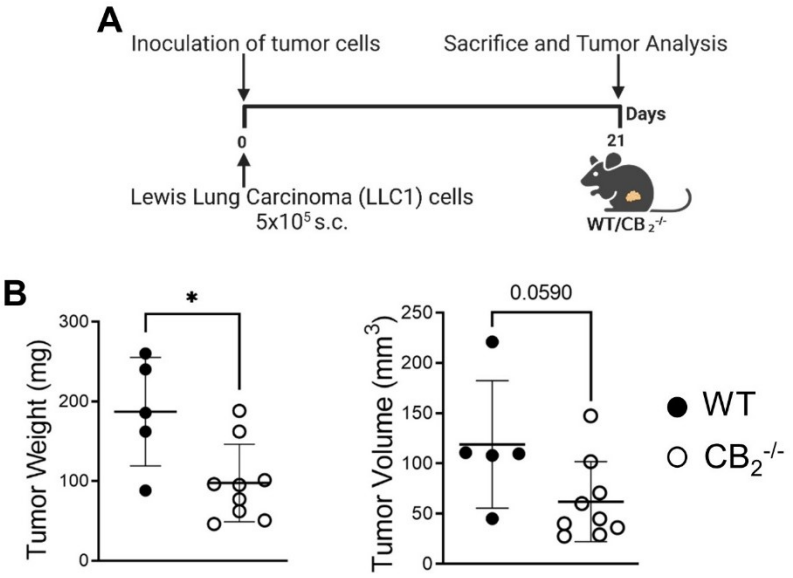

Figure 7. *In mice lacking CB_2 in the TME, growth of LLC1 cell tumors is reduced.*

(A-B) Experimental scheme: on day 0, $5x10^5$ Lewis lung carcinoma (LLC1) cells were subcutaneously (s.c.) injected into the flanks of $CB_2^{-/-}$ mice and wild type (WT) littermates. Three weeks later, tumors were harvested and measured *ex vivo*. Data are presented as mean values ± SD. n=5-9. *p<.05, analyzed by unpaired student`s *t*-test. This figure has been adapted from (197).

3.2 Reduction of tumor burden uniquely depends on the absence of CB_2 in the TME host cells

3.2.1 CB_2 expression in KP tumor cells

We showed that, apart from immune cells, approximately 20-25% of tumor cells in murine tumors (**Figure 5 B**, **Figure 8 A)** and almost 20% of tumor cells in human NSCLC tissue express CB_2 mRNA (**Figure 6 B**; using cytokeratin as a marker for tumor cells) or protein (**Figure 6 C**; using EPCAM as a marker for tumor cells). Based on RT-qPCR, tumors of $CB_2^{-/-}$ mice demonstrated reduced expression of CB_2 transcripts as compared to WT mice (**Figure 8 B**), most likely because host cells infiltrating the TME in $CB_2^{-/-}$ mice lacked CB_2 expression. The content of CB_2 mRNA in the tumors of CB_2 knockout mice measured by RT-qPCR, therefore, should have derived from tumor cells. Interestingly, KP cells in culture hardly expressed any CB_2 (**Figure 8 B**). The specificity of the CB_2 primers was demonstrated by absence of CB_2 mRNA in spleen tissue of $CB_2^{-/-}$ vs. WT mice (**Figure 8 C**).

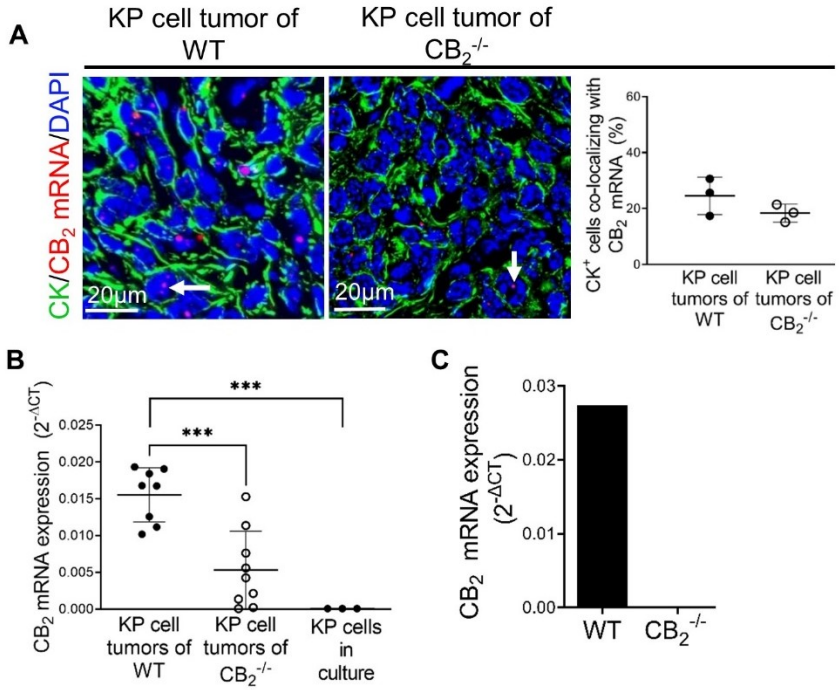

Figure 8. *Expression of CB_2 in murine tumor cells.*

(A) Representative ISH-IF images of KP cell tumor of WT and $CB_2^{-/-}$ mice stained with cytokeratin (CK). Arrows point at CB_2 co-localizing with cytokeratin positive (CK^+) cells. Calibration bars = 20 µm. The graph shows percentage of CK^+ cells expressing CB_2 mRNA. Data show mean values ± SD. n=3/group (sections from three different tumors, 75-150 cells counted per section). **(B)** qPCR data demonstrating relative CB_2 expression in lysates from KP cell tumor of WT and $CB_2^{-/-}$ mice and KP cells in culture. Data are presented as mean values ± SD. n≥8 per group; n=3 for KP cells (3 consecutive passages of KP cells). **(C)** The specificity of the CB_2 primers is depicted through relative expression of CB_2 mRNA in lysates of spleen extracted from healthy WT and $CB_2^{-/-}$ mice. ***p<.001, analyzed by unpaired student`s *t*-test

(A), one-way ANOVA with Tukey's multiple comparison test **(B)**. *ISH/IF*, in situ hybridization and immunofluorescence; *WT*, wild type. This figure has been adapted from (197).

3.2.2 CB_2 found on KP tumor cells does not control tumor growth

To identify the role of CB_2 expressed in KP tumor cells and its influence on tumor growth *in vivo*, we pharmacologically activated or blocked CB_2 in tumor-bearing $CB_2^{-/-}$ mice using the CB_2 agonist JWH133 **(Figure 9 A)** and the CB_2 antagonist SR144528 **(Figure 9 B)** at previously described doses (201; 202). The results demonstrated neither activation nor inhibition of CB_2 in tumor cells had an effect on tumor growth (**Figure 9 A-B**), signifying that the reduction in tumor burden detected in $CB_2^{-/-}$ mice was entirely influenced by CB_2 expressed on host cells infiltrating the TME.

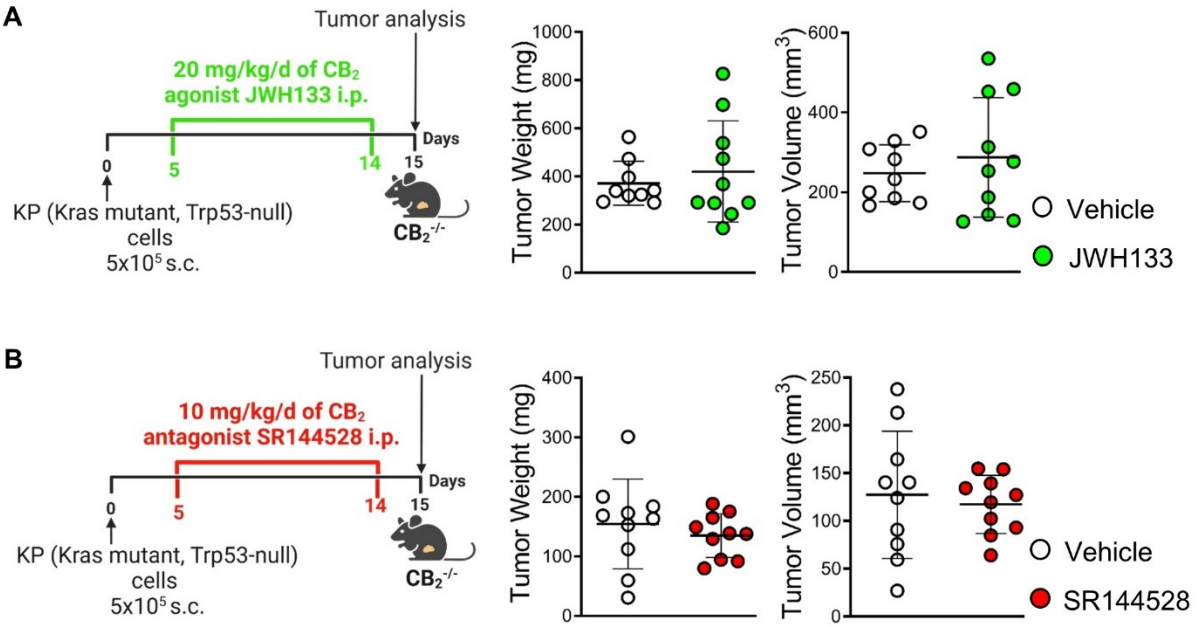

Figure 9. *CB_2 expressed on tumor cells has no influence on tumor growth.*

(A-B) Experimental scheme as in Figure 4. From day 5 until day 14, $CB_2^{-/-}$ mice received intraperitoneal (i.p.) injections of either **(A)** 20 mg/kg/d of CB_2 agonist JWH133 or **(B)** 10 mg/kg/d of CB_2 antagonist SR144528 (or vehicle). On day 15, tumor weight and volume were measured *ex vivo*. Representative results from one independent experiment are shown. Data are presented as means ± SD. n≥9; analyzed by unpaired student`s *t*-test. This figure has been adapted from (197).

3.3 Genetic deletion of CB_2 in host cells provides an anti-tumorigenic TME

3.3.1 Tumor immune microenvironment (TME)

We used flow cytometry to identify immune cell profiles in tumor tissues of $CB_2^{-/-}$ knockout and WT mice. Our results showed significant differences in infiltration between the tumors of mice

lacking CB_2 and WT mice, particularly, in the lymphoid cell populations (gating strategy in **Figure 21 A-B**). As for the percentages of tumor-infiltrating leukocytes and myeloid cells, there were no significant differences between tumors of $CB_2^{-/-}$ knockout and WT mice (**Figure 10 A-B**). The lymphoid immune cell composition in tumors of $CB_2^{-/-}$ and WT mice revealed the following: we noticed a significant increase in the infiltration of T cells ($CD3^+$), NK cells ($NKp46^+$) and $CD8^+$ T cells into tumors of $CB_2^{-/-}$ knockout mice (**Figure 10 C-D**). No significant differences in the infiltration of $CD4^+$ T cells and Tregs were seen into tumors of $CB_2^{-/-}$ vs. WT mice. However, we identified differences in subtypes of $CD8^+$ T cells, as percentages of naïve $CD8^+$ T cells were reduced while effector $CD8^+$ T cells were increased in tumors of $CB_2^{-/-}$ vs. WT mice (**Figure 10 E**), suggesting that $CD8^+$ T cells from $CB_2^{-/-}$, but not WT mice, differentiated to become $CD44^+$ $CD8^+$ T effector cells. Moreover, there was a negative correlation between tumor weight of $CB_2^{-/-}$ mice with the percentages of infiltrated $CD8^+$ T and NK cells (**Figure 10 F-G**). Additionally, we did not observe significant differences in the percentages of T, B, NK, and NKT cells within spleens (**Figure 11 A**) and lungs (**Figure 11 B**) of healthy $CB_2^{-/-}$ and WT mice, indicating that the observed differences in infiltration are likely linked to the tumor growth.

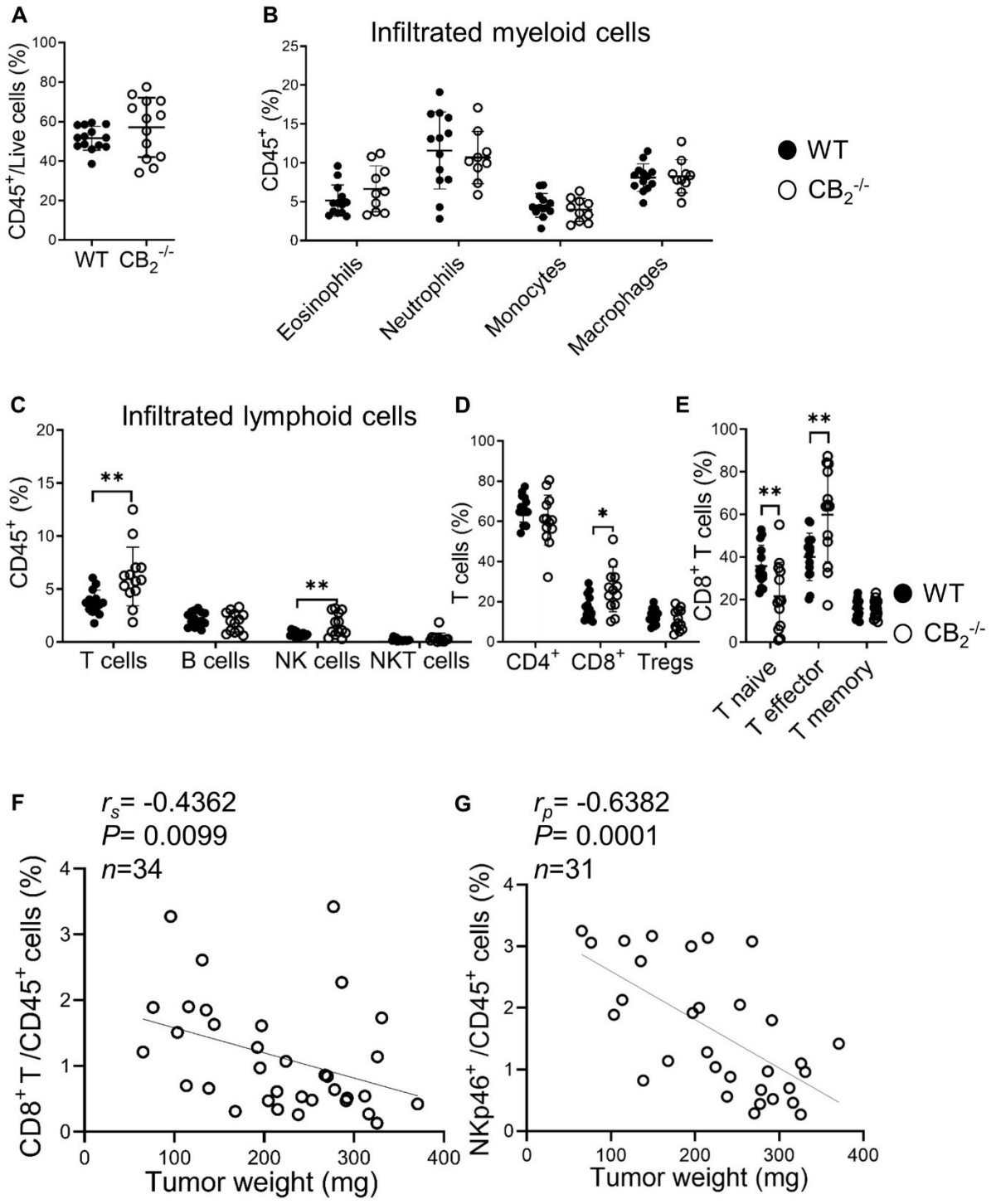

Figure 10. *CB_2 influences the immune cell profile of the TME.*

(A-E) The graphs show percentages of immune cells, including myeloid and lymphoid cells infiltrating KP cell tumors of $CB_2^{-/-}$ knockout and WT mice. Data are presented as mean values ± SD from two pooled independent experiments. n≥10. **(F-G)** Tumor weights from $CB_2^{-/-}$ mice were plotted against the percentages of tumor-infiltrating $CD8^+$ T ($CD45^+/CD3^+/CD8^+$) and NK ($CD45^+/CD3^-/CD19^-/NKp46^+$) cells (out of $CD45^+$ cells). Data were from four pooled independent experiments. n=31-34. Correlation of samples was evaluated using Spearman (r_s) and Pearson (r_p) correlation coefficients after testing for normality. *p<.05; **p<.01,

analyzed by unpaired student`s *t*-test **(A)**, multiple *t*-tests **(B-E)**. *NK*, natural killer cells, *NKT*, natural killer T cells; *Tregs*, Regulatory T cells; *WT*, wild type. This figure has been adapted from (197).

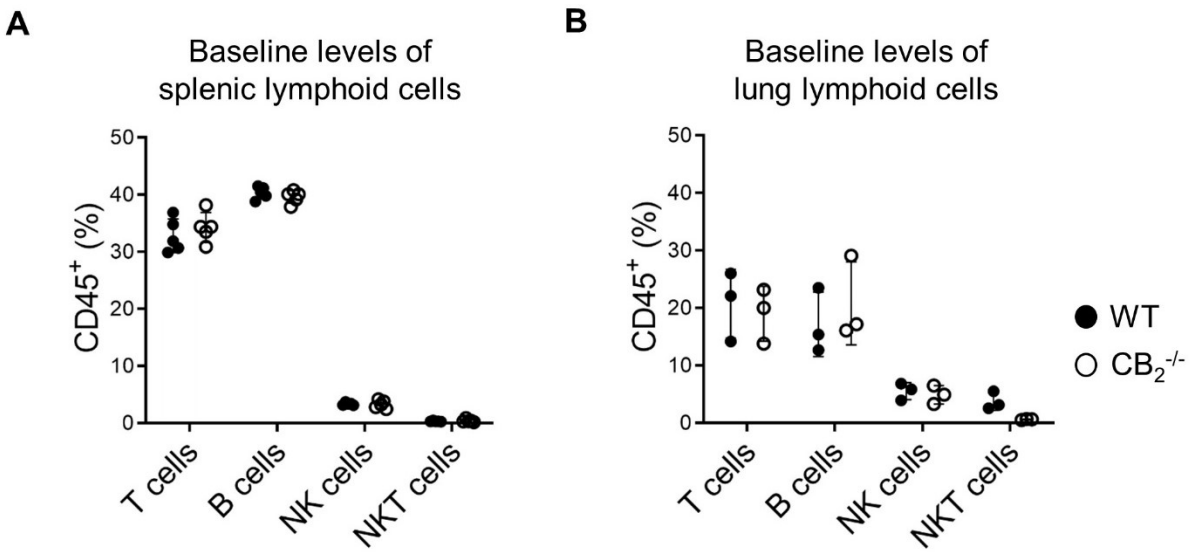

Figure 11. *Baseline levels of splenic and lung lymphoid immune cells in mice lacking CB_2.*

(A-B) The graphs demonstrate flow cytometric analysis of single cell suspensions from spleens **(A)** and lungs **(B)** of healthy $CB_2^{-/-}$ and WT mice. The percentages of T ($CD3^+$) cells, B ($CD45^+/CD3^-/CD19^+$) cells, NK ($CD45^+/CD3^-/CD19^-/NKp46^+$), and NKT ($CD45^+/CD3^+/NKp46^+$) cells (out of $CD45^+$ cells) are demonstrated. Data are shown as mean values ± SD. n=5/group **(A)**, n=3/group **(B)**; analyzed by multiple *t*-tests. *NK*, natural killer cells; NKT, natural killer T cells; *WT*, wild type. This figure has been adapted from (197).

3.3.2 Enhanced cytotoxic activity of $CD8^+$ T and NK cells

To assess the cytotoxic activity of $CD8^+$ T and NK cells within the TME, we stimulated single cell suspensions from tumors of $CB_2^{-/-}$ and WT mice with PMA/Ionomycin *ex vivo* and used flow cytometry to measure their activity. We identified a significant rise in the expression of IFN-γ in $CD8^+$ T cells (**Figure 12 A**), and of CD107a on NK cells (**Figure 12 B-C**), indicating local activation and increased tumoricidal activity of $CD8^+$ T and NK cells.

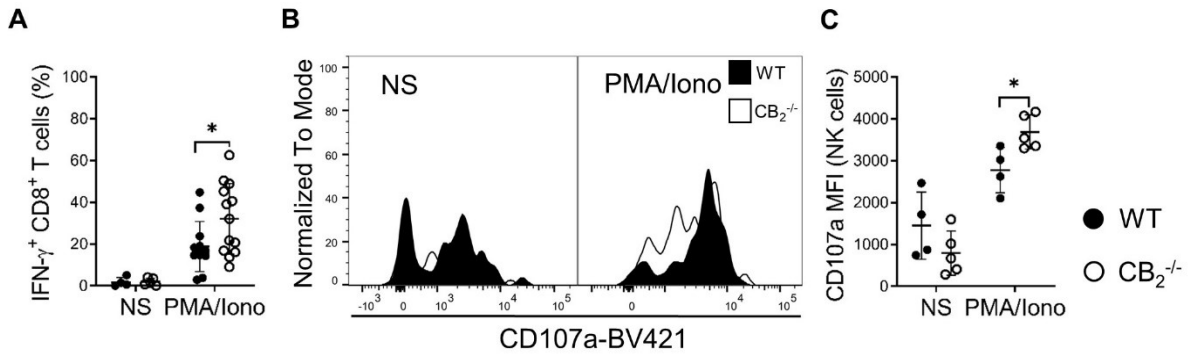

Figure 12. *Increased cytotoxic activity CD8⁺ T and NK cells in the absence of CB_2 on host cells.*

(A) The graph shows the percentage of tumor-infiltrated CD8⁺ T cells expressing IFN-γ before (non-stimulated, NS) and after stimulation with phorbol myristate acetate/ionomycin (PMA/Iono) *ex vivo*. Data are presented as mean values ±SD from two pooled independent experiments. n=4 (for NS per group); n≥11 (for PMA/Iono per group). **(B-C)** Degranulation capacity of intratumoral NK cells before (NS) and after *ex vivo* stimulation with PMA/Iono. **(C)** The graph demonstrates median fluorescence intensity (MFI) of CD107a on NK cells. n≥4. *p<.05, analyzed by multiple *t*-tests (**A, C**). NK, natural killer cells; WT, wild type. This figure has been adapted from (197).

Collectively, the results from flow cytometry indicate that a TME free of CB_2 expression favors an anti-tumorigenic immune cell profile, and enhances cytotoxic activity in lymphocytes.

3.4 Proliferation and apoptosis rates of tumor cells and tumor-infiltrated immune cells

To determine primary mechanisms for the reduction of tumor burden in $CB_2^{-/-}$ mice, we checked for changes in cellular processes, such as apoptosis and cell proliferation in the tumor. We performed flow cytometric analysis and cleaved-caspase-3/caspase-3 immunoblotting of tumors from $CB_2^{-/-}$ and WT mice. Our data revealed no significant differences in apoptotic behavior of both tumor cells ($CD45^-$) and infiltrated leukocytes ($CD45^+$) between $CB_2^{-/-}$ and WT mice (**Figure 13 A-C**). Furthermore, results based on BrdU incorporation assays and Ki-67 immunofluorescence, revealed no significant differences in the proliferation of tumor cells as well as tumor-infiltrated immune cells between $CB_2^{-/-}$ and WT mice (**Figure 13 D-E**), suggesting that other underlying mechanisms were responsible for the tumor reduction.

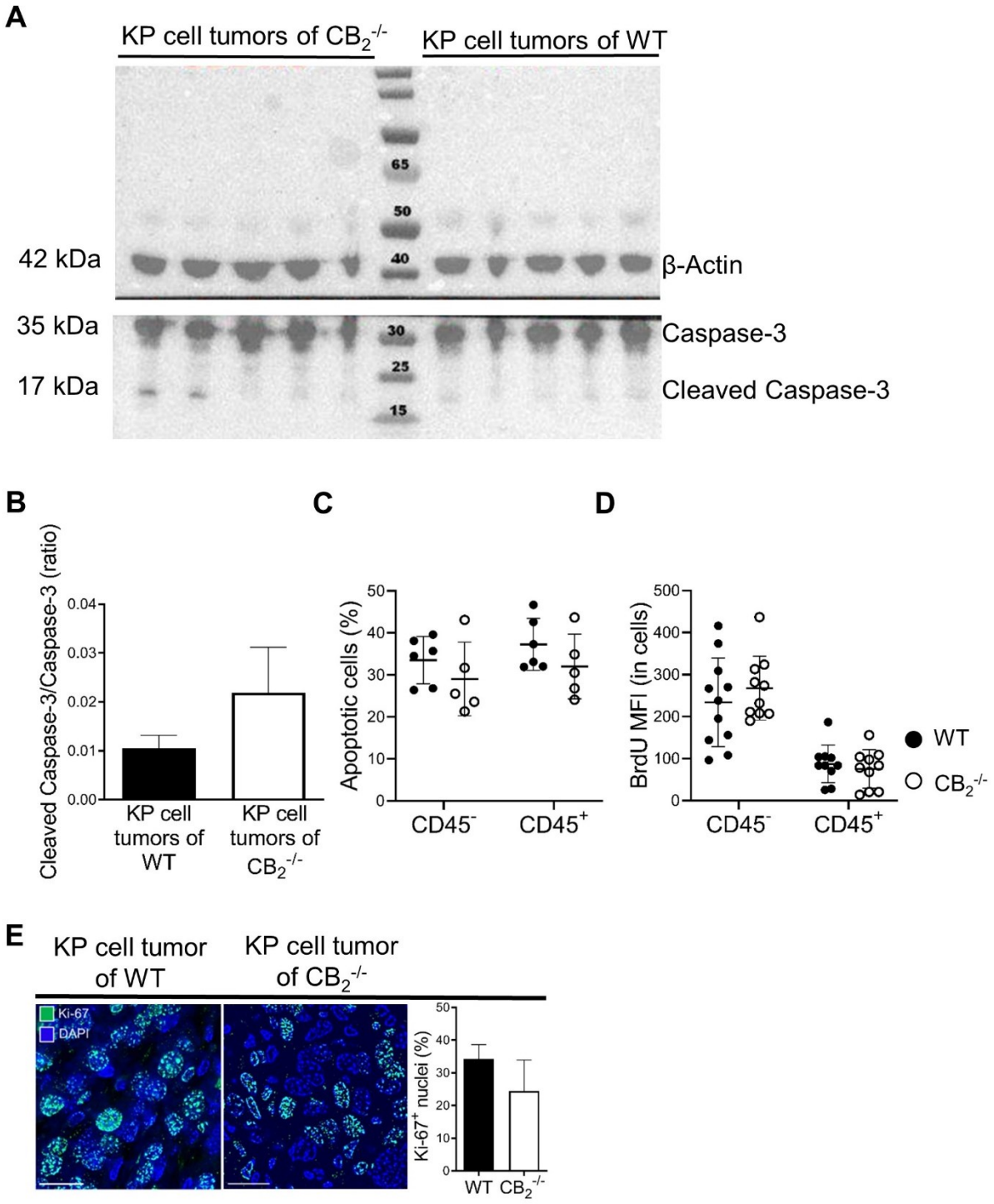

***Figure 13**. Rate of apoptosis and proliferation within the tumor.*

(A-B) Protein extracts from KP cell tumors of $CB_2^{-/-}$ and WT mice were checked for expression of caspase-3/cleaved caspase-3 and β-actin proteins using Western blotting. Data are presented as mean values ± SEM. n = 5 mice per group. **(C)** The graph shows the percentage of apoptotic CD45 negative ($CD45^-$, tumor cells) and CD45 positive ($CD45^+$, leukocytes) cells within the tumor tissue. Data are presented as mean values ± SD. n= ≥ 5 mice per group. **(D)** Flow cytometric analysis of tumors of $CB_2^{-/-}$ and WT mice demonstrates median fluorescence intensity (MFI) of BrdU in tumor and tumor-infiltrated immune cells. Data indicate mean values

±SD. n≥10. **(E)** KP cell tumors of WT and $CB_2^{-/-}$ mice were stained with anti-Ki-67 proliferation marker. Calibration bars = 20 µm. Data are presented as mean values + SD. n=3 (sections from three different tumors, 30-125 cells were counted per section), analyzed by unpaired student`s *t*-test (**B, E**), multiple *t*-tests **(C-D)**. This figure has been adapted from (197).

3.5 Lack of CB_2 in the TME increases CCL21 expression within the tumor

To assess changes in soluble factors within the TME, we performed a cytokine array in tumor supernatants of $CB_2^{-/-}$ and WT mice and detected increased levels of CCL21 in tumor supernatants of $CB_2^{-/-}$ vs. WT mice. To verify the changes, we also performed an ELISA with the supernatants and found that concentrations of CCL21 were indeed increased in $CB_2^{-/-}$ vs. WT mice (**Figure 14 A**). Baseline serum levels of CCL21 did not differ between healthy $CB_2^{-/-}$ and WT mice (**Figure 14 B**).

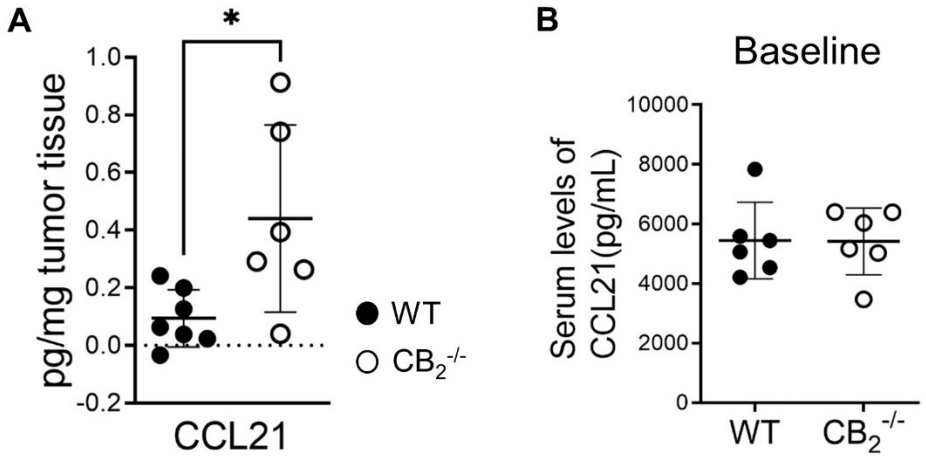

Figure 14. *Level of CCL21 within tumor supernatants.*

(A) An ELISA for CCL21 was performed in tumor supernatants of KP cell tumors of $CB_2^{-/-}$ and WT mice, and values were normalized against tumor weights. Data indicate mean values ± SD. n=6-7. **(B)** Concentration of CCL21 was measured in serum samples of healthy $CB_2^{-/-}$ and WT mice. Data are presented as mean values ± SD. n=6. **p<.05*, analyzed by unpaired student`s *t*-test.

3.5.1.1 CCL21 and its receptor (CCR7)

To determine the source of CCL21 within the tumors, we assessed non-immune cells of the TME, such as endothelial cells and fibroblasts for CCL21 expression by flow cytometry. We noticed that endothelial cells expressed CCL21 at a higher level than fibroblasts in tumors of $CB_2^{-/-}$ and WT mice. Furthermore, we identified that CCL21 expression was increased in endothelial cells of $CB_2^{-/-}$ vs. WT mice (**Figure 15 A**), indicating that the absence of CB_2 on host cells of the TME caused increased expression of CCL21 by endothelial cells. We next assessed surface expression of CCR7, the receptor for CCL21, in tumor-infiltrating immune

cells. The results revealed reduced surface expression of CCR7 in $CD8^+$ T and NK cells within tumors of $CB_2^{-/-}$ mice compared to WT littermates (**Figure 15 B-C**), suggesting that the high levels of CCL21 ligand within the TME of $CB_2^{-/-}$ mice has possibly led to CCR7 endocytosis into early endosomes, as previously demonstrated by Otero et al. (66).

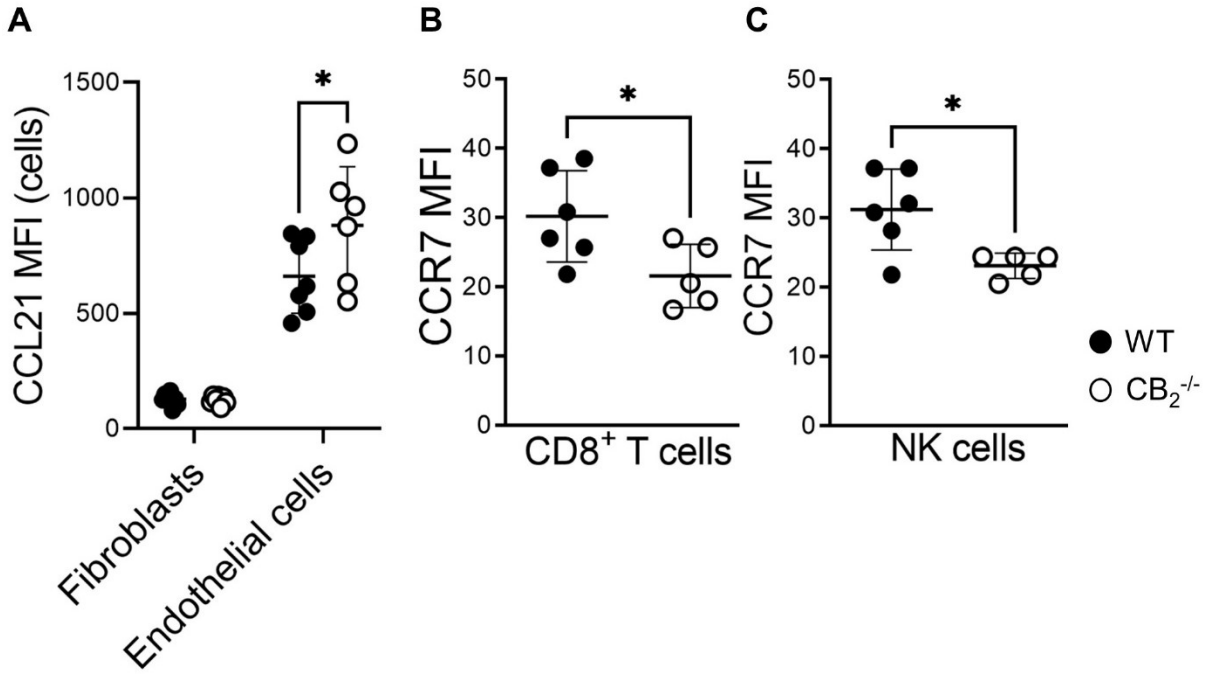

Figure 15. *Expression of CCL21 and its receptor, CCR7, within the TME.*

(A) Flow cytometric analysis of stromal cells (fibroblasts and endothelial cells) was performed to investigate expression of CCL21 within KP cell tumors from $CB_2^{-/-}$ and WT mice. The graph shows median fluorescence intensity (MFI) of CCL21 on fibroblasts and endothelial cells. Data are presented as mean values ±SD. n≥6. **(B-C)** MFI of CCR7 on $CD8^+$ T and NK cells is shown. Data indicate mean values ±SD. n≥5. **p<.05*; analyzed by two-way ANOVA, Sidak's multiple comparisons test **(A)**, unpaired student`s *t*-test **(B-C)**.

3.5.1.2 CCL21 chemoattracts $CD8^+$ T and NK cells

Since we demonstrated increased infiltration of $CD8^+$ T and NK cells at the tumor site of $CB_2^{-/-}$ mice (**Figure 10 C-D**) we hypothesized that CCL21 may act as a chemoattractant of immune cells to the tumor site. We, therefore, assessed the chemotactic capability of $CD8^+$ T and NK cells (isolated from the spleens of tumor-bearing $CB_2^{-/-}$ and WT mice) *in vitro,* and we measured migration of these cells towards increased concentrations of CCL21. $CD8^+$ T and NK cells from $CB_2^{-/-}$ and WT littermates migrated to CCL21 in a concentration-responsive but similar manner (**Figure 16 A-B**), indicating that the increased infiltration of $CD8^+$ T and NK cells seen in the tumors of $CB_2^{-/-}$ mice was not a direct effect of CB_2 deletion in these cell types.

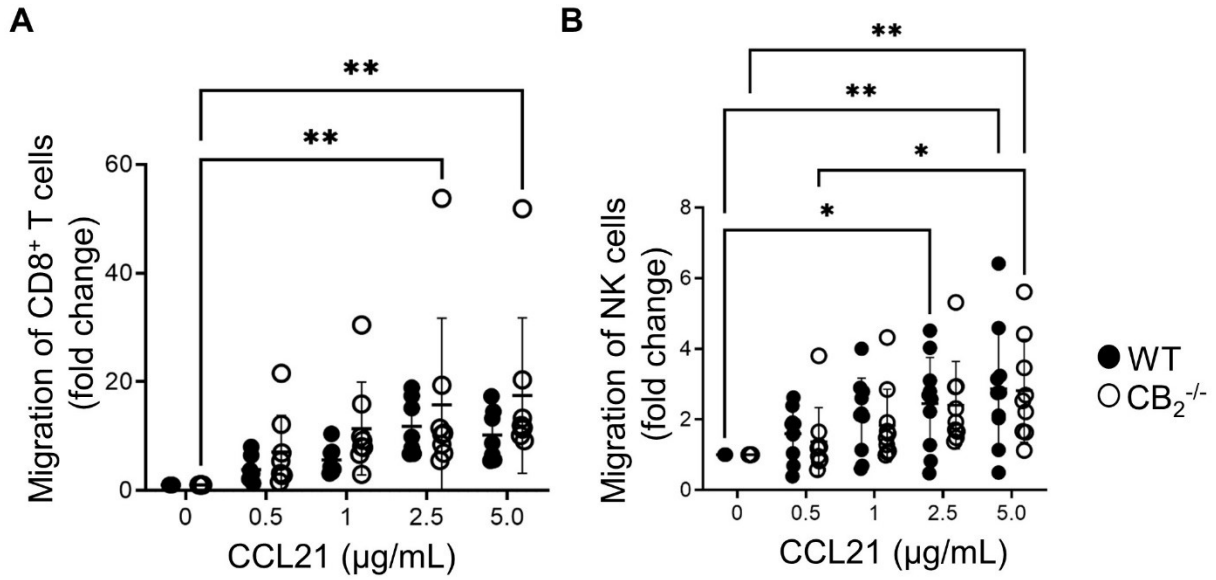

Figure 16. *Migration of CD8⁺ T and NK cells towards CCL21.*

(A-B) Graphs show migration of CD8⁺ T and NK cells isolated from the spleens of tumor-bearing $CB_2^{-/-}$ and WT mice towards increased concentrations of CCL21 (µg/mL). Data are presented as mean values ±SD from three pooled independent experiments. n=7-10. *p<.05; **p<.01, analyzed by two-way ANOVA, Tukey's multiple comparisons test **(A-B)**. *WT*, wild type.

3.6 The CB_2-free TME shows increased expression of immune checkpoint proteins

We next measured surface expression of various immune checkpoint proteins on tumor-infiltrated immune cells. We identified that tumor-infiltrated CD8⁺ T cells of $CB_2^{-/-}$ mice had a higher expression of PD-1 than those of WT mice (**Figure 17 A**), whereas PD-1 expression on NK cells did not differ between $CB_2^{-/-}$ knockout and WT mice (**Figure 17 B**). Furthermore, there was an increased expression of PD-L1 on tumor-infiltrated myeloid cells (macrophages and DCs) in $CB_2^{-/-}$ vs. WT mice (**Figure 17 C**). Our dual ISH-IF analysis on KP tumors demonstrated that about 40% of PD-1⁺ and PD-L1⁺ cells expressed CB_2 mRNA (**Figure 17 D**). In human lung cancer, approximately 20% of PD-1⁺ and PD-L1⁺ cells co-localized with CB_2 mRNA (**Figure 17 E**). We, therefore, hypothesized that a TME deficient in CB_2 would favor an outcome in immune-based therapeutic strategies, such as immune checkpoint blockade.

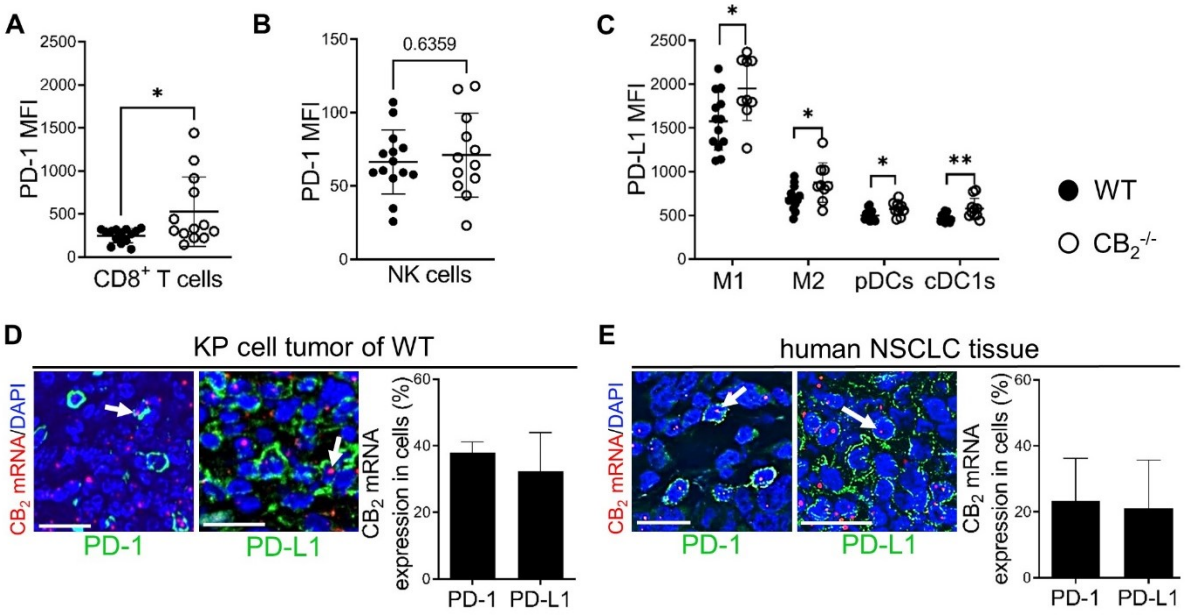

Figure 17. *PD-1 and PD-L1 expression on immune cells of the TME.*

(A-B) Flow cytometric analysis of PD-1 on tumor-infiltrated $CD8^+$ T and NK cells is shown. Data are presented as mean values ±SD from two pooled independent experiments. n=13-14. **(C)** MFI of PD-L1 on tumor-infiltrated myeloid cells. Data are presented as mean values ±SD from two pooled independent experiments. n=10-13 **(D)** Representative image of ISH-IF staining of KP cell tumors. Arrows point at positively stained PD-1/PD-L1 cells co-localizing with CB_2 mRNA. Data show mean values +SD. n=3 (sections from three different tumors, 30-150 cells counted per section). **(E)** ISH-IF staining of human NSCLC tissue sections. The graph shows the percentage of $PD\text{-}1^+/PD\text{-}L1^+$ stained cells co-localizing with CB_2 mRNA. Data demonstrate mean values +SD. n=3 (for quantification, tumor sections from three different patients with NSCLC were used, 30-150 cells counted per section). Arrows point at co-localization of CB_2 mRNA with $PD\text{-}1^+/PD\text{-}L1^+$ cells. Calibration bars = 20 µm. *p<.05; **p<.01, analyzed by unpaired student`s *t*-test **(A-B)**, multiple *t*-tests **(C)**. *NK*, natural killer cells; *MFI*, median fluorescence intensity; *PD-1*, programmed death-1; *PD-L1*, programmed death-ligand 1; *M1*, M1 macrophages; *M2*, M2 macrophages, *pDCs*, plasmacytoid dendritic cells; *cDC1*, type 1 conventional dendritic cells, *ISH-IF*, in situ hybridization and immunofluorescence; *WT*, wild type; *NSCLC*, non-small cell lung cancer. This figure has been adapted from (197).

Apart from the PD-1/PD-L1 axis, we observed no significant differences in the expression of other immune checkpoint proteins like TIGIT, CTLA-4, TIM-3, and LAG-3 on tumor-infiltrated $CD8^+$ T cells between $CB_2^{-/-}$ and WT mice (**Figure 18 A-D**). Only TIGIT demonstrated higher expression on NK cells, but did not reach statistical significance (p=0.06) (**Figure 18 E**), whereas other checkpoint proteins on NK cells from $CB_2^{-/-}$ mice were, similar to $CD8^+$ T cells, not different to WT mice (**Figure 18 F-H**).

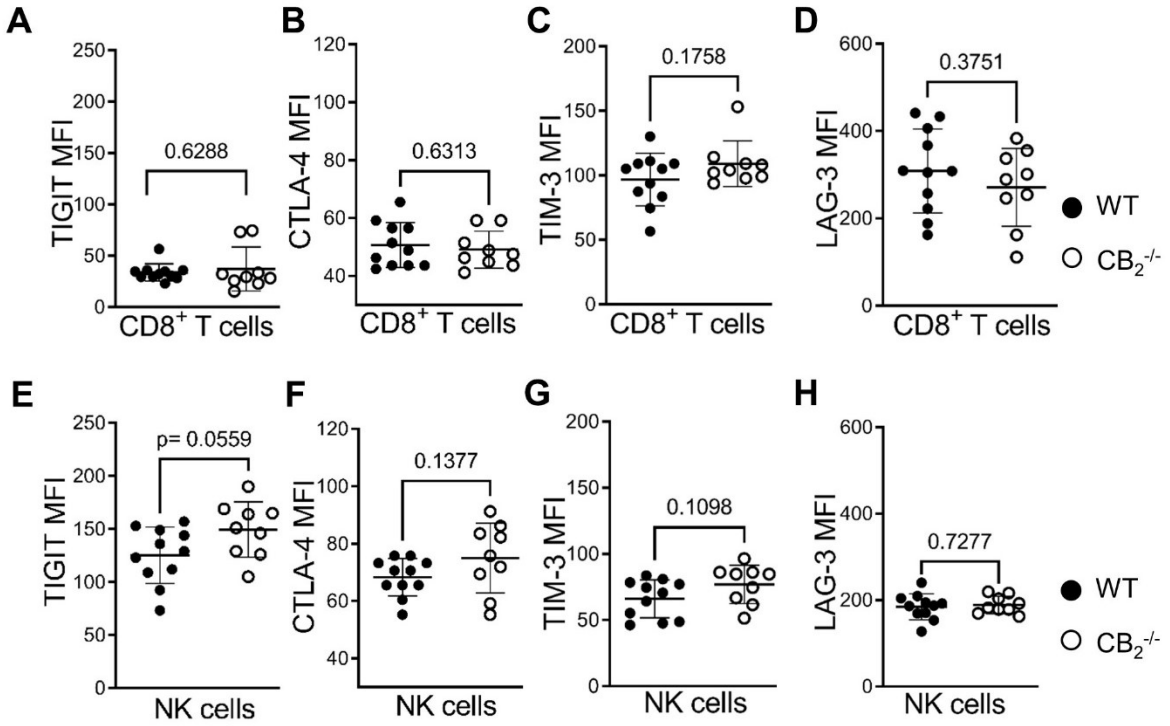

Figure 18. *Expression of immune checkpoint proteins on tumor-infiltrated CD8⁺ T and NK cells.*

(A-H) Flow cytometric analysis demonstrate MFIs of immune checkpoint proteins on tumor-infiltrated CD8⁺ T **(A-D)** and NKp46⁺ NK **(E-H)** cells of $CB_2^{-/-}$ and WT mice. Data demonstrate mean values ±SD from two pooled independent experiments. n=9-14, analyzed by unpaired student`s *t*-test. *MFI*, median fluorescence intensity; *TIGIT*, T cell immunoglobulin and ITIM domain; *CTLA-4*, cytotoxic T-lymphocyte antigen-4; *TIM-3*, T cell immunoglobulin and mucin domain-containing protein-3; *LAG-3*, lymphocyte activation gene-3; *NK*, natural killer cells; *WT*, wild type. This figure has been adapted from (197).

3.7 A TME devoid of CB_2 reveals improved responsiveness to anti-PD-1 therapy

To investigate whether $CB_2^{-/-}$ knockout mice may respond better to ICI therapy than WT mice, we treated the mice with anti-PD-1 antibodies to enhance activity in immune cells (**Figure 19 A**). Indeed, the responsiveness to PD-1 antibody treatment was amplified in the absence of CB_2 on host cells, leading to a significant reduction of tumor growth in $CB_2^{-/-}$ vs. WT mice (**Figure 19 B-C**). WT mice only showed a slight and non-significant decrease in tumor weight (6.6% ± 9.7; WT+ isotype control vs. WT+ anti-PD-1) and volume (18.7% ± 8.2; WT+ isotype control vs. WT+ anti-PD-1). In contrast, tumor weight (45.2% ± 5.0) and volume (41.5% ± 6.9) were significantly decreased in $CB_2^{-/-}$ mice treated with anti-PD-1 antibodies in comparison to isotype control-treated $CB_2^{-/-}$ mice (**Figure 19 D-E**). Regarding changes in the immune cell populations of the TME, anti-PD-1 therapy resulted in a further increase in tumor-infiltrated CD3⁺ T, CD8⁺ T and NK cells, and a higher percentage of CD8⁺ effector T cells in tumors of

$CB_2^{-/-}$ (**Figure 19 J-M**) vs. WT mice (**Figure 19 F-I**), implying that the deletion of CB_2 within the TME strongly favored an improved response to anti-PD-1 therapy which led to a significant reduction of tumor burden in the $CB_2^{-/-}$ vs. WT mice (**Figure 20**).

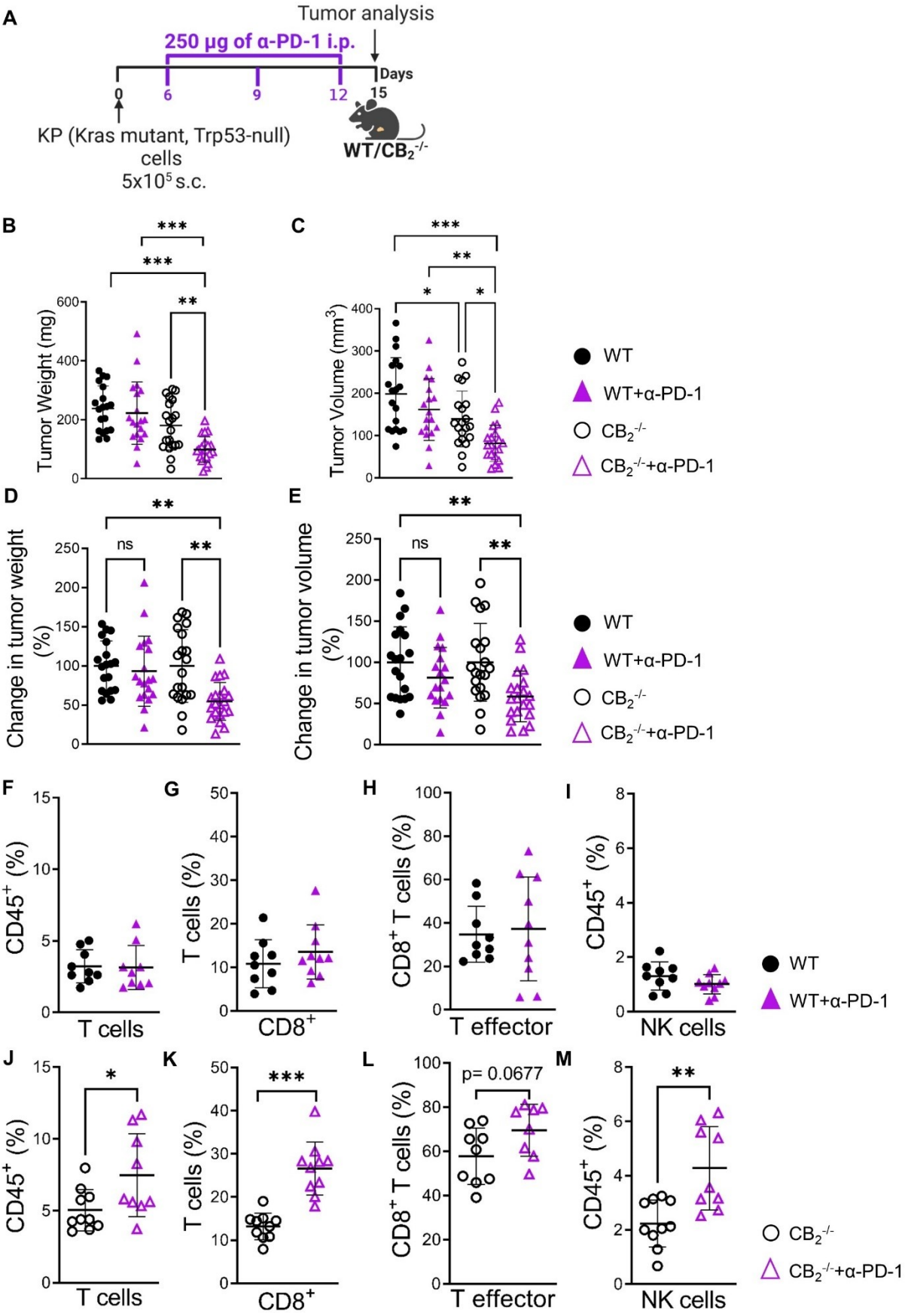

Figure 19. *CB_2 knockout mice respond to anti-PD-1 treatment more favorably than WT mice.*

(A) Experimental scheme: $5x10^5$ KP (Kras mutant, Trp53-null) lung adenocarcinoma cells were subcutaneously (s.c.) injected into flanks of $CB_2^{-/-}$ mice and WT littermates on day 0. Mice were treated with 250 µg of anti-PD-1 (α-PD-1) antibody (or isotype control) on days 6, 9, and 12. **(B-C)** On day 15, both tumor weight and volume were measured *ex vivo,* and tumors were collected for analysis. Data indicate mean values ± SD from two pooled independent experiments. n=19-21. **(D-E)** The graphs demonstrate the percentage changes in tumor weight and volume. To compare treatments, WT and $CB_2^{-/-}$ groups were set at 100%. Data indicate mean values ± SD from two pooled independent experiments. n=19-21. **(F-M)** Graphs demonstrate percentages of tumor-infiltrated immune cells in $CB_2^{-/-}$ and WT mice treated with α-PD-1 or isotype control. Data demonstrate mean values ±SD. One representative experiment is shown. n≥8. *p<.05; **p<.01; ***p<.001, analyzed by one-way ANOVA, Tukey's multiple comparisons test **(B-E)**, unpaired student`s *t*-test **(F-M)**. *WT*, wild type; ns, not significant; *NK*, natural killer cells. This figure has been adapted from (197).

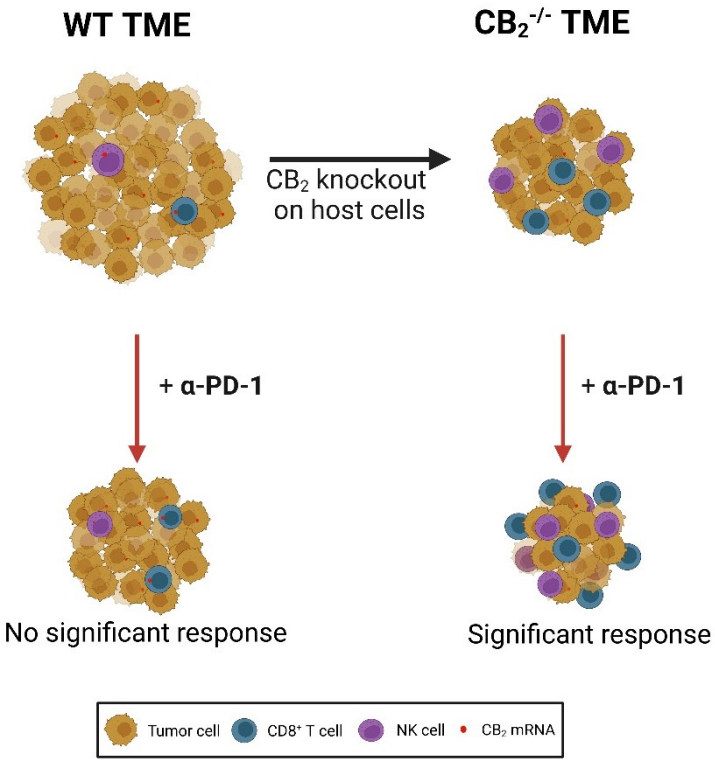

Figure 20. *CB_2 in TME cells provides a pro-tumorigenic microenvironment by reducing cytotoxic activity of lymphocytes in a mouse model of NSCLC.*

Knockout of CB_2 on host cells leads to tumor growth reduction, increased infiltration and higher tumoricidal activity of $CD8^+$ T and NK cells *in situ*. The response to anti-PD-1 antibody (α-PD-1) treatment was better in $CB_2^{-/-}$ knockout than WT mice, resulting in smaller tumors. The therapy further increased infiltration of $CD8^+$ T and NK cells in the TME of $CB_2^{-/-}$ mice. *TME,* tumor microenvironment; *NSCLC*, non-small cell lung cancer. This figure has been adapted from (197).

4 Discussion

The concept that tumor cells and cells of the immune system are present in a shared microenvironment is not new. In 1863, Rudolf Virchow, a German pathologist noticed white blood cells in neoplastic tissues and hypothesized that there could be a link between chronic inflammation and cancer (211; 212). However, five decades later, a renowned biologist, Paul Ehrlich, postulated that the immune system could combat cancer growth (213). These opposing perceptions already indicated that the immune system is a double-edged sword in cancer. On the one hand, inflammation can promote oncogenesis, and on the other hand, the immune system is a powerful tool of the body to fight cancer when appropriately regulated (214). Since then, significant progress has been made in our understanding about the role of the immune system in controling tumor development through shaping the tumor microenvironment (TME). Accordingly, new approaches in the therapy of cancer, such as immune checkpoint inhibitor therapy, have been introduced, and have improved the survival rate of cancer patients. However, a low response rate and resistance to immunotherapy are still an obstacle, indicating that novel targets need to be found in immune cells of the TME to overcome these challenges.

The classical CB receptors, CB_1 and CB_2, constitute a main part of the ECS (154; 155). Since the discovery of CB receptors in the early 1990s, a number of studies identified the expression sites of these receptors as well as their (patho)physiological roles. CB receptors are abundantly present in cells of the immune system, with CB_2 being expressed at much higher levels than CB_1 (154, 156; 163; 164). This suggests that CB receptors could have an important role in regulating the immune system (161; 163). Moreover, CB_1 and CB_2 were found to be over-expressed in cancers of the skin (215) and breast (216), and also in NSCLC (188). Hence, CB receptors could be demonstrated to control cancer growth (194; 195; 215–217). However, there is no universal pro- or anti-tumorigenic role of CB receptors across cancer types, suggesting that their role in tumor development depends on the tumor entity and their influence on the TME or vice versa.

Therefore, the purpose of this thesis was to elucidate the role of CB receptors in host cells of the TME and how TME-derived CB receptors affect the immune cell profile, tumor burden, and response to anti-PD-1 blocking therapy in a NSCLC model.

The TME is composed of various cellular and non-cellular components (10). Among the numerous cell types, cytotoxic lymphocytes are vital members of tumor-fighting cells. In our study, we used ISH RNAscope® in combination with IF to identify and quantify gene expression

of CB receptors in murine and human lung cancer tissues. The ISH probes against CB_1 and CB_2 were all checked in the respective knockout mouse indicating a clear evidence for the specificity of the probes (162). We demonstrated that in murine and human lung cancer tissues, tumor cells as well as cells of the TME, like $CD8^+$ T cells, NK cells, and macrophages express higher levels of CB_2 than CB_1. Dual ISH-IF analysis of murine tumors revealed that around 20-40% of tumor-infiltrated immune cells and approximately 25% of tumor cells expressed CB_2 transcripts. These results were the basis of our hypothesis that CB_2 might have TME cell-mediated and/or possible direct effects on the growth of tumor cells. To identify the influence of CB_2-expressing TME cells on tumor growth, we used a s.c. lung cancer model in mice deficient in the *Cnr1* or the *Cnr2* gene (encoding CB_1 or CB_2 protein, respectively). We could report that mice lacking CB_1 had no change in tumor growth vs. WTs, while $CB_2^{-/-}$ knockout mice demonstrated a significant tumor reduction in comparison to WT mice. These findings indicate that the tumor reduction was mediated via a TME free of CB_2 expression. It also means that presence of CB_2 in the TME favors tumor growth.

Moreover, pharmacological inhibition of CB receptors using CB_1 and CB_2 antagonists showed analogous findings, supporting the fact that only deletion of CB_2, but not of CB_1, caused reduction of tumor burden in the NSCLC model. In addition, we hypothesized a potential direct role of tumor cell-derived CB_2 on tumor growth. Several studies have reported a direct role of CB_1 and CB_2 receptors located in tumor cells in reducing tumor growth of cancers, such as skin cancer (215), mantle cell lymphoma (218), and glioma (219). Using pharmacological activation or inhibition of the CB_2 receptor in $CB_2^{-/-}$ knockout mice (only KP tumor cells expressing CB_2 were targeted here), we demonstrated that CB_2 in tumor cells played no role in the reduction of tumor growth, signifying that only CB_2 expressed on TME host cells influenced tumor growth.

CB_2 is widely expressed in the cells of the immune system, where it influences either anti- or pro-inflammatory cellular functions depending on the presence of stimuli and the nature of the TME (160). Since we identified a widespread expression of CB_2 in tumor-infiltrated immune cells of the TME by ISH, we characterized the profile of tumor-infiltrated immune cells by identifying and quantifying lymphoid and myeloid immune cells using flow cytometry. The absence of CB_2 within the TME resulted in an alteration of the immune landscape and led to an anti-tumorigenic immune cell profile. We detected enhanced infiltration of cytotoxic lymphocytes, mostly of cytotoxic $CD8^+$ T and NK cells, into tumors of $CB_2^{-/-}$ knockout vs. WT mice. A more focused investigation of these cells demonstrated that tumor-infiltrated $CD8^+$ T and NK cells of mice deficient in CB_2 had an increased cytotoxic activity. These data agree

with several studies demonstrating that enhanced infiltration of cytotoxic lymphocytes into the TME is correlated with a good prognosis (220–222). In NSCLC, infiltration and activity of $CD8^+$ T and NK cells may be restricted: NK cells have been demonstrated to infiltrate NSCLC tissues at reduced numbers and they are more localized in normal lung than cancerous tissues (223). Additionally, NK cells may be dysfunctional and less proliferative in lung cancer and they can overexpress inhibitory receptors that compromise their tumor-fighting ability (224; 225). Furthermore, it was observed that within NSCLC tissues, cytotoxic T cells are reduced in their number, and they show low IFN-γ expression (226; 227). As a consequence, the CB_2-deficient TME reversed the reduced infiltration of $CD8^+$ T and NK cells in our lung cancer model and improved activity of these cells, thus most likely contributing to a reduction in tumor growth.

Immune cells recruited to the tumor site via the actions of chemokines and their specific receptors have been broadly connected to tumor development and metastasis (228). In our study, we observed that tumors of $CB_2^{-/-}$ knockout mice displayed an increased concentration of CCL21 in the TME, along with reduced expression of its receptor, CCR7, on tumor-infiltrated $CD8^+$ T and NK cells. CCR7 is usually expressed at low levels on activated T cells (60), supporting our findings that tumor-infiltrated $CD8^+$ T cells of $CB_2^{-/-}$ knockout mice were active. Reduced expression of CCR7 occurs due to internalization of the receptor upon binding to its ligands, CCL19 and CCL21 (66). In lung cancer, CCL21 can control tumor growth either in a lymphocyte dependent (229) or independent manner (230–232). For instance, Sharma et al. demonstrated that intratumoral administration of CCL21 into tumor-bearing mice resulted in tumor reduction and increased infiltration of $CD4^+$, $CD8^+$ T cells, and additionally to a higher level of Th_1 cytokines at the tumor site (229). These findings are concordant with our results showing that CCL21 chemoattracts $CD8^+$ T and NK cells of $CB_2^{-/-}$ knockout and WT mice at a similar rate. However, since we failed to see differences in CCL21-induced migration of $CD8^+$ T and NK cells between $CB_2^{-/-}$ knockout and WT mice, the rise in CCL21 in the tumors of $CB_2^{-/-}$ knockout mice could be unrelated to the tumor growth reduction, and other mechanisms are responsible for our observations. Further studies are required to identify mechanisms that resulted in the increase of CCL21 in endothelial cells of the TME of mice lacking CB_2.

Immune checkpoint inhibitors have been shown to prolong survival of patients with various cancers, including skin and lung cancer (233; 234). The PD-1/PD-L1 axis is the most important immune checkpoint target of all checkpoints as it has been demonstrated to be an effective target in the treatment of several types of cancer (233–235). Earlier studies indicated that one of the important prerequisites for ICIs to work is an adequate infiltration of cytotoxic lymphocytes, including $CD8^+$ T cells, at the tumor sites (236; 237). Of note, our study revealed

that $CB_2^{-/-}$ knockout tumor-bearing mice responded significantly better than WT mice to anti-PD-1 therapy (as evidenced by the substantial reduction in tumor burden). We also observed an increase in PD-1 expression on $CD8^+$ T cells isolated from tumors of $CB_2^{-/-}$ knockout mice. It has been shown that PD-1^+ $CD8^+$ T cells reflect the functional avidity and anti-tumor reactivity of $CD8^+$ T cells and their presence in the TME also predict response rate and survival in patients with NSCLC treated with anti-PD-1 (238–240). Additionally, we found increased PD-L1 expression in tumor-infiltrating myeloid cells in $CB_2^{-/-}$ knockout mice. This is another key finding suggesting that the tumor may respond favorably to ICI therapy, including an anti-PD-1 therapy (21; 241; 242). Increased levels of PD-L1 are usually complemented by high levels of T cells within the TME (reviewed in (243), which was also the case in tumors of $CB_2^{-/-}$ knockout mice. Consequently, identification of the PD-L1 expression rate in cancer tissues is considered the most direct method for predicting the response rate to PD-1/PD-L1 inhibitors (243). While cytotoxic $CD8^+$ T cells are the most important focus for improving immune checkpoint blockade treatments, other immune cells such as NK cells could be also an important contributor to the efficacy of checkpoint inhibitors (reviewed in (244)). It has been demonstrated that intratumoral NK cells support the response to immunotherapies targeting the PD-1/PD-L1 axis (245; 246). Furthermore, high numbers of intratumoral NK cells have been correlated with a good prognosis and a positive response to the therapy of breast cancer (247–249), melanoma (250–252), gastrointestinal cancer (253–255), prostate cancer (256), neuroblastoma (257), and head and neck cancer (258). Recent research has shown that high NK cell counts correlate with a favorable response to anti-PD-1 treatment, and with the overall survival of patients with melanoma or metastatic melanoma (222; 259). Zhang et al. demonstrated that the clinical benefits of PD-L1 and TIGIT-based immunotherapies were enhanced by the presence of NK cells because they increased anti-tumor functions of $CD8^+$ T cells and/or reduced their exhaustion (260). The TME of $CB_2^{-/-}$ knockout mice showed significantly higher infiltration of NK cells than the TME of WT mice. The presence of NK cells in tumors, hence, may increase the susceptibility to immunotherapy with anti-PD-1. To further determine the susceptibility to checkpoint blockade, we measured other immune checkpoint proteins that dampen proliferation and tumoricidal activity of T and NK cells, such as CTLA-4, TIM-3, TIGIT, and LAG-3 (94; 261–264). There were no significant differences in the expression rates of these proteins between $CB_2^{-/-}$ knockout and WT mice, except for an increased expression of TIGIT on NK cells. Our results, therefore, demonstrated that tumor-infiltrated $CD8^+$ T and NK cells of $CB_2^{-/-}$ knockout mice were in an active, functional, and non-exhausted state (high levels of IFN-γ and PD-1 on $CD8^+$ T cells, and of CD107a on NK cells).

Anti-PD-1/PDL1 therapy has been shown to improve the immune cell composition and restore the effector activity of $CD8^+$ T cells to kill tumor cells (265). In addition, NK cells and other cytotoxic lymphocytes positively respond to immunotherapy (reviewed in (266)). Lee et al. found that melanoma patients who responded well to anti-PD-1 therapy demonstrated enhanced frequency of intratumoral and peritumoral NK cells (259). Hsu et al. similarly found that the effect of anti-PD-1/PD-L1 therapy can be mediated by T cells and additionally by NK cells (245). Our results show that the anti-PD-1 blocking therapy further enhanced the infiltration of $CD8^+$ T and NK cells in the TME of $CB_2^{-/-}$ knockout vs. WT mice. This supports the notion that an effective anti-PD-1 therapy is intrinsically connected with the presence of cytotoxic lymphocytes within the TME. It is worth to mention that tumor-infiltrated NK cells of $CB_2^{-/-}$ knockout and WT mice showed no difference in PD-1 expression, and that the expression of PD-1 on NK cells was lower than on $CD8^+$ T cells. This raises a question whether antibodies against PD-1 can have a direct effect on NK cells, as the ICI may have indirectly modulated anti-tumorigenic NK cell functions through the interaction with other immune cells of the TME, as previously described (267; 268). Liu et al. could show that PD-1 acts as a negative regulator of NK cells in digestive cancers including esophageal, liver, colorectal, gastric and biliary cancer. Interestingly, blockade of the PD-1/PD-L1 axis distinctly enhanced capacity of NK cells to degranulate, release cytokines and resist to apoptosis *in vitro.* It also reduced the growth of xenografts in nude mice (269), indicating that PD-1 blockade may be an effective approach in NK cell-associated tumor immunotherapy. During the preparation of our manuscript, another study described that THC and cannabinoid drugs suppressed the therapeutic effect of anti-PD-1 blockade (210), reconfirming our study findings. In addition, a recent retrospective study observed a reduced response rate to nivolumab when used with cannabis in patients with NSCLC, advanced melanoma, and renal clear cell carcinoma (270). With our findings, we demonstrate a possible mechanism for a suppressed immune response, which involves CB_2, $CD8^+$ T and NK cells. Further experiments to verify the role of $CD8^+$ T and NK cells in tumor reduction would include depletion of both cell types in tumor-bearing $CB_2^{-/-}$ knockout and WT mice as both cells play an important role in controling tumor growth in mice lacking CB_2.

Conclusion

Our data show that the presence of the CB_2 receptor in the TME of NSCLC tumors suppresses the activity of cytotoxic lymphocytes, particularly of $CD8^+$ T and NK cells, hence endorsing tumor growth. We failed to observe a role for TME-derived CB_1 in our model of NSCLC. Knockout of CB_2 in the TME removes the immunosuppressive break causing tumors to be more responsive to PD-1 blockade therapy. The findings also suggest that the consumption of cannabis or cannabinoid-based medicine during immune checkpoint therapy may result in a

reduced treatment response. Overall, the CB_2 receptor maybe an interesting additional target for ICI therapy.

5 Bibliography

1. Sung H, Ferlay J, Siegel RL, Laversanne M, Soerjomataram I, Jemal A, Bray F. Global Cancer Statistics 2020: GLOBOCAN Estimates of Incidence and Mortality Worldwide for 36 Cancers in 185 Countries. CA Cancer J Clin. 2021;71(3):209-249. doi:10.3322/caac.21660

2. Govindan R, Page N, Morgensztern D, Read W, Tierney R, Vlahiotis A, Spitznagel EL, Piccirillo J. Changing epidemiology of small-cell lung cancer in the United States over the last 30 years: Analysis of the surveillance, epidemiologic, and end results database. J Clin Oncol. 2006;24(28):4539-4544. doi:10.1200/JCO.2005.04.4859

3. Travis WD, Brambilla E, Riely GJ. New pathologic classification of lung cancer: Relevance for clinical practice and clinical trials. J Clin Oncol. 2013;31(8):992-1001. doi:10.1200/JCO.2012.46.9270

4. Gridelli C, Rossi A, Carbone DP, Guarize J, Karachaliou N, Mok T, Petrella F, Spaggiari L, Rosell R. Non-small-cell lung cancer. Nat Rev Dis Prim. 2015;1:15009. doi:10.1038/nrdp.2015.9

5. Couraud S, Zalcman G, Milleron B, Morin F, Souquet PJ. Lung cancer in never smokers - a review. Eur J Cancer. 2012;48(9):1299-1311. doi:10.1016/j.ejca.2012.03.007

6. Lee T, Lee B, Choi Y La, Han J, Ahn MJ, Um SW. Non-small cell lung cancer with concomitant EGFR, KRAS, and ALK mutation: Clinicopathologic features of 12 cases. J Pathol Transl Med. 2016;50(3):197-203. doi:10.4132/jptm.2016.03.09

7. Duan Q, Zhang H, Zheng J, Zhang L. Turning Cold into Hot: Firing up the Tumor Microenvironment. Trends in Cancer. 2020;6(7):605-618. doi:10.1016/j.trecan.2020.02.022

8. Busch SE, Hanke ML, Kargl J, Metz HE, MacPherson D, Houghton AM. Lung Cancer Subtypes Generate Unique Immune Responses. J Immunol. 2016;197(11):4493-4503. doi:10.4049/jimmunol.1600576

9. Hanahan D. Hallmarks of Cancer: New Dimensions. Cancer Discov. 2022;12(1):31-46. doi:10.1158/2159-8290.CD-21-1059

10. Balkwill FR, Capasso M, Hagemann T. The tumor microenvironment at a glance. J Cell Sci. 2012;125(23):5591-5596. doi:10.1242/jcs.116392

11. Fernández JP, Luddy KA, Harmon C, O'Farrelly C. Hepatic tumor microenvironments and effects on NK cell phenotype and function. Int J Mol Sci. 2019;20(17):4131. doi:10.3390/ijms20174131

12. Terry S, Buart S, Chouaib S. Hypoxic stress-induced tumor and immune plasticity, suppression, and impact on tumor heterogeneity. Front Immunol. 2017;8:1625. doi:10.3389/fimmu.2017.01625

13. Giese MA, Hind LE, Huttenlocher A. Neutrophil plasticity in the tumor microenvironment. Blood. 2019;133(20):2159-2167. doi:10.1182/blood-2018-11-844548

14. Gonzalez-Gugel E, Saxena M, Bhardwaj N. Modulation of innate immunity in the tumor microenvironment. Cancer Immunol Immunother. 2016;65(10):1261-1268. doi:10.1007/s00262-016-1859-9

15. Davoodzadeh Gholami M, kardar GA, Saeedi Y, Heydari S, Garssen J, Falak R. Exhaustion of T lymphocytes in the tumor microenvironment: Significance and effective mechanisms. Cell Immunol. 2017;322:1-14. doi:10.1016/j.cellimm.2017.10.002

16. Hasmim M, Messai Y, Ziani L, Thiery J, Bouhris JH, Noman MZ, Chouaib S. Critical role of tumor microenvironment in shaping NK cell functions: Implication of hypoxic stress. Front Immunol. 2015;6:482. doi:10.3389/fimmu.2015.00482

17. Chen DS, Mellman I. Elements of cancer immunity and the cancer-immune set point. Nature. 2017;541(7637):321-330. doi:10.1038/nature21349

18. Hegde PS, Chen DS. Top 10 Challenges in Cancer Immunotherapy. Immunity. 2020;52(1):17-35. doi:10.1016/j.immuni.2019.12.011

19. Hegde PS, Karanikas V, Evers S. The where, the when, and the how of immune monitoring for cancer immunotherapies in the era of checkpoint inhibition. Clin Cancer Res. 2016;22(8):1865-1874. doi:10.1158/1078-0432.CCR-15-1507

20. Galon J, Bruni D. Approaches to treat immune hot, altered and cold tumours with combination immunotherapies. Nat Rev Drug Discov. 2019;18(3):197-218. doi:10.1038/s41573-018-0007-y

21. Herbst RS, Soria JC, Kowanetz M, Fine GD, Hamid O, Gordon MS, Sosman JA, McDermott DF, Powderly JD, Gettinger SN, Kohrt HEK, Horn L, Lawrence DP, Rost S,

Leabman M, Xiao Y, Mokatrin A, Koeppen H, Hegde PS, Mellman I, Chen DS, Hodi FS. Predictive correlates of response to the anti-PD-L1 antibody MPDL3280A in cancer patients. Nature. 2014;515(7528):563-567. doi:10.1038/nature14011

22. Iwahori K. Cytotoxic CD8+ Lymphocytes in the Tumor Microenvironment. Adv Experimetal Med Biol. 2020;1224:53-62. doi:10.1007/978-3-030-35723-8_4

23. Maimela NR, Liu S, Zhang Y. Fates of CD8+ T cells in Tumor Microenvironment. Comput Struct Biotechnol J. 2019;17:1-13. doi:10.1016/j.csbj.2018.11.004

24. Zhang N, Bevan MJ. CD8+ T Cells: foot soldiers of the immune system. Immunity. 2011;35(2):161-168. doi:10.1016/j.immuni.2011.07.010

25. Wherry EJ, Ahmed R. Memory CD8 T-Cell differentiation during viral infection. J Virol. 2004;78(11):5535-5545. doi:10.1128/jvi.78.11.5535-5545.2004

26. Kim PS, Ahmed R. Features of responding T cells in cancer and chronic infection. Curr Opin Immunol. 2010;22(2):223-230. doi:10.1016/j.coi.2010.02.005

27. Baitsch L, Fuertes-Marraco SA, Legat A, Meyer C, Speiser DE. The three main stumbling blocks for anticancer T cells. Trends Immunol. 2012;33(7):364-372. doi:10.1016/j.it.2012.02.006

28. Clark WH. Tumour progression and the nature of cancer. Br J Cancer. 1991;64(4):631-644. doi:10.1038/bjc.1991.375

29. Mahmoud SMA, Paish EC, Powe DG, Macmillan RD, Grainge MJ, Lee AHS, Ellis IO, Green AR. Tumor-infiltrating CD8+ lymphocytes predict clinical outcome in breast cancer. J Clin Oncol. 2011;29(15):1949-1955. doi:10.1200/JCO.2010.30.5037

30. Galon J, Costes A, Sanchez-Cabo F, Kirilovsky A, Mlecnik B, Lagorce-Pagès C, Tosolini M, Camus M, Berger A, Wind P, Zinzindohoué F, Bruneval P, Cugnenc PH, Trajanoski Z, Wolf-Herm, Pagès F. Type, density, and location of immune cells within human colorectal tumors predict clinical outcome. Science (80-). 2006;313(5795):1960-1964. doi:10.1126/science.1129139

31. Sato E, Olson SH, Ahn J, Bundy B, Nishikawa H, Qian F, Jungbluth AA, Frosina D, Gnjatic S, Ambrosone C, Kepner J, Odunsi T, Ritter G, Lele S, Chen YT, Ohtani H, Old LJ, Odunsi K. Intraepithelial CD8 tumor-infiltrating lymphocytes and a high CD8 regulatory T cell ratio are associated with favorable prognosis in ovarian cancer. Proc Natl Acad Sci U S A. 2005;102(51):18538-18543.

doi:doi.org/10.1073/pnas.050918210

32. Sharma P, Shen Y, Wen S, Yamada S, Jungbluth AA, Gnjatic S, Bajorin DF, Reuter VE, Herr H, Old LJ, Sato E. CD8 tumor-infiltrating lymphocytes are predictive of survival in muscle-invasive urothelial carcinoma. Proc Natl Acad Sci U S A. 2007;104(10):3967-3972. doi:10.1073/pnas.0611618104

33. Schulze AB, Evers G, Görlich D, Mohr M, Marra A, Hillejan L, Rehkämper J, Schmidt LH, Heitkötter B. Tumor infiltrating T cells influence prognosis in stage I-III non-small cell lung cancer. J Thorac Dis. 2020;12(5):1824-1842. doi:10.21037/jtd-19-3414a

34. Soo RA, Chen Z, Siew R, Teng Y, Tan HL, Iacopetta B, Tai BC, Soong R. Prognostic significance of immune cells in non-small cell lung cancer: meta-analysis. Oncotarget. 2018;9(37):24801-24820. doi:10.18632/oncotarget.24835

35. Al-Shibli KI, Donnem T, Al-Saad S, Persson M, Bremnes RM, Busund LT. Prognostic effect of epithelial and stromal lymphocyte infiltration in non-small cell lung cancer. Clin Cancer Res. 2008;14(16):5220-5227. doi:10.1158/1078-0432.CCR-08-0133

36. Miotto D, Cascio N Lo, Stendardo M, Querzoli P, Pedriali M, De Rosa E, Fabbri LM, Mapp CE, Boschetto P. CD8+ T cells expressing IL-10 are associated with a favourable prognosis in lung cancer. Lung Cancer. 2010;69(3):355-360. doi:10.1016/j.lungcan.2009.12.012

37. Carstens JL, De Sampaio PC, Yang D, Barua S, Wang H, Rao A, Allison JP, Le Bleu VS, Kalluri R. Spatial computation of intratumoral T cells correlates with survival of patients with pancreatic cancer. Nat Commun. 2017;8:15095. doi:10.1038/ncomms15095

38. Seo AN, Lee HJ, Kim EJ, Kim HJ, Jang MH, Lee HE, Kim YJ, Kim JH, Park SY. Tumour-infiltrating CD8+ lymphocytes as an independent predictive factor for pathological complete response to primary systemic therapy in breast cancer. Br J Cancer. 2013;109(10):2705-2713. doi:10.1038/bjc.2013.634

39. Brown JR, Wimberly H, Lannin DR, Nixon C, Rimm DL, Bossuyt V. Multiplexed quantitative analysis of CD3, CD8, and CD20 predicts response to neoadjuvant chemotherapy in breast cancer. Clin Cancer Res. 2014;20(23):5995-6005. doi:10.1158/1078-0432.CCR-14-1622

40. Murakami E, Shionoya T, Komenoi S, Suzuki Y, Sakane F. The value of tumor

infiltrating lymphocytes (TILs) for predicting response to neoadjuvant chemotherapy in breast cancer: a systematic review and meta-analysis. PLoS One. 2014;9(12):e115103. doi:10.1371/journal.pone.0115103

41. Rashidian M, Ingram JR, Dougan M, Dongre A, Whang KA, LeGall C, Cragnolini JJ, Bierie B, Gostissa M, Gorman J, Grotenbreg GM, Bhan A, Weinberg RA, Ploegh HL. Predicting the response to CTLA-4 blockade by longitudinal noninvasive monitoring of CD8 T cells. J Exp Med. 2017;214(8):2243-2255. doi:10.1084/jem.20161950

42. Tumeh PC, Harview CL, Yearley JH, Shintaku IP, Taylor EJM, Robert L, Chmielowski B, Spasic M, Henry G, Ciobanu V, West AN, Carmona M, Kivork C, Seja E, Cherry G, Gutierrez AJ, Grogan TR, Mateus C, Tomasic G, Glaspy JA, Emerson RO, Robins H, Pierce RH, Elashoff DA, Robert C, Ribas A. PD-1 blockade induces responses by inhibiting adaptive immune resistance. Nature. 2014;515(7528):568-571. doi:10.1038/nature13954

43. Chen PL, Roh W, Reuben A, Cooper ZA, Spencer CN, Prieto PA, Miller JP, Bassett RL, Gopalakrishnan V, Wani K, De Macedo MP, Austin-Breneman JL, Jiang H, Chang Q, Reddy SM, Chen WS, Tetzlaff MT, Broaddus RJ, Davies MA, Gershenwald JE, Haydu L, Lazar AJ, Patel SP, Hwu P, Hwu WJ, Diab A, Glitza IC, Woodman SE, Vence LM, Wistuba II, Amaria RN, Kwong LN, Prieto V, Eric Davis R, Ma W, Overwijk WW, Sharpe AH, Hu J, Andrew Futreal P, Blando J, Sharma P, Allison JP, Chin L, Wargo JA. Analysis of immune signatures in longitudinal tumor samples yields insight into biomarkers of response and mechanisms of resistance to immune checkpoint blockade. Cancer Discov. 2016;6(8):827-837. doi:10.1158/2159-8290.CD-15-1545

44. Masopust D, Schenkel JM. The integration of T cell migration, differentiation and function. Nat Rev Immunol. 2013;13(5):309-320. doi:10.1038/nri3442

45. Slaney CY, Kershaw MH, Darcy PK. Trafficking of T cells into tumors. Cancer Res. 2014;74(24):7168-7174. doi:10.1158/0008-5472.CAN-14-2458

46. Anderson KG, Stromnes IM, Greenberg PD. Obstacles Posed by the Tumor Microenvironment to T cell Activity: A Case for Synergistic Therapies. Cancer Cell. 2017;31(3):311-325. doi:10.1016/j.ccell.2017.02.008

47. Buckanovich RJ, Facciabene A, Kim S, Benencia F, Sasaroli D, Balint K, Katsaros D, O'Brien-Jenkins A, Gimotty PA, Coukos G. Endothelin B receptor mediates the endothelial barrier to T cell homing to tumors and disables immune therapy. Nat Med.

2008;14(1):28-36. doi:10.1038/nm1699

48. Musha H, Ohtani H, Mizoi T, Kinouchi M, Nakayama T, Shiiba K, Miyagawa K, Nagura H, Yoshie O, Sasaki I. Selective infiltration of CCR5+CXCR3+ T lymphocytes in human colorectal carcinoma. Int J Cancer. 2005;116(6):949-956. doi:10.1002/ijc.21135

49. Mulligan AM, Raitman I, Feeley L, Pinnaduwage D, Nguyen LT, O'Malley FP, Ohashi PS, Andrulis IL. Tumoral lymphocytic infiltration and expression of the chemokine CXCL10 in breast cancers from the ontario familial breast cancer registry. Clin Cancer Res. 2013;19(2):336-346. doi:10.1158/1078-0432.CCR-11-3314

50. Harlin H, Meng Y, Peterson AC, Zha Y, Tretiakova M, Slingluff C, McKee M, Gajewski TF. Chemokine expression in melanoma metastases associated with CD8+ T-cell recruitment. Cancer Res. 2009;69(7):3077-3085. doi:10.1158/0008-5472.CAN-08-2281

51. Mikucki ME, Fisher DT, Matsuzaki J, Skitzki JJ, Gaulin NB, Muhitch JB, Ku AW, Frelinger JG, Odunsi K, Gajewski TF, Luster AD, Evans SS. Non-redundant requirement for CXCR3 signalling during tumoricidal T-cell trafficking across tumour vascular checkpoints. Nat Commun. 2015;6:7458. doi:10.1038/ncomms8458

52. Wennerberg E, Kremer V, Childs R, Lundqvist A. CXCL10-induced migration of adoptively transferred human natural killer cells toward solid tumors causes regression of tumor growth in vivo. Cancer Immunol Immunother. 2015;64(2):225-235. doi:10.1007/s00262-014-1629-5

53. Kunz M, Toksoy A, Goebeler M, Engelhardt E, Bröcker EB, Gillitzer R. Strong expression of the lymphoattractant C-X-C chemokine Mig is associated with heavy infiltration of T cells in human malignant melanoma. J Pathol. 1999;189(4):552-558. doi:10.1002/(SICI)1096-9896(199912)189:4<552::AID-PATH469>3.0.CO;2-I

54. Hong M, Puaux AL, Huang C, Loumagne L, Tow C, Mackay C, Kato M, Prévost-Blondel A, Avril MF, Nardin A, Abastado JP. Chemotherapy induces intratumoral expression of chemokines in cutaneous melanoma, favoring T-cell infiltration and tumor control. Cancer Res. 2011;71(22):6997-7009. doi:10.1158/0008-5472.CAN-11-1466

55. Guirnalda P, Wood L, Goenka R, Crespo J, Paterson Y. Interferon γ-induced intratumoral expression of CXCL9 alters the local distribution of T cells following

immunotherapy with Listeria monocytogenes. Oncoimmunology. 2013;2(8):e25752. doi:10.4161/onci.25752

56. Groom JR, Luster AD. CXCR3 ligands: Redundant, collaborative and antagonistic functions. Immunol Cell Biol. 2011;89(2):207-215. doi:10.1038/icb.2010.158

57. Matsumura S, Wang B, Kawashima N, Braunstein S, Badura M, Babb JS, Schneider RJ, Formenti SC, Dustin ML, Demaria S. Radiation-induced CXCL16 release by breast cancer cells attracts effector T cells. J Immunol. 2008;181(5):3099-3107. doi:10.4049/jimmunol.181.5.3099

58. Mossanen JC, Kohlhepp M, Wehr A, Krenkel O, Liepelt A, Roeth AA, Möckel D, Heymann F, Lammers T, Gassler N, Hermann J, Jankowski J, Neumann UP, Luedde T, Trautwein C, Tacke F. CXCR6 Inhibits Hepatocarcinogenesis by Promoting Natural Killer T- and CD4+ T-Cell–Dependent Control of Senescence. Gastroenterology. 2019;156(6):1877-1889.e4. doi:10.1053/j.gastro.2019.01.247

59. Wang B, Wang Y, Sun X, Deng G, Huang W, Wu X, Gu Y, Tian Z, Fan Z, Xu Q, Chen H, Sun Y. CXCR6 is required for antitumor efficacy of intratumoral CD8+ T cell. J Immunother Cancer. 2021;9(8):e003100. doi:10.1136/jitc-2021-003100

60. Willimann K, Legler DF, Loetscher M, Roos RS, Delgado MB, Clark-Lewis I, Baggiolini M, Moser B. The chemokine SLC is expressed in T cell areas of lymph nodes and mucosal lymphoid tissues and attracts activated T cells via CCR7. Eur J Immunol. 1998;28(6):2025-2034. doi:10.1002/(SICI)1521-4141(199806)28:06<2025::AID-IMMU2025>3.0.CO;2-C

61. Sallusto F, Lenig D, Förster R, Lipp M, Antonio L. Two subsets of memory T lymphocytes with distinct homing potentials and effector functions. Nature. 1999;401:708-712. doi:doi.org/10.1038/44385

62. Sallusto F, Schaerli P, Loetscher P, Schaniel C, Lenig D, Mackay CR, Qin S, Lanzavecchia A. Rapid and coordinated switch in chemokine receptor expression during dendritic cell maturation. Eur J Immunol. 1998;28(9):2760-2769. doi:10.1002/(SICI)1521-4141(199809)28:09<2760::AID-IMMU2760>3.0.CO;2-N

63. Sozzani S, Allavena P, D'Amico G, Luini W, Bianchi G, Kataura M, Imai T, Yoshie O, Bonecchi R, Mantovani A. Differential regulation of chemokine receptors during dendritic cell maturation: a model for their trafficking properties. J Immunol. 1998;161:1083-1086. http://www.jimmunol.org/content/161/3/1083

64. Gunn MD. Chemokine mediated control of dendritic cell migration and function. Semin Immunol. 2003;15(5):271-276. doi:10.1016/j.smim.2003.08.004

65. Yoshida R, Imai T, Hieshima K, Kusuda J, Baba M, Kitaura M, Nishimura M, Kakizaki M, Nomiyama H, Yoshie O. Molecular cloning of a novel human CC chemokine EBI1-ligand chemokine that is a specific functional ligand for EBI1, CCR7. J Biol Chem. 1997;272(21):13803-13809. doi:10.1074/jbc.272.21.13803

66. Otero C, Groettrup M, Legler DF. Opposite fate of endocytosed CCR7 and its ligands: recycling versus degradation. J Immunol. 2006;177(4):2314-2323. doi:10.4049/jimmunol.177.4.2314

67. Förster R, Andreas Schubel, Dagmar Breitfeld, Kremmer E, Renner-Müller I, Wolf E, Lipp M. CCR7 coordinates the primary immune response by establishing functional microenvironments in secondary lymphoid organs. Cell. 1999;99(1):23-33. doi:10.1016/s0092-8674(00)80059-8

68. Ohl L, Mohaupt M, Czeloth N, Hintzen G, Kiafard Z, Rg Zwirner J, Blankenstein T, Henning G. CCR7 governs skin dendritic cell migration under inflammatory and steady-state conditions. Immunity. 2004;21(2):279-288. doi:10.1016/j.immuni.2004.06.014

69. Xie Q, Ding J, Chen Y. Role of CD8+ T lymphocyte cells: Interplay with stromal cells in tumor microenvironment. Acta Pharm Sin B. 2021;11(6):1365-1378. doi:10.1016/j.apsb.2021.03.027

70. Anderson AC, Joller N, Kuchroo VK. Lag-3, Tim-3, and TIGIT: Co-inhibitory Receptors with Specialized Functions in Immune Regulation. Immunity. 2016;44(5):989-1004. doi:10.1016/j.immuni.2016.05.001

71. Kurachi M. CD8+ T cell exhaustion. Semin Immunopathol. 2019;41(3):327-337. doi:10.1007/s00281-019-00744-5

72. Sakuishi K, Apetoh L, Sullivan JM, Blazar BR, Kuchroo VK, Anderson AC. Targeting Tim-3 and PD-1 pathways to reverse T cell exhaustion and restore anti-tumor immunity. J Exp Med. 2010;207(10):2187-2194. doi:10.1084/jem.20100643

73. Fourcade J, Sun Z, Benallaoua M, Guillaume P, Luescher IF, Sander C, Kirkwood JM, Kuchroo V, Zarour HM. Upregulation of Tim-3 and PD-1 expression is associated with tumor antigen-specific CD8+ T cell dysfunction in melanoma patients. J Exp Med.

2010;207(10):2175-2186. doi:10.1084/jem.20100637

74. He Y, Cao J, Zhao C, Li X, Zhou C, Hirsch FR. TIM-3, a promising target for cancer immunotherapy. Onco Targets Ther. 2018;11:7005-7009. doi:10.2147/OTT.S170385

75. Fife BT, Bluestone JA. Control of peripheral T-cell tolerance and autoimmunity via the CTLA-4 and PD-1 pathways. Immunol Rev. 2008;224(1):166-182. doi:10.1111/j.1600-065X.2008.00662.x

76. Krummel MF, Allison JP. CD28 and CTLA-4 have opposing effects on the response of T cells to stimulation. J Exp Med. 1995;182(2):459-465. doi:10.1084/jem.182.2.459

77. Pérez-García A, Osca G, Bosch-Vizcaya A, Kelleher N, Santos NY, Rodríguez R, González Y, Roncero JM, Coll R, Serrando M, Lloveras N, Tuset E, Gallardo D. Kinetics of the CTLA-4 isoforms expression after T-lymphocyte activation and role of the promoter polymorphisms on CTLA-4 gene transcription. Hum Immunol. 2013;74(9):1219-1224. doi:10.1016/j.humimm.2013.05.012

78. Perkins D, Wang Z, Donovan C, He H, Mark D, Guan G, Wang Y, Walunas T, Bluestone J, Listman J, Finn PW. Regulation of CTLA-4 expression during T cell activation. J Immunol. 1996;156(11):4154-4159. http://www.jimmunol.org/content/156/11/4154

79. Lindsten T, Lee KP, Harris ES, Petryniak B, Craighead N, Reynolds PJ, Lombard DB, Freeman GJ, Nadler LM, Gray GS, Thompson C 6., June CH. Characterization of CTLA-4 structure and expression on human T cells. J Immunol. 1993;151(7):3489-3499. http://www.jimmunol.org/content/151/7/3489

80. Linsley PS, Greene JL, Brady W, Bajorath J, Ledbetter JA, Peach R. Human B7-1 (CD80) and B7-2 (CD86) bind with similar avidities but distinct kinetics to CD28 and CTLA-4 receptors. Immunity. 1994;1(9):793-801. doi:10.1016/s1074-7613(94)80021-9

81. Read S, Malmström V, Powrie F. Cytotoxic T lymphocyte-associated antigen 4 plays an essential role in the function of CD25(+) CD4(+) regulatory cells that control intestinal inflammation. J Exp Med. 2000;192(2):295-302. doi:10.1084/jem.192.2.295

82. Takahashi T, Tagami T, Yamazaki S, Uede T, Shimizu J, Sakaguchi N, Mak TW, Sakaguchi S. Immunologic self-tolerance maintained by CD25(+) CD4(+) regulatory T Cells constitutively expressing cytotoxic T lymphocyte-associated antigen 4. J Exp Med. 2000;192(2):303-309. doi:10.1084/jem.192.2.303

83. Oyewole-Said D, Konduri V, Vazquez-Perez J, Weldon SA, Levitt JM, Decker WK. Beyond T-Cells: Functional Characterization of CTLA-4 Expression in Immune and Non-Immune Cell Types. Front Immunol. 2020;11:608024. doi:10.3389/fimmu.2020.608024

84. Okazaki T, Chikuma S, Iwai Y, Fagarasan S, Honjo T. A rheostat for immune responses: The unique properties of PD-1 and their advantages for clinical application. Nat Immunol. 2013;14(12):1212-1218. doi:10.1038/ni.2762

85. Xiao Y, Yu S, Zhu B, Bedoret D, Bu X, Duke-Cohan LMF, Umetsu DT, Sharpe AH, DeKruyff RH, Freeman GJ. RGMb is a novel binding partner for PD-l2 and its engagement with PD-l2 promotes respiratory tolerance. J Exp Med. 2014;211(5):943-959. doi:10.1084/jem.20130790

86. Patel SP, Kurzrock R. PD-L1 expression as a predictive biomarker in cancer immunotherapy. Mol Cancer Ther. 2015;14(4):847-856. doi:10.1158/1535-7163.MCT-14-0983

87. Yearley JH, Gibson C, Yu N, Moon C, Murphy E, Juco J, Lunceford J, Cheng J, Chow LQM, Seiwert TY, Handa M, Tomassini JE, McClanahan T. PD-L2 expression in human tumors: Relevance to anti-PD-1 therapy in cancer. Clin Cancer Res. 2017;23(12):3158-3167. doi:10.1158/1078-0432.CCR-16-1761

88. Dominguez-Gutierrez PR, Kwenda EP, Donelan W, Miranda M, Doty A, O'Malley P, Crispen PL, Kusmartsev S. Detection of PD-L1–Expressing Myeloid Cell Clusters in the Hyaluronan-Enriched Stroma in Tumor Tissue and Tumor-Draining Lymph Nodes. J Immunol. 2022;208(12):2829-2836. doi:10.4049/jimmunol.2100026

89. Yu X, Harden K, Gonzalez LC, Francesco M, Chiang E, Irving B, Tom I, Ivelja S, Refino CJ, Clark H, Eaton D, Grogan JL. The surface protein TIGIT suppresses T cell activation by promoting the generation of mature immunoregulatory dendritic cells. Nat Immunol. 2009;10(1):48-57. doi:10.1038/ni.1674

90. Stanietsky N, Simic H, Arapovic J, Toporik A, Levy O, Novik A, Levine Z, Beiman M, Dassa L, Achdout H, Stern-Ginossar N, Tsukerman P, Jonjic S, Mandelboim O. The interaction of TIGIT with PVR and PVRL2 inhibits human NK cell cytotoxicity. Proc Natl Acad Sci U S A. 2009;106(42):17858-17863. doi:10.1073/pnas.0903474106

91. Boles KS, Vermi W, Facchetti F, Fuchs A, Wilson TJ, Diacovo TG, Cella M, Colonna M. A novel molecular interaction for the adhesion of follicular CD4 T cells to follicular

DC. Eur J Immunol. 2009;39(3):695-703. doi:10.1002/eji.200839116

92. Joller N, Hafler JP, Brynedal B, Kassam N, Spoerl S, Levin SD, Sharpe AH, Kuchroo VK. Cutting edge: TIGIT has T cell-intrinsic inhibitory functions. J Immunol. 2011;186(3):1338-1342. doi:10.4049/jimmunol.1003081

93. Wu H, Chen Y, Liu H, Xu LL, Teuscher P, Wang S, Lu S, Dent AL. Follicular regulatory T cells repress cytokine production by follicular helper T cells and optimize IgG responses in mice. Eur J Immunol. 2016;46(5):1152-1161. doi:10.1002/eji.201546094

94. Chauvin JM, Pagliano O, Fourcade J, Sun Z, Wang H, Sander C, Kirkwood JM, Chen THT, Maurer M, Korman AJ, Zarour HM. TIGIT and PD-1 impair tumor antigen-specific CD8+ T cells in melanoma patients. J Clin Invest. 2015;125(5):2046-2058. doi:10.1172/JCI80445

95. Fuchs A, Cella M, Giurisato E, Shaw AS, Colonna M. Cutting edge: CD96 (tactile) promotes NK cell-target cell adhesion by interacting with the poliovirus receptor (CD155). J Immunol. 2004;172(7):3994-3998. doi:10.4049/jimmunol.172.7.3994

96. Lozano E, Dominguez-Villar M, Kuchroo V, Hafler DA. The TIGIT/CD226 axis regulates human T cell function. J Immunol. 2012;188(8):3869-3875. doi:10.4049/jimmunol.1103627

97. Pende D, Bottino C, Castriconi R, Cantoni C, Marcenaro S, Rivera P, Spaggiari GM, Dondero A, Carnemolla B, Reymond N, Mingari MC, Lopez M, Moretta L, Moretta A. PVR (CD155) and Nectin-2 (CD112) as ligands of the human DNAM-1 (CD226) activating receptor: Involvement in tumor cell lysis. Mol Immunol. 2005;42(4):463-469. doi:10.1016/j.molimm.2004.07.028

98. Reches A, Ophir Y, Stein N, Kol I, Isaacson B, Charpak Amikam Y, Elnekave A, Tsukerman P, Kucan Brlic P, Lenac T, Seliger B, Jonjic S, Mandelboim O. Nectin4 is a novel TIGIT ligand which combines checkpoint inhibition and tumor specificity. J Immunother Cancer. 2020;8(1):e000266. doi:10.1136/jitc-2019-000266

99. Laurent Monney, Catherine A. Sabatos, Jason L. Gaglia, Akemi Ryu, Hanspeter Waldner, Tatyana Chernova, Stephen Manning, Edward A. Greenfield, Anthony J. Coyle, Raymond A. Sobelß, Gordon J. Freeman, Vijay K. Kuchroo. Th1-specific cell surface protein Tim-3 regulates macrophage activation and severity of an autoimmune disease. Nature. 2002;415(6871):536-540. doi:10.1038/415536a

100. Das M, Zhu C, Kuchroo VK. Tim-3 and its role in regulating anti-tumor immunity. Immunol Rev. 2017;276(1):97-111. doi:10.1111/imr.12520

101. Zhu C, Anderson AC, Schubart A, Xiong H, Imitola J, Khoury SJ, Zheng XX, Strom TB, Kuchroo VK. The Tim-3 ligand galectin-9 negatively regulates T helper type 1 immunity. Nat Immunol. 2005;6(12):1245-1252. doi:10.1038/ni1271

102. DeKruyff RH, Bu X, Ballesteros A, Santiago C, Chim YLE, Lee HH, Karisola P, Pichavant M, Kaplan GG, Umetsu DT, Freeman GJ, Casasnovas JM. T cell/transmembrane, Ig, and mucin-3 allelic variants differentially recognize phosphatidylserine and mediate phagocytosis of apoptotic cells. J Immunol. 2010;184(4):1918-1930. doi:10.4049/jimmunol.0903059

103. Chiba S, Baghdadi M, Akiba H, Yoshiyama H, Kinoshita I, Dosaka-Akita H, Fujioka Y, Ohba Y, Gorman J V., Colgan JD, Hirashima M, Uede T, Takaoka A, Yagita H, Jinushi M. Tumor-infiltrating DCs suppress nucleic acid-mediated innate immune responses through interactions between the receptor TIM-3 and the alarmin HMGB1. Nat Immunol. 2012;13(9):832-842. doi:10.1038/ni.2376

104. Huang YH, Zhu C, Kondo Y, Anderson AC, Gandhi A, Russell A, Dougan SK, Petersen BS, Melum E, Pertel T, Clayton KL, Raab M, Chen Q, Beauchemin N, Yazaki PJ, Pyzik M, Ostrowski MA, Glickman JN, Rudd CE, Ploegh HL, Franke A, Petsko GA, Kuchroo VK, Blumberg RS. CEACAM1 regulates TIM-3-mediated tolerance and exhaustion. Nature. 2015;517(7534):386-390. doi:10.1038/nature13848

105. Mao X, Ou MT, Karuppagounder SS, Kam TI, Yin X, Xiong Y, Ge P, Umanah GE, Brahmachari S, Shin JH, Kang HC, Zhang J, Xu J, Chen R, Park H, Andrabi SA, Kang SU, Gonçalves RA, Liang Y, Zhang S, Qi C, Lam S, Keiler JA, Tyson J, Kim D, Panicker N, Yun SP, Workman CJ, Vignali DAA, Dawson VL, Ko HS, Dawson TM. Pathological α-synuclein transmission initiated by binding lymphocyte-activation gene 3. Science (80-). 2016;353(6307):aah3374. doi:10.1126/science.aah3374

106. Camisaschi C, De Filippo A, Beretta V, Vergani B, Villa A, Vergani E, Santinami M, Cabras AD, Arienti F, Triebel F, Rodolfo M, Rivoltini L, Castelli C. Alternative activation of human plasmacytoid DCs in vitro and in melanoma lesions: Involvement of LAG-3. J Invest Dermatol. 2014;134(7):1893-1902. doi:10.1038/jid.2014.29

107. Belkina AC, Starchenko A, Drake KA, Proctor EA, Pihl RMF, Olson A, Lauffenburger DA, Lin N, Snyder-Cappione JE. Multivariate Computational Analysis of Gamma Delta

T Cell Inhibitory Receptor Signatures Reveals the Divergence of Healthy and ART-Suppressed HIV+ Aging. Front Immunol. 2018;9:2783. doi:10.3389/fimmu.2018.02783

108. Golden D, Kolmakova A, Sura S, Vella AT, Manichaikul A, Wang XQ, Bielinski SJ, Taylor KD, Chen YDI, Rich SS, Rodriguez A. Lymphocyte activation gene 3 and coronary artery disease. JCI Insight. 2016;1(17):e88628. doi:10.1172/jci.insight.88628

109. Triebel F, Jitsukawa S, Baixeras E, Roman-Roman S, Genevee C, Viegas-Pequignot,' And E, Hercend T. LAG-3, a novel lymphocyte activation gene closely related to CD4. J Exp Med. 1990;171(5):1393-1405. doi:10.1084/jem.171.5.1393

110. Huard B, Mastrangeli R, Prigent P, Bruniquel D, Donini S, El-Tayar N, Maigret B, Dréano M, Triebel F. Characterization of the major histocompatibility complex class II binding site on LAG-3 protein. Proc Natl Acad Sci U S A. 1997;94(11):5744-5749. doi:10.1073/pnas.94.11.5744

111. Xu F, Liu J, Liu D, Liu B, Wang M, Hu Z, Du X, Tang L, He F. LSECtin expressed on melanoma cells promotes tumor progression by inhibiting antitumor T-cell responses. Cancer Res. 2014;74(13):3418-3428. doi:10.1158/0008-5472.CAN-13-2690

112. Kouo T, Huang L, Pucsek AB, Cao M, Solt S, Armstrong T, Jaffee E. Galectin-3 shapes antitumor immune responses by suppressing CD8 T Cells via LAG-3 and Inhibiting Expansion of Plasmacytoid Dendritic Cells. Cancer Immunol Res. 2015;3(4):412-423. doi:10.1158/2326-6066.CIR-14-0150

113. Graydon CG, Mohideen S, Fowke KR. LAG3's Enigmatic Mechanism of Action. Front Immunol. 2021;11:615317. doi:10.3389/fimmu.2020.615317

114. Wang J, Sanmamed MF, Datar I, Su TT, Ji L, Sun J, Chen L, Chen Y, Zhu G, Yin W, Zheng L, Zhou T, Badri T, Yao S, Zhu S, Boto A, Sznol M, Melero I, Vignali DAA, Schalper K, Chen L. Fibrinogen-like Protein 1 Is a Major Immune Inhibitory Ligand of LAG-3. Cell. 2019;176(1-2):334-347.e12. doi:10.1016/j.cell.2018.11.010

115. Serriari NE, Gondois-Rey F, Guillaume Y, Remmerswaal EBM, Pastor S, Messal N, Truneh A, Hirsch I, van Lier RAW, Olive D. B and T lymphocyte attenuator is highly expressed on CMV-specific T cells during infection and regulates their function. J Immunol. 2010;185(6):3140-3148. doi:10.4049/jimmunol.0902487

116. Yu X, Zheng Y, Mao R, Su Z, Zhang J. BTLA/HVEM Signaling: Milestones in Research and Role in Chronic Hepatitis B Virus Infection. Front Immunol.

2019;10:617. doi:10.3389/fimmu.2019.00617

117. Cai G, Freeman GJ. The CD160, BTLA, LIGHT/HVEM pathway: A bidirectional switch regulating T-cell activation. Immunol Rev. 2009;229(1):244-258. doi:10.1111/j.1600-065X.2009.00783.x

118. Hurchla MA, Sedy JR, Gavrielli M, Drake CG, Murphy TL, Murphy KM. B and T lymphocyte attenuator exhibits structural and expression polymorphisms and is highly induced in anergic CD4+ T cells. J Immunol. 2005;174(6):3377-3385. doi:10.4049/jimmunol.174.6.3377

119. Huntington ND, Cursons J, Rautela J. The cancer–natural killer cell immunity cycle. Nat Rev Cancer. 2020;20(8):437-454. doi:10.1038/s41568-020-0272-z

120. Zhang Y, Huang B. The Development and Diversity of ILCs, NK Cells and Their Relevance in Health and Diseases. Adv Exp Med Biol. 2017;1024:225-244. doi:10.1007/978-981-10-5987-2_11

121. Carrega P, Ferlazzo G. Natural killer cell distribution and trafficking in human tissues. Front Immunol. 2012;3:347. doi:10.3389/fimmu.2012.00347

122. Rosmaraki EE, Douagi I, Roth C, Colucci F, Cumano A, Di Santo JP. Identification of committed NK cell progenitors in adult murine bone marrow. Eur J Immunol. 2001;31(6):1900-1909. doi:10.1002/1521-4141(200106)31:6<1900::AID-IMMU1900>3.0.CO;2-M

123. Sojka DK, Tian Z, Yokoyama WM. Tissue-resident natural killer cells and their potential diversity. Semin Immunol. 2014;26(2):127-131. doi:10.1016/j.smim.2014.01.010

124. Kondo M, Weissman IL, Akashi K. Identification of clonogenic common lymphoid progenitors in mouse bone marrow. Cell. 1997;91(5):661-672. doi:10.1016/s0092-8674(00)80453-5

125. Claude Gregoire, Lionel Chasson, Carmelo Luci, Elena Tomasello, Frederic Geissmann, Eric Vivier, Thierry Walzer. The trafficking of natural killer cells. Immunol Rev. 2007;220(1):169-182. doi:10.1111/j.1600-065X.2007.00563.x

126. Sun H, Sun C, Tian Z, Xiao W. NK cells in immunotolerant organs. Cell Mol Immunol. 2013;10(3):202-212. doi:10.1038/cmi.2013.9

127. Kumar S. Natural killer cell cytotoxicity and its regulation by inhibitory receptors. Immunology. 2018;154(3):383-393. doi:10.1111/imm.12921

128. Guethlein LA, Norman PJ, Hilton HHG, Parham P. Co-evolution of MHC class I and variable NK cell receptors in placental mammals. Immunol Rev. 2015;267(1):259-282. doi:10.1111/imr.12326

129. Lanier LL. NKG2D receptor and its ligands in host defense. Cancer Immunol Res. 2015;3(6):575-582. doi:10.1158/2326-6066.CIR-15-0098

130. Vivier E, Artis D, Colonna M, Diefenbach A, Di Santo JP, Eberl G, Koyasu S, Locksley RM, McKenzie ANJ, Mebius RE, Powrie F, Spits H. Innate Lymphoid Cells: 10 Years On. Cell. 2018;174(5):1054-1066. doi:10.1016/j.cell.2018.07.017

131. Topham NJ, Hewitt EW. Natural killer cell cytotoxicity: How do they pull the trigger? Immunology. 2009;128(1):7-15. doi:10.1111/j.1365-2567.2009.03123.x

132. Carson WE, Giri JG, Lindemann MJ, Linett ML, Ahdieh M, Paxton R, Anderson D, Eisenmann J, Grabstein K, Caligiuri MA. Interleukin (IL) 15 is a novel cytokine that activates human natural killer cells via components of the IL-2 receptor. J Exp Med. 1994;180(4):1395-1403. doi:10.1084/jem.180.4.1395

133. Poli A, Michel T, Thérésine M, Andrès E, Hentges F, Zimmer J. CD56bright natural killer (NK) cells: An important NK cell subset. Immunology. 2009;126(4):458-465. doi:10.1111/j.1365-2567.2008.03027.x

134. Cichocki F, Verneris MR, Cooley S, Bachanova V, Brunstein CG, Blazar BR, Wagner J, Schlums H, Bryceson YT, Weisdorf DJ, Miller JS. The past, present, and future of NK cells in hematopoietic cell transplantation and adoptive transfer. Curr Top Microbiol Immunol. 2016;395:225-243. doi:10.1007/82_2015_445

135. Cooper MA, Fehniger TA, Turner SC, Chen KS, Ghaheri BA, Ghayur T, Carson WE, Caligiuri MA. Human natural killer cells: a unique innate immunoregulatory role for the CD56 bright subset. Blood. 2001;97(10):3146-3151. doi:10.1182/blood.v97.10.3146

136. Russick J, Torset C, Hemery E, Cremer I. NK cells in the tumor microenvironment: Prognostic and theranostic impact. Recent advances and trends. Semin Immunol. 2020;48:101407. doi:10.1016/j.smim.2020.101407

137. Dalbeth N, Gundle R, Davies RJO, Lee YCG, McMichael AJ, Callan MFC. CD56 bright NK Cells Are Enriched at Inflammatory Sites and Can Engage with Monocytes in a

Reciprocal Program of Activation. J Immunol. 2004;173(10):6418-6426. doi:10.4049/jimmunol.173.10.6418

138. Della Chiesa M, Vitale M, Carlomagno S, Ferlazzo G, Moretta L, Moretta A. The natural killer cell-mediated killing of autologous dendritic cells is confined to a cell subset expressing CD94/NKG2A, but lacking inhibitory killer Ig-like receptors. Eur J Immunol. 2003;33(6):1657-1666. doi:10.1002/eji.200323986

139. Morandi B, Mortara L, Chiossone L, Accolla RS, Mingari MC, Moretta L, Moretta A, Ferlazzo G. Dendritic cell editing by activated natural killer cells results in a more protective cancer-specific immune response. PLoS One. 2012;7(6):e39170. doi:10.1371/journal.pone.0039170

140. Chen DS, Mellman I. Oncology meets immunology: The cancer-immunity cycle. Immunity. 2013;39(1):1-10. doi:10.1016/j.immuni.2013.07.012

141. Gadgeel SM. Personalized Therapy of Non-small Cell Lung Cancer (NSCLC). Adv Exp Med Biol. 2016;890:203-222. doi:10.1007/978-3-319-24932-2_11

142. Nivolumab Approved for Lung Cancer. Cancer Discov. 2015;5(5):OF1. doi:10.1158/2159-8290.CD-NB2015-042

143. Garon EB, Rizvi NA, Hui R, Leighl N, Balmanoukian AS, Eder JP, Patnaik A, Aggarwal C, Gubens M, Horn L, Carcereny E, Ahn MJ, Felip E, Lee JS, Hellmann MD, Hamid O, Goldman JW, Soria JC, Dolled-Filhart M, Rutledge RZ, Zhang J, Lunceford JK, Rangwala R, Lubiniecki GM, Roach C, Emancipator K, Gandhi L. Pembrolizumab for the treatment of non-small-cell lung cancer. N Engl J Med. 2015;372(21):2018-2028. doi:10.1056/nejmoa1501824

144. Shiravand Y, Khodadadi F, Kashani SMA, Hosseini-Fard SR, Hosseini S, Sadeghirad H, Ladwa R, O'byrne K, Kulasinghe A. Immune Checkpoint Inhibitors in Cancer Therapy. Curr Oncol. 2022;29(5):3044-3060. doi:10.3390/curroncol29050247

145. Sharma P, Hu-Lieskovan S, Wargo JA, Ribas A. Primary, Adaptive, and Acquired Resistance to Cancer Immunotherapy. Cell. 2017;168(4):707-723. doi:10.1016/j.cell.2017.01.017

146. Jenkins RW, Barbie DA, Flaherty KT. Mechanisms of resistance to immune checkpoint inhibitors. Br J Cancer. 2018;118(1):9-16. doi:10.1038/bjc.2017.434

147. Boyero L, Sánchez-Gastaldo A, Alonso M, Noguera-Uclés JF, Molina-Pinelo S,

Bernabé-Caro R. Primary and acquired resistance to immunotherapy in lung cancer: Unveiling the mechanisms underlying of immune checkpoint blockade therapy. Cancers (Basel). 2020;12(12):3729. doi:10.3390/cancers12123729

148. Luchini C, Bibeau F, Ligtenberg MJL, Singh N, Nottegar A, Bosse T, Miller R, Riaz N, Douillard JY, Andre F, Scarpa A. ESMO recommendations on microsatellite instability testing for immunotherapy in cancer, and its relationship with PD-1/PD-L1 expression and tumour mutational burden: A systematic review-based approach. Ann Oncol. 2019;30(8):1232-1243. doi:10.1093/annonc/mdz116

149. Reck M, Rodríguez-Abreu D, Robinson AG, Hui R, Csőszi T, Fülöp A, Gottfried M, Peled N, Tafreshi A, Cuffe S, O'Brien M, Rao S, Hotta K, Leiby MA, Lubiniecki GM, Shentu Y, Rangwala R, Brahmer JR. Pembrolizumab versus Chemotherapy for PD-L1–Positive Non–Small-Cell Lung Cancer. N Engl J Med. 2016;375(19):1823-1833. doi:10.1056/nejmoa1606774

150. Nicoś M, Krawczyk P, Crosetto N, Milanowski J. The Role of Intratumor Heterogeneity in the Response of Metastatic Non-Small Cell Lung Cancer to Immune Checkpoint Inhibitors. Front Oncol. 2020;10:569202. doi:10.3389/fonc.2020.569202

151. Turajlic S, Litchfield K, Xu H, Rosenthal R, McGranahan N, Reading JL, Wong YNS, Rowan A, Kanu N, Al Bakir M, Chambers T, Salgado R, Savas P, Loi S, Birkbak NJ, Sansregret L, Gore M, Larkin J, Quezada SA, Swanton C. Insertion-and-deletion-derived tumour-specific neoantigens and the immunogenic phenotype: a pan-cancer analysis. Lancet Oncol. 2017;18(8):1009-1021. doi:10.1016/S1470-2045(17)30516-8

152. Tran L, Theodorescu D. Determinants of resistance to checkpoint inhibitors. Int J Mol Sci. 2020;21(5):1594. doi:10.3390/ijms21051594

153. Robert C. A decade of immune-checkpoint inhibitors in cancer therapy. Nat Commun. 2020;11(1):3801. doi:10.1038/s41467-020-17670-y

154. Lu HC, Mackie K. Review of the Endocannabinoid System. Biol Psychiatry Cogn Neurosci Neuroimaging. 2021;6(6):607-615. doi:10.1016/j.bpsc.2020.07.016

155. Cristino L, Bisogno T, Di Marzo V. Cannabinoids and the expanded endocannabinoid system in neurological disorders. Nat Rev Neurol. 2020;16(1):9-29. doi:10.1038/s41582-019-0284-z

156. Galiègue S, Mary S, Marchand J, Dussossoy D, Carrière D, Carayon P, Bouaboula M,

Shire D, LE Fur G, Casellas P. Expression of Central and Peripheral Cannabinoid Receptors in Human Immune Tissues and Leukocyte Subpopulations. Eur J Biochem. 1995;232(1):54-61. doi:10.1111/j.1432-1033.1995.tb20780.x

157. Khan MI, Sobociiska AA, Czarnecka AM, Król M, Botta B, Szczylik C. The Therapeutic Aspects of the Endocannabinoid System (ECS) for Cancer and their Development: From Nature to Laboratory. Curr Pharm Des. 2016;22(12):1756-1766. doi:10.2174/1381612822666151211094901

158. Maurya N, Velmurugan BK. Therapeutic applications of cannabinoids. Chem Biol Interact. 2018;293:77-88. doi:10.1016/j.cbi.2018.07.018

159. Di Marzo V, Piscitelli F. The Endocannabinoid System and its Modulation by Phytocannabinoids. Neurotherapeutics. 2015;12(4):692-698. doi:10.1007/s13311-015-0374-6

160. Kienzl M, Kargl J, Schicho R. The immune endocannabinoid system of the tumor microenvironment. Int J Mol Sci. 2020;21(23):1-25. doi:10.3390/ijms21238929

161. Kaplan BLF. The role of CB1 in immune modulation by cannabinoids. Pharmacol Ther. 2013;137(3):365-374. doi:10.1016/j.pharmthera.2012.12.004

162. Grill M, Hasenoehrl C, Kienzl M, Kargl J, Schicho R. Cellular localization and regulation of receptors and enzymes of the endocannabinoid system in intestinal and systemic inflammation. Histochem Cell Biol. 2019;151(1):5-20. doi:10.1007/s00418-018-1719-0

163. Basu S, Dittel BN. Unraveling the complexities of cannabinoid receptor 2 (CB2) immune regulation in health and disease. Immunol Res. 2011;51(1):26-38. doi:10.1007/s12026-011-8210-5

164. Simard M, Rakotoarivelo V, Di Marzo V, Flamand N. Expression and Functions of the CB2 Receptor in Human Leukocytes. Front Pharmacol. 2022;13:826400. doi:10.3389/fphar.2022.826400

165. Braile M, Marcella S, Marone G, Galdiero MR, Varricchi G, Loffredo S. The Interplay between the Immune and the Endocannabinoid Systems in Cancer. Cells. 2021;10(6):1282. doi:10.3390/cells10061282

166. Turcotte C, Blanchet MR, Laviolette M, Flamand N. The CB2 receptor and its role as a regulator of inflammation. Cell Mol Life Sci. 2016;73(23):4449-4470.

doi:10.1007/s00018-016-2300-4

167. Demuth DG, Molleman A. Cannabinoid signalling. Life Sci. 2006;78(6):549-563. doi:10.1016/j.lfs.2005.05.055

168. Jourdan T, Godlewski G, Cinar R, Bertola A, Szanda G, Liu J, Tam J, Han T, Mukhopadhyay B, Skarulis MC, Ju C, Aouadi M, Czech MP, Kunos G. Activation of the Nlrp3 inflammasome in infiltrating macrophages by endocannabinoids mediates beta cell loss in type 2 diabetes. Nat Med. 2013;19(9):1132-1140. doi:10.1038/nm.3265

169. Mai P, Yang L, Tian L, Wang L, Jia S, Zhang Y, Liu X, Yang L, Li L. Endocannabinoid System Contributes to Liver Injury and Inflammation by Activation of Bone Marrow–Derived Monocytes/Macrophages in a CB1-Dependent Manner. J Immunol. 2015;195(7):3390-3401. doi:10.4049/jimmunol.1403205

170. Buckley NE. The peripheral cannabinoid receptor knockout mice: An update. Br J Pharmacol. 2008;153(2):309-318. doi:10.1038/sj.bjp.0707527

171. Nagarkatti P, Pandey R, Rieder SA, Hegde VL, Nagarkatti M. Cannabinoids as novel anti-inflammatory drugs. Future Med Chem. 2009;1(7):1333-1349. doi:10.4155/fmc.09.93

172. Maresz K, Pryce G, Ponomarev ED, Marsicano G, Croxford JL, Shriver LP, Ledent C, Cheng X, Carrier EJ, Mann MK, Giovannoni G, Pertwee RG, Yamamura T, Buckley NE, Hillard CJ, Lutz B, Baker D, Dittel BN. Direct suppression of CNS autoimmune inflammation via the cannabinoid receptor CB1 on neurons and CB2 on autoreactive T cells. Nat Med. 2007;13(4):492-497. doi:10.1038/nm1561

173. Börner C, Höllt V, Sebald W, Kraus J. Transcriptional regulation of the cannabinoid receptor type 1 gene in T cells by cannabinoids. J Leukoc Biol. 2007;81(1):336-343. doi:10.1189/jlb.0306224

174. Börner C, Höllt V, Kraus J. Activation of human T cells induces upregulation of cannabinoid receptor type 1 transcription. Neuroimmunomodulation. 2007;14(6):281-286. doi:10.1159/000117809

175. Börner C, Bedini A, Höllt V, Kraus J. Analysis of promoter regions regulating basal and interleukin-4-inducible expression of the human CB1 receptor gene in T lymphocytes. Mol Pharmacol. 2008;73(3):1013-1019. doi:10.1124/mol.107.042945

176. Börner C, Martella E, Höllt V, Kraus J. Regulation of opioid and cannabinoid receptor genes in human neuroblastoma and T cells by the epigenetic modifiers trichostatin A and 5-Aza-2'- deoxycytidine. Neuroimmunomodulation. 2012;19(3):180-186. doi:10.1159/000331474

177. Derocq JM, Ségui M, Marchand J, Le Fur G, Casellas P. Cannabinoids enhance human B-cell growth at low nanomolar concentrations. FEBS Lett. 1995;369(2-3):177-182. doi:10.1016/0014-5793(95)00746-V

178. Agudelo M, Newton C, Widen R, Sherwood T, Nong L, Friedman H, Klein TW. Cannabinoid receptor 2 (CB2) mediates immunoglobulin class switching from IgM to IgE in cultures of murine purified B lymphocytes. J Neuroimmune Pharmacol. 2008;3(1):35-42. doi:10.1007/s11481-007-9088-9

179. Newton CA, Chou PJ, Perkins I, Klein TW. CB1 and CB2 cannabinoid receptors mediate different aspects of delta-9-tetrahydrocannabinol (THC)-induced T helper cell shift following immune activation by legionella pneumophila infection. J Neuroimmune Pharmacol. 2009;4(1):92-102. doi:10.1007/s11481-008-9126-2

180. Correa F, Docagne F, Mestre L, Clemente D, Hernangómez M, Loría F, Guaza C. A role for CB2 receptors in anandamide signalling pathways involved in the regulation of IL-12 and IL-23 in microglial cells. Biochem Pharmacol. 2009;77(1):86-100. doi:10.1016/j.bcp.2008.09.014

181. Correa F, Hernangómez M, Mestre L, Loría F, Spagnolo A, Docagne F, Di Marzo V, Guaza C. Anandamide enhances IL-10 production in activated microglia by targeting CB2 receptors: Roles of ERK1/2, JNK, and NF-κB. Glia. 2010;58(2):135-147. doi:10.1002/glia.20907

182. Massi P, Fuzio D, Vigano D, Sacerdote P, Parolaro D. Relative involvement of cannabinoid CB and CB receptors in the Δ9-tetrahydrocannabinol-induced inhibition of natural killer activity. Eur J Pharmacol. 2000;387(3):343-347. doi:doi.org/10.1016/S0014-2999(99)00860-2

183. Do Y, McKallip RJ, Nagarkatti M, Nagarkatti PS. Activation through Cannabinoid Receptors 1 and 2 on Dendritic Cells Triggers NF-κB-Dependent Apoptosis: Novel Role for Endogenous and Exogenous Cannabinoids in Immunoregulation. J Immunol. 2004;173(4):2373-2382. doi:10.4049/jimmunol.173.4.2373

184. Lombard C, Nagarkatti M, Nagarkatti P. CB2 cannabinoid receptor agonist, JWH-015

triggers apoptosis in immune cells: Potential role for CB2 selective ligands as immunosuppressive agents. Clin Immunol. 2007;122(3):259-270. doi:10.1016/j.clim.2006.11.002

185. Laezza C, Pagano C, Navarra G, Pastorino O, Proto MC, Fiore D, Piscopo C, Gazzerro P, Bifulco M. The endocannabinoid system: A target for cancer treatment. Int J Mol Sci. 2020;21(3):747. doi:10.3390/ijms21030747

186. Turcotte C, Blanchet MR, Laviolette M, Flamand N. Impact of cannabis, cannabinoids, and endocannabinoids in the lungs. Front Pharmacol. 2016;7:317. doi:10.3389/fphar.2016.00317

187. Staiano RI, Loffredo S, Borriello F, Iannotti FA, Piscitelli F, Orlando P, Secondo A, Granata F, Lepore MT, Fiorelli A, Varricchi G, Santini M, Triggiani M, Di Marzo V, Marone G. Human lung-resident macrophages express CB1 and CB2 receptors whose activation inhibits the release of angiogenic and lymphangiogenic factors. J Leukoc Biol. 2016;99(4):531-540. doi:10.1189/jlb.3hi1214-584r

188. Preet A, Qamri Z, Nasser MW, Prasad A, Shilo K, Zou X, Groopman JE, Ganju RK. Cannabinoid receptors, CB1 and CB2, as novel targets for inhibition of non-small cell lung cancer growth and metastasis. Cancer Prev Res. 2011;4(1):65-75. doi:10.1158/1940-6207.CAPR-10-0181

189. Boyacıoğlu Ö, Bilgiç E, Varan C, Bilensoy E, Nemutlu E, Sevim D, Kocaefe Ç, Korkusuz P. ACPA decreases non-small cell lung cancer line growth through Akt/PI3K and JNK pathways in vitro. Cell Death Dis. 2021;12(1):56. doi:10.1038/s41419-020-03274-3

190. Preet A, Ganju RK, Groopman JE. Δ9-Tetrahydrocannabinol inhibits epithelial growth factor-induced lung cancer cell migration in vitro as well as its growth and metastasis in vivo. Oncogene. 2008;27(3):339-346. doi:10.1038/sj.onc.1210641

191. Vidinský B, Gál P, Pilátová M, Vidová Z, Solár P, Varinská L, Ivanová L, Mojžiš J, Gál P. Anti-proliferative and Anti-angiogenic Effects of CB2 R Agonist (JWH-133) in Non-small Lung Cancer Cells (A549) and Human Umbilical Vein Endothelial Cells: an in Vitro Investigation. CzechRepublic Folia Biol. 2012;58(2):75-80.

192. Preet A, Qamri Z, Nasser MW, Prasad A, Shilo K, Zou X, Groopman JE, Ganju RK. Cannabinoid receptors, CB1 and CB2, as novel targets for inhibition of non-small cell lung cancer growth and metastasis. Cancer Prev Res. 2011;4(1):65-75.

doi:10.1158/1940-6207.CAPR-10-0181

193. Ravi J, Elbaz M, Wani NA, Nasser MW, Ganju RK. Cannabinoid receptor-2 agonist inhibits macrophage induced EMT in non-small cell lung cancer by downregulation of EGFR pathway. Mol Carcinog. 2016;55(12):2063-2076. doi:10.1002/mc.22451

194. Milian L, Mata M, Alcacer J, Oliver M, Sancho-Tello M, de Llano JJM, Camps C, Galbis J, Carretero J, Carda C. Cannabinoid receptor expression in non-small cell lung cancer. Effectiveness of tetrahydrocannabinol and cannabidiol inhibiting cell proliferation and epithelial-mesenchymal transition in vitro. PLoS One. 2020;15(2):e0228909. doi:10.1371/journal.pone.0228909

195. Xu S, Ma H, Bo Y, Shao M. The oncogenic role of CB2 in the progression of non-small-cell lung cancer. Biomed Pharmacother. 2019;117:109080. doi:10.1016/j.biopha.2019.109080

196. Kienzl M, Hasenoehrl C, Maitz K, Sarsembayeva A, Taschler U, Valadez-Cosmes P, Kindler O, Ristic D, Raftopoulou S, Santiso A, Bärnthaler T, Brcic L, Hahnefeld L, Gurke R, Thomas D, Geisslinger G, Kargl J, Schicho R. Monoacylglycerol lipase deficiency in the tumor microenvironment slows tumor growth in non-small cell lung cancer. Oncoimmunology. 2021;10(1):e1965319. doi:10.1080/2162402X.2021.1965319

197. Sarsembayeva A, Kienzl M, Gruden E, Ristic D, Maitz K, Valadez-Cosmes P, Santiso A, Hasenoehrl C, Brcic L, Lindenmann J, Kargl J, Schicho R. Cannabinoid receptor 2 plays a pro-tumorigenic role in non-small cell lung cancer by limiting anti-tumor activity of CD8+ T and NK cells. Front Immunol. 2023;13:997115. doi:10.3389/fimmu.2022.997115

198. Mathsyaraja H, Catchpole J, Freie B, Eastwood E, Babaeva E, Geuenich M, Cheng PF, Ayers J, Yu M, Wu N, Moorthi S, Poudel KR, Koehne A, Grady W, Houghton AM, Berger AH, Shiio Y, Macpherson D, Eisenman RN. Loss of MGA repression mediated by an atypical polycomb complex promotes tumor progression and invasiveness. Elife. 2021;10:e64212. doi:10.7554/eLife.64212

199. Kienzl M, Hasenoehrl C, Valadez-Cosmes P, Maitz K, Sarsembayeva A, Sturm E, Heinemann A, Kargl J, Schicho R. IL-33 reduces tumor growth in models of colorectal cancer with the help of eosinophils. Oncoimmunology. 2020;9(1):1-12. doi:10.1080/2162402X.2020.1776059

200. Rinaldi-Carmona M, Barth F, Hkaulme M, Shireb D, Calandrab B, Congy C, Martinez S, Maruani J, Ncliat G, Caputb D, Ferrarab P, Soubric P, Brelike JC, Le Fura G. SR141716A, a potent and selective antagonist of the brain cannabinoid receptor. FEBS Lett. 1994;350:240-244. doi:10.1016/0014-5793(94)00773-x

201. Di Marzo V. Targeting the endocannabinoid system: To enhance or reduce? Nat Rev Drug Discov. 2008;7(5):438-455. doi:10.1038/nrd2553

202. Storr MA, Keenan CM, Zhang H, Patel KD, Makriyannis A, Sharkey KA. Activation of the cannabinoid 2 receptor (CB2) protects against experimental colitis. Inflamm Bowel Dis. 2009;15(11):1678-1685. doi:10.1002/ibd.20960

203. Rinaldi-Carmona M, Barth F,´Millan J, Jean-Marie Derocq, Pierre Casellas, Christian Congy, Didier Oustric, Martine Sarran, Monsif Bouaboula, Bernard Calandra, Marielle Portier, David Shire, Jean-Claude BrelieRe, Ge Rard Lefur. SR144528, the First Potent and Selective Antagonist of the CB2 Cannabinoid Receptor. J Pharmacol Exp Ther. 1998;284(2):644-650. http://www.jpet.org

204. Strauss L, Mahmoud MAA, Weaver JD, Tijaro-Ovalle NM, Christofides A, Wang Q, Pal R, Yuan M, Asara J, Patsoukis N, Boussiotis VA. Targeted deletion of PD-1 in myeloid cells induces antitumor immunity. Sci Immunol. 2020;5(43):1-27. doi:10.1126/sciimmunol.aay1863

205. Lucarini V, Zicchedda G, Macchia I, La Sorsa V, Peschiaroli F, Buccione C, Sistigu A, Sanchez M, Andreone S, D'Urso MT, Spada M, Macchia D, Afferni C, Mattei F, Schiavoni G. IL-33 restricts tumor growth and inhibits pulmonary metastasis in melanoma-bearing mice through eosinophils. Oncoimmunology. 2017;6(6):e1317420. doi:10.1080/2162402X.2017.1317420

206. Alter G, Malenfant JM, Altfeld M. CD107a as a functional marker for the identification of natural killer cell activity. J Immunol Methods. 2004;294(1-2):15-22. doi:10.1016/j.jim.2004.08.008

207. Eberlein J, Nguyen TT, Victorino F, Golden-Mason L, Rosen HR, Homann D. Comprehensive assessment of chemokine expression profiles by flow cytometry. J Clin Invest. 2010;120(3):907-923. doi:10.1172/JCI40645

208. Pfaffl MW. A new mathematical model for relative quantification in real-time RT-PCR. Nucleic Acids Res. 2001;29(9):e45. doi:10.1093/nar/29.9.e45

209. Wei M, Guo M, Meng X, Li L, Wang H, Zhang M, Bei Y. PPARγ Mediates the Cardioprotective Roles of Danlou Tablet After Acute Myocardial Ischemia-Reperfusion Injury. Front Cardiovasc Med. 2022;9:858909. doi:10.3389/fcvm.2022.858909

210. Xiong X, Chen S, Shen J, You H, Yang H, Yan C, Fang Z, Zhang J, Cai X, Dong X, Kang T, Li W, Zhou P. Cannabis suppresses antitumor immunity by inhibiting JAK/STAT signaling in T cells through CNR2. Signal Transduct Target Ther. 2022;7(1):99. doi:10.1038/s41392-022-00918-y

211. Coussens LM, Werb Z. Inflammation and cancer. Nature. 2002;420(6917):860-867. doi:10.1038/nature01322

212. Virchow Rudolf. An address on the value of pathological experiments. Br Med J. 1881;2:198-203.

213. Ehrlich P. Über den jetzigen stand der karzinomforschung. Ned Tijdschr voor Geneeskd. 1909;5:273-290.

214. Garner H, de Visser KE. Immune crosstalk in cancer progression and metastatic spread: a complex conversation. Nat Rev Immunol. 2020;20(8):483-497. doi:10.1038/s41577-019-0271-z

215. Llanos Casanova M, Blázquez C, Martínez-Palacio J, Villanueva C, Fernández-Aceñero MJ, Huffman JW, Jorcano JL, Guzmán M. Inhibition of skin tumor growth and angiogenesis in vivo by activation of cannabinoid receptors. J Clin Invest. 2003;111(1):43-50. doi:10.1172/JCI200316116

216. Caffarel MM, Sarrió D, Palacios J, Guzmán M, Sánchez C. Δ9-tetrahydrocannabinol inhibits cell cycle progression in human breast cancer cells through Cdc2 regulation. Cancer Res. 2006;66(13):6615-6621. doi:10.1158/0008-5472.CAN-05-4566

217. Pyszniak M, Tabarkiewicz J, Łuszczki JJ. Endocannabinoid system as a regulator of tumor cell malignancy – Biological pathways and clinical significance. Onco Targets Ther. 2016;9:4323-4336. doi:10.2147/OTT.S106944

218. Gustafsson K, Christensson B, Sander B, Flygare J. Cannabinoid receptor-mediated apoptosis induced by R(+)-methanandamide and Win55,212-2 is associated with ceramide accumulation and p38 activation in mantle cell lymphoma. Mol Pharmacol. 2006;70(5):1612-1620. doi:10.1124/mol.106.025981

219. Sánchez C, de Ceballos ML, Gómez del Pulgar T, Rueda D, Corbacho C, Velasco G,

Galve-Roperh I, Huffman JW, Ramón Cajal S, Guzmán M. Inhibition of glioma growth in vivo by selective activation of the CB(2) cannabinoid receptor. Cancer Res. 2001;61(15):5784-5789. http://aacrjournals.org/cancerres/article-pdf/61/15/5784/2485361/5784.pdf

220. Martínez-Lostao L, Anel A, Pardo J. How Do Cytotoxic Lymphocytes Kill Cancer Cells? Clin Cancer Res. 2015;21(22):5047-5056. doi:10.1158/1078-0432.CCR-15-0685

221. Takanami I, Takeuchi K, Giga M. The prognostic value of natural killer cell infiltration in resected pulmonary adenocarcinoma. J Thorac Cardiovasc Surg. 2001;121(6):1058-1063. doi:10.1067/mtc.2001.113026

222. Barry KC, Hsu J, Broz ML, Cueto FJ, Binnewies M, Combes AJ, Nelson AE, Loo K, Kumar R, Rosenblum MD, Alvarado MD, Wolf DM, Bogunovic D, Bhardwaj N, Daud AI, Ha PK, Ryan WR, Pollack JL, Samad B, Asthana S, Chan V, Krummel MF. A natural killer–dendritic cell axis defines checkpoint therapy–responsive tumor microenvironments. Nat Med. 2018;24(8):1178-1191. doi:10.1038/s41591-018-0085-8

223. Stankovic B, Bjørhovde HAK, Skarshaug R, Aamodt H, Frafjord A, Müller E, Hammarström C, Beraki K, Bækkevold ES, Woldbæk PR, Helland Å, Brustugun OT, Øynebråten I, Corthay A. Immune Cell Composition in Human Non-small Cell Lung Cancer. Front Immunol. 2019;9:3101. doi:10.3389/fimmu.2018.03101

224. Jin S, Deng Y, Hao JW, Li Y, Liu B, Yu Y, Shi FD, Zhou QH. NK cell phenotypic modulation in lung cancer environment. PLoS One. 2014;9(10):e109976. doi:10.1371/journal.pone.0109976

225. Cong J, Wang X, Zheng X, Wang D, Fu B, Sun R, Tian Z, Wei H. Dysfunction of Natural Killer Cells by FBP1-Induced Inhibition of Glycolysis during Lung Cancer Progression. Cell Metab. 2018;28(2):243-255.e5. doi:10.1016/j.cmet.2018.06.021

226. Prado-Garcia H, Romero-Garcia S, Aguilar-Cazares D, Meneses-Flores M, Lopez-Gonzalez JS. Tumor-induced CD8+ T-cell dysfunction in lung cancer patients. Clin Dev Immunol. 2012;2012:741741. doi:10.1155/2012/741741

227. Sheng SY, Gu Y, Lu CG, Zou JY, Hong H, Wang RF. The distribution and function of human memory T cell subsets in lung cancer. Immunol Res. 2017;65(3):639-650. doi:10.1007/s12026-016-8882-y

228. Muller A, Homey B, Soto H, Ge N, Catron D, Buchanan ME, McClanahan T, Murphy E, Yuan W, Wagner SN, Luis Barrerak J, Mohark A, Vera Â steguik E, Zlotnik A. Involvement of chemokine receptors in breast cancer metastasis. Nature. 2001;410(6824):50-56. doi:10.1038/35065016

229. Sharma S, Stolina M, Luo J, Strieter RM, Burdick M, Zhu LX, Batra RK, Dubinett SM. Secondary Lymphoid Tissue Chemokine Mediates T Cell-Dependent Antitumor Responses In Vivo. J Immunol. 2000;164(9):4558-4563. doi:10.4049/jimmunol.164.9.4558

230. Arenberg DA, Zlotnick A, Strom SRB, Burdick MD, Strieter RM. The murine CC chemokine, 6C-kine, inhibits tumor growth and angiogenesis in a human lung cancer SCID mouse model. Cancer Immunol Immunother. 2001;49(11):587-592. doi:10.1007/s002620000147

231. Xu Y, Liu L, Qiu X, Jiang L, Huang B, Li H, Li Z, Luo W, Wang E. CCL21/CCR7 promotes G2/M phase progression via the ERK pathway in human non-small cell lung cancer cells. PLoS One. 2011;6(6):e21119. doi:10.1371/journal.pone.0021119

232. Xu Y, Liu L, Qiu X, Liu Z, Li H, Li Z, Luo W, Wang E. CCL21/CCR7 prevents apoptosis via the ERK pathway in human non-small cell lung cancer cells. PLoS One. 2012;7(3):e33262. doi:10.1371/journal.pone.0033262

233. Amaria RN, Reddy SM, Tawbi HA, Davies MA, Ross MI, Glitza IC, Cormier JN, Lewis C, Hwu WJ, Hanna E, Diab A, Wong MK, Royal R, Gross N, Weber R, Lai SY, Ehlers R, Blando J, Milton DR, Woodman S, Kageyama R, Wells DK, Hwu P, Patel SP, Lucci A, Hessel A, Lee JE, Gershenwald J, Simpson L, Burton EM, Posada L, Haydu L, Wang L, Zhang S, Lazar AJ, Hudgens CW, Gopalakrishnan V, Reuben A, Andrews MC, Spencer CN, Prieto V, Sharma P, Allison J, Tetzlaff MT, Wargo JA. Neoadjuvant immune checkpoint blockade in high-risk resectable melanoma. Nat Med. 2018;24(11):1649-1654. doi:10.1038/s41591-018-0197-1

234. Suresh K, Naidoo J, Lin CT, Danoff S. Immune Checkpoint Immunotherapy for Non-Small Cell Lung Cancer: Benefits and Pulmonary Toxicities. Chest. 2018;154(6):1416-1423. doi:10.1016/j.chest.2018.08.1048

235. Sun C, Mezzadra R, Schumacher TN. Regulation and Function of the PD-L1 Checkpoint. Immunity. 2018;48(3):434-452. doi:10.1016/j.immuni.2018.03.014

236. Farhood B, Najafi M, Mortezaee K. CD8+ cytotoxic T lymphocytes in cancer

immunotherapy: A review. J Cell Physiol. 2019;234(6):8509-8521. doi:10.1002/jcp.27782

237. Leclerc M, Voilin E, Gros G, Corgnac S, de Montpréville V, Validire P, Bismuth G, Mami-Chouaib F. Regulation of antitumour CD8 T-cell immunity and checkpoint blockade immunotherapy by Neuropilin-1. Nat Commun. 2019;10(1):3345. doi:10.1038/s41467-019-11280-z

238. Simon S, Labarriere N. PD-1 expression on tumor-specific T cells: Friend or foe for immunotherapy? Oncoimmunology. 2018;7(1):e1364828. doi:10.1080/2162402X.2017.1364828

239. Thommen DS, Koelzer VH, Herzig P, Roller A, Trefny M, Dimeloe S, Kiialainen A, Hanhart J, Schill C, Hess C, Prince SS, Wiese M, Lardinois D, Ho PC, Klein C, Karanikas V, Mertz KD, Schumacher TN, Zippelius A. A transcriptionally and functionally distinct PD-1+ CD8+ T cell pool with predictive potential in non-small-cell lung cancer treated with PD-1 blockade. Nat Med. 2018;24(7):994-1004. doi:10.1038/s41591-018-0057-z

240. Legat A, Speiser DE, Pircher H, Zehn D, Fuertes Marraco SA. Inhibitory receptor expression depends more dominantly on differentiation and activation than “exhaustion” of human CD8 T cells. Front Immunol. 2013;4:455. doi:10.3389/fimmu.2013.00455

241. Topalian SL, Hodi FS, Brahmer JR, Gettinger SN, Smith DC, McDermott DF, Powderly JD, Carvajal RD, Sosman JA, Atkins MB, Leming PD, Spigel DR, Antonia SJ, Horn L, Drake CG, Pardoll DM, Chen L, Sharfman WH, Anders RA, Taube JM, McMiller TL, Xu H, Korman AJ, Jure-Kunkel M, Agrawal S, McDonald D, Kollia GD, Gupta A, Wigginton JM, Sznol M. Safety, Activity, and Immune Correlates of Anti–PD-1 Antibody in Cancer. N Engl J Med. 2012;366(26):2443-2454. doi:10.1056/nejmoa1200690

242. Taube JM, Klein A, Brahmer JR, Xu H, Pan X, Kim JH, Chen L, Pardoll DM, Topalian SL, Anders RA. Association of PD-1, PD-1 ligands, and other features of the tumor immune microenvironment with response to anti-PD-1 therapy. Clin Cancer Res. 2014;20(19):5064-5074. doi:10.1158/1078-0432.CCR-13-3271

243. Tang S, Qin C, Hu H, Liu T, He Y, Guo H, Yan H, Zhang J, Tang S, Zhou H. Immune Checkpoint Inhibitors in Non-Small Cell Lung Cancer: Progress, Challenges, and

Prospects. Cells. 2022;11(3):320. doi:10.3390/cells11030320

244. Shaver KA, Croom-Perez TJ, Copik AJ. Natural Killer Cells: The Linchpin for Successful Cancer Immunotherapy. Front Immunol. 2021;12:679117. doi:10.3389/fimmu.2021.679117

245. Hsu J, Hodgins JJ, Marathe M, Nicolai CJ, Bourgeois-Daigneault MC, Trevino TN, Azimi CS, Scheer AK, Randolph HE, Thompson TW, Zhang L, Iannello A, Mathur N, Jardine KE, Kirn GA, Bell JC, McBurney MW, Raulet DH, Ardolino M. Contribution of NK cells to immunotherapy mediated by PD-1/PD-L1 blockade. J Clin Invest. 2018;128(10):4654-4668. doi:10.1172/JCI99317

246. Dong W, Wu X, Ma S, Wang Y, Nalin AP, Zhu Z, Zhang J, Benson DM, He K, Caligiuri MA, Yu J. The Mechanism of Anti–PD-L1 Antibody Efficacy against PD-L1–Negative Tumors Identifies NK Cells Expressing PD-L1 as a Cytolytic Effector. Cancer Discov. 2019;9(10):1422-1437. doi:10.1158/2159-8290.CD-18-1259

247. Arnould L, Gelly M, Penault-Llorca F, Benoit L, Bonnetain F, Migeon C, Cabaret V, Fermeaux V, Bertheau P, Garnier J, Jeannin JF, Coudert B. Trastuzumab-based treatment of HER2-positive breast cancer: An antibody-dependent cellular cytotoxicity mechanism? Br J Cancer. 2006;94(2):259-267. doi:10.1038/sj.bjc.6602930

248. Muntasell A, Rojo F, Servitja S, Rubio-Perez C, Cabo M, Tamborero D, Costa-García M, Martínez-Garcia M, Menendez S, Vazquez I, Lluch A, Gonzalez-Perez A, Rovira A, Lopez-Botet M, Albanell J. NK Cell Infiltrates and HLA Class I Expression in Primary HER2+ Breast Cancer Predict and Uncouple Pathological Response and Disease-free Survival. Clin Cancer Res. 2019;25(5):1535-1545. doi:10.1158/1078-0432.CCR-18-2365

249. Muntasell A, Servitja S, Cabo M, Bermejo B, Pérez-Buira S, Rojo F, Costa-García M, Arpí O, Moraru M, Serrano L, Tusquets I, Martínez MT, Heredia G, Vera A, Martínez-García M, Soria L, Comerma L, Santana-Hernández S, Eroles P, Rovira A, Vilches C, Lluch A, Albanell J, López-Botet M. High Numbers of Circulating CD57+ NK Cells Associate with Resistance to HER2-Specific Therapeutic Antibodies in HER2+ Primary Breast Cancer. Cancer Immunol Res. 2019;7(8):1280-1292. doi:10.1158/2326-6066.CIR-18-0896

250. Ali TH, Pisanti S, Ciaglia E, Mortarini R, Anichini A, Garofalo C, Tallerico R, Santinami M, Gulletta E, Ietto C, Galgani M, Matarese G, Bifulco M, Ferrone S, Colucci F,

Moretta A, Kärre K, Carbone E. Enrichment of CD56(dim)KIR+ CD57+ highly cytotoxic NK cells in tumour-infiltrated lymph nodes of melanoma patients. Nat Commun. 2014;5:5639. doi:10.1038/ncomms6639

251. Messaoudene M, Fregni G, Fourmentraux-Neves E, Chanal J, Maubec E, Mazouz-Dorval S, Couturaud B, Girod A, Sastre-Garau X, Albert S, Guédon C, Deschamps L, Mitilian D, Cremer I, Jacquelot N, Rusakiewicz S, Zitvogel L, Avril MF, Caignard A. Mature cytotoxic CD56bright/CD16+ natural killer cells can infiltrate lymph nodes adjacent to metastatic melanoma. Cancer Res. 2014;74(1):81-92. doi:10.1158/0008-5472.CAN-13-1303

252. Cursons J, Souza-Fonseca-Guimaraes F, Foroutan M, Anderson A, Hollande F, Hediyeh-Zadeh S, Behren A, Huntington ND, Davis MJ. A gene signature predicting natural killer cell infiltration and improved survival in melanoma patients. Cancer Immunol Res. 2019;7(7):1162-1174. doi:10.1158/2326-6066.CIR-18-0500

253. Pernot S, Terme M, Radosevic-Robin N, Castan F, Badoual C, Marcheteau E, Penault-Llorca F, Bouche O, Bennouna J, Francois E, Ghiringhelli F, De La Fouchardiere C, Samalin E, Baptiste Bachet J, Borg C, Boige V, Voron T, Stanbury T, Tartour E, Gourgou S, Malka D, Taieb J. Infiltrating and peripheral immune cell analysis in advanced gastric cancer according to the Lauren classification and its prognostic significance. Gastric Cancer. 2020;23(1):73-81. doi:10.1007/s10120-019-00983-3

254. Ménard C, Blay JY, Borg C, Michiels S, Ghiringhelli F, Robert C, Nonn C, Chaput N, Taïeb J, Delahaye NF, Flament C, Emile JF, Cesne A Le, Zitvogel L. Natural killer cell IFN-γ levels predict long-term survival with imatinib mesylate therapy in gastrointestinal stromal tumor-bearing patients. Cancer Res. 2009;69(8):3563-3569. doi:10.1158/0008-5472.CAN-08-3807

255. Delahaye NF, Rusakiewicz S, Martins I, Ménard C, Roux S, Lyonnet L, Paul P, Sarabi M, Chaput N, Semeraro M, Minard-Colin V, Poirier-Colame V, Chaba K, Flament C, Baud V, Authier H, Kerdine-Römer S, Pallardy M, Cremer I, Peaudecerf L, Rocha B, Valteau-Couanet D, Gutierrez JC, Nunès JA, Commo F, Bonvalot S, Ibrahim N, Terrier P, Opolon P, Bottino C, Moretta A, Tavernier J, Rihet P, Coindre JM, Blay JY, Isambert N, Emile JF, Vivier E, Lecesne A, Kroemer G, Zitvogel L. Alternatively spliced NKp30 isoforms affect the prognosis of gastrointestinal stromal tumors. Nat Med. 2011;17(6):700-707. doi:10.1038/nm.2366

256. Pasero C, Gravis G, Guerin M, Granjeaud S, Thomassin-Piana J, Rocchi P, Paciencia-Gros M, Poizat F, Bentobji M, Azario-Cheillan F, Walz J, Salem N, Brunelle S, Moretta A, Olive D. Inherent and tumor-driven immune tolerance in the prostate microenvironment impairs natural killer cell antitumor activity. Cancer Res. 2016;76(8):2153-2165. doi:10.1158/0008-5472.CAN-15-1965

257. Semeraro M, Rusakiewicz S, Minard-Colin V, Delahaye NF, Enot D, Vély F, Marabelle A, Papoular B, Piperoglou C, Ponzoni M, Perri P, Tchirkov A, Matta J, Lapierre V, Shekarian T, Valsesia-Wittmann S, Commo F, Prada N, Poirier-Colame V, Bressac B, Cotteret S, Brugieres L, Farace F, Chaput N, Kroemer G, Dominique Valteau-Couanet †, Zitvogel L. Clinical impact of the NKp30/B7-H6 axis in high-risk neuroblastoma patients. Sci Transl Med. 2015;7(283):283ra55. doi:10.1126/scitranslmed.aaa2327

258. Habif G, Crinier A, André P, Vivier E, Narni-Mancinelli E. Targeting natural killer cells in solid tumors. Cell Mol Immunol. 2019;16(5):415-422. doi:10.1038/s41423-019-0224-2

259. Lee H, Quek C, Silva I, Tasker A, Batten M, Rizos H, Lim SY, Nur Gide T, Shang P, Attrill GH, Madore J, Edwards J, Carlino MS, Guminski A, Saw RPM, Thompson JF, Ferguson PM, Palendira U, Menzies AM, Long G V., Scolyer RA, Wilmott JS. Integrated molecular and immunophenotypic analysis of NK cells in anti-PD-1 treated metastatic melanoma patients. Oncoimmunology. 2019;8(2):e1537581. doi:10.1080/2162402X.2018.1537581

260. Zhang Q, Bi J, Zheng X, Chen Y, Wang H, Wu W, Wang Z, Wu Q, Peng H, Wei H, Sun R, Tian Z. Blockade of the checkpoint receptor TIGIT prevents NK cell exhaustion and elicits potent anti-tumor immunity. Nat Immunol. 2018;19(7):723-732. doi:10.1038/s41590-018-0132-0

261. Pansy K, Uhl B, Krstic J, Szmyra M, Fechter K, Santiso A, Thüminger L, Greinix H, Kargl J, Prochazka K, Feichtinger J, Deutsch AJ. Immune regulatory processes of the tumor microenvironment under malignant conditions. Int J Mol Sci. 2021;22(24):13311. doi:10.3390/ijms222413311

262. Marin-Acevedo JA, Dholaria B, Soyano AE, Knutson KL, Chumsri S, Lou Y. Next generation of immune checkpoint therapy in cancer: New developments and challenges. J Hematol Oncol. 2018;11(1):39. doi:10.1186/s13045-018-0582-8

263. Lanitis E, Dangaj D, Irving M, Coukos G. Mechanisms regulating T-cell infiltration and

activity in solid tumors. Ann Oncol. 2017;28:xii18-xii32. doi:10.1093/annonc/mdx238

264. Harjunpää H, Guillerey C. TIGIT as an emerging immune checkpoint. Clin Exp Immunol. 2020;200(2):108-119. doi:10.1111/cei.13407

265. Huang AC, Postow MA, Orlowski RJ, Mick R, Bengsch B, Manne S, Xu W, Harmon S, Giles JR, Wenz B, Adamow M, Kuk D, Panageas KS, Carrera C, Wong P, Quagliarello F, Wubbenhorst B, D'Andrea K, Pauken KE, Herati RS, Staupe RP, Schenkel JM, McGettigan S, Kothari S, George SM, Vonderheide RH, Amaravadi RK, Karakousis GC, Schuchter LM, Xu X, Nathanson KL, Wolchok JD, Gangadhar TC, Wherry EJ. T-cell invigoration to tumour burden ratio associated with anti-PD-1 response. Nature. 2017;545(7652):60-65. doi:10.1038/nature22079

266. Pesce S, Greppi M, Grossi F, Del Zotto G, Moretta L, Sivori S, Genova C, Marcenaro E. PD/1-PD-Ls checkpoint: Insight on the potential role of NK cells. Front Immunol. 2019;10:1242. doi:10.3389/fimmu.2019.01242

267. Alvarez M, Simonetta F, Baker J, Morrison AR, Wenokur AS, Pierini A, Berraondo P, Negrin RS. Indirect Impact of PD-1/PD-L1 Blockade on a Murine Model of NK Cell Exhaustion. Front Immunol. 2020;11:7. doi:10.3389/fimmu.2020.00007

268. Oyer JL, Gitto SB, Altomare DA, Copik AJ. PD-L1 blockade enhances anti-tumor efficacy of NK cells. Oncoimmunology. 2018;7(11):e1509819. doi:10.1080/2162402X.2018.1509819

269. Liu Y, Cheng Y, Xu Y, Wang Z, Du X, Li C, Peng J, Gao L, Liang X, Ma C. Increased expression of programmed cell death protein 1 on NK cells inhibits NK-cell-mediated anti-tumor function and indicates poor prognosis in digestive cancers. Oncogene. 2017;36(44):6143-6153. doi:10.1038/onc.2017.209

270. Taha T, Meiri D, Talhamy S, Wollner M, Peer A, Bar-Sela G. Cannabis Impacts Tumor Response Rate to Nivolumab in Patients with Advanced Malignancies. Oncologist. 2019;24(4):549-554. doi:10.1634/theoncologist.2018-0383

6 Appendix

6.1 Flow cytometry

Table 3. *List of antibodies used in flow cytometry.*

Antibody	Dilution	Clone	Company	Catalogue #
CD45-AF700	1:200	30-F11	BioLegend	103128
CD3-BUV395	1:40	145-2C11	BD Biosciences	563565
CD8-PerCPCy5.5	1:80	53-6.7	BioLegend	100734
CD4-BUV496	1:80	GK1.5	BD Biosciences	564667
PD-1-APC	1:40	29F.1A12	BioLegend	135210
CD62L-BV605	1:50	MEL-14	BioLegend	104438
CD44-BUV737	1:160	IM7	BD Biosciences	612799
NKp46-BV510	1:20	29A1.4	BioLegend	137623
CD19-FITC	1:160	6D5	BioLegend	115506
FoxP3-PE	1:40	FJK-16s	eBioscience™	12-5773-82
CD45-BV785	1:160	30-F11	BioLegend	103149
Ly6C-APC	1:79	HK1.4	BioLegend	128015
Ly6G-PE /Dazzle	1:166	1A8	BioLegend	127648
CD11c-BV605	1:20	N418	BioLegend	117334
PD-L1-PeCy7	1:79	10F.9G2	BioLegend	124313
CD206-FITC	1:160	C068C2	BioLegend	141703
MHCII-PerCP-Cy5.5	1:160	M5/114.15.2	BioLegend	107625
CD103-BV510	1:40	2E7	BioLegend	121423
CD11b-BUV737	1:80	M1/70	BD Biosciences	612801
F4/80-BUV395	1:40	T45-2342	BD Biosciences	565614
Siglec-F-PE	1:40	E50-2440	BD Biosciences	562068
CD107a-BV421	1:100	1D4B	BioLegend	121618
IFN-γ-PE-CF594	1:25	XMG1.2	BD Biosciences	562303
CD19-PECy7	1:161	6D5	BioLegend	115520
TIGIT-BV421	1:33	1G9	BD Biosciences	565270
TIM-3-BV785	1:40	RMT3-23	BioLegend	119725
LAG-3-BV650	1:161	C9B7W	BioLegend	125227
CTLA-4-PE	1:20	UC10-4B9	BioLegend	106305
CCR7-PE	1:20	4B12	BioLegend	120105
CD45-AF700	1:100	HI30	BioLegend	304024
CD3-APC	1:40	UCHT1	BioLegend	300411
CD8-BV650	1:50	RPA-T8	BioLegend	301041
CD56-PE	1:80	HCD56	BioLegend	318306
Epcam-PE/Dazzle	1:17	9C4	BioLegend	324231
CD4-BUV395	1:20	SK3	BD Biosciences	563550
CD45-APC	1:100	30-F11	BioLegend	103112
BrdU-FITC	1:50	3D4	BioLegend	364104
Annexin V FITC	1:50		BioLegend	640906
Propidium Iodide (PI)-PE	1:50		BD Biosciences	51-66211E
CD90.2-PE	1:25	53-2.1	BioLegend	140307
CD31-APC	1:160	390	BioLegend	102409

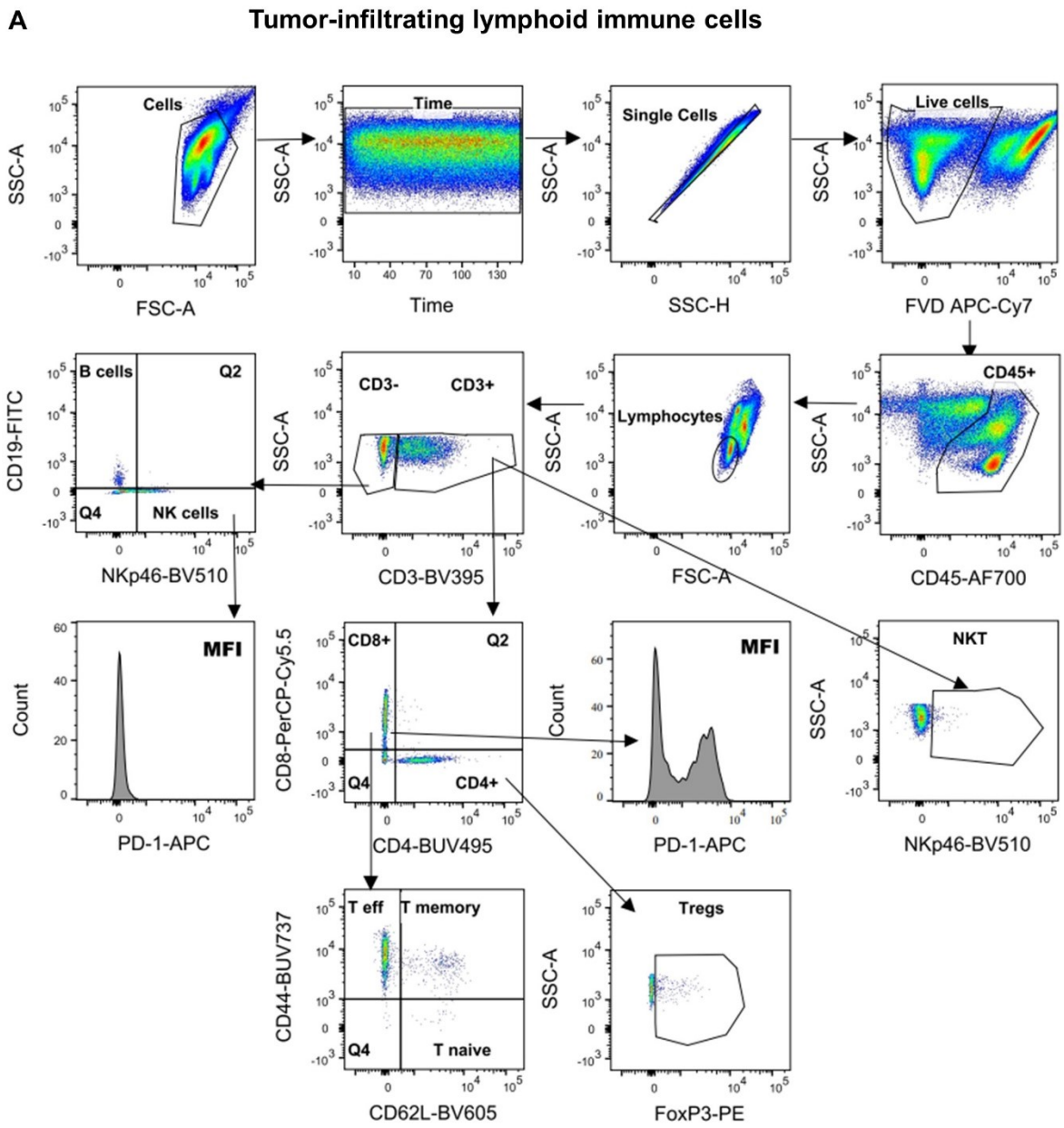
A
Tumor-infiltrating lymphoid immune cells
Cells
SSC-A
FSC-A
Time
Time
Single Cells
SSC-H
Live cells
FVD APC-Cy7
CD45+
CD45-AF700
Lymphocytes
FSC-A
CD3-
CD3+
CD3-BV395
B cells
Q2
Q4
NK cells
CD19-FITC
NKp46-BV510
MFI
Count
PD-1-APC
CD8+
Q2
Q4
CD4+
CD8-PerCP-Cy5.5
CD4-BUV495
MFI
Count
PD-1-APC
NKT
NKp46-BV510
T eff
T memory
Q4
T naive
CD44-BUV737
CD62L-BV605
Tregs
FoxP3-PE

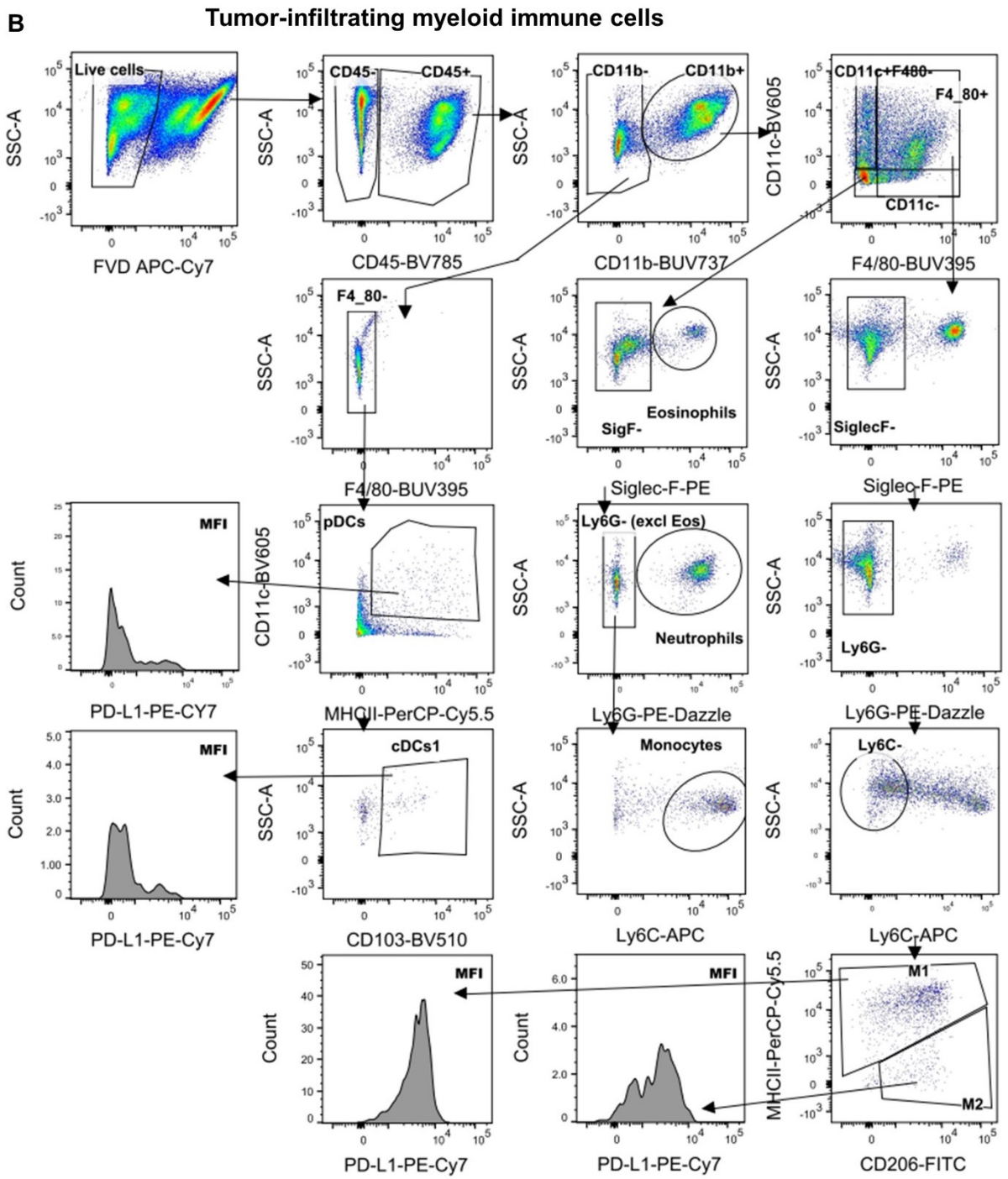
B
Tumor-infiltrating myeloid immune cells
Live cells
SSC-A
FVD APC-Cy7
CD45-
CD45+
CD45-BV785
CD11b-
CD11b+
CD11b-BUV737
CD11c+F480-
F4_80+
CD11c-
CD11c-BV605
F4/80-BUV395
F4_80-
F4/80-BUV395
SigF-
Eosinophils
Siglec-F-PE
SiglecF-
Siglec-F-PE
MFI
Count
PD-L1-PE-CY7
pDCs
CD11c-BV605
MHCII-PerCP-Cy5.5
Ly6G- (excl Eos)
Neutrophils
Ly6G-PE-Dazzle
Ly6G-
Ly6G-PE-Dazzle
MFI
PD-L1-PE-Cy7
cDCs1
CD103-BV510
Monocytes
Ly6C-APC
Ly6C-
Ly6C-APC
MFI
PD-L1-PE-Cy7
MFI
PD-L1-PE-Cy7
M1
M2
MHCII-PerCP-Cy5.5
CD206-FITC

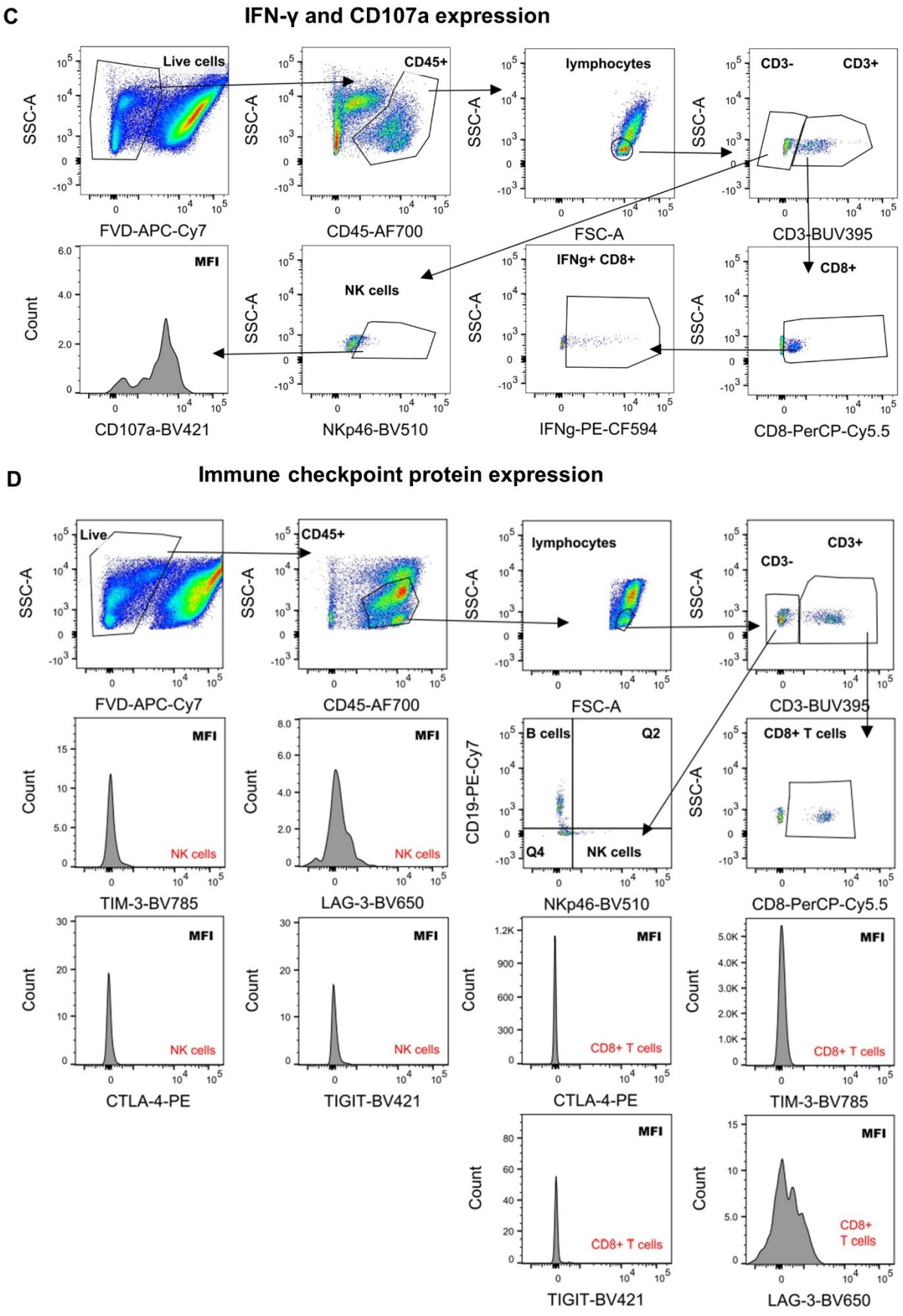
C
IFN-γ and CD107a expression
Live cells
CD45+
lymphocytes
CD3-
CD3+
SSC-A
FVD-APC-Cy7
CD45-AF700
FSC-A
CD3-BUV395
MFI
Count
CD107a-BV421
NK cells
NKp46-BV510
IFNg+ CD8+
IFNg-PE-CF594
CD8+
CD8-PerCP-Cy5.5
D
Immune checkpoint protein expression
Live
B cells
Q2
Q4
NK cells
CD8+ T cells
CD19-PE-Cy7
TIM-3-BV785
LAG-3-BV650
CTLA-4-PE
TIGIT-BV421

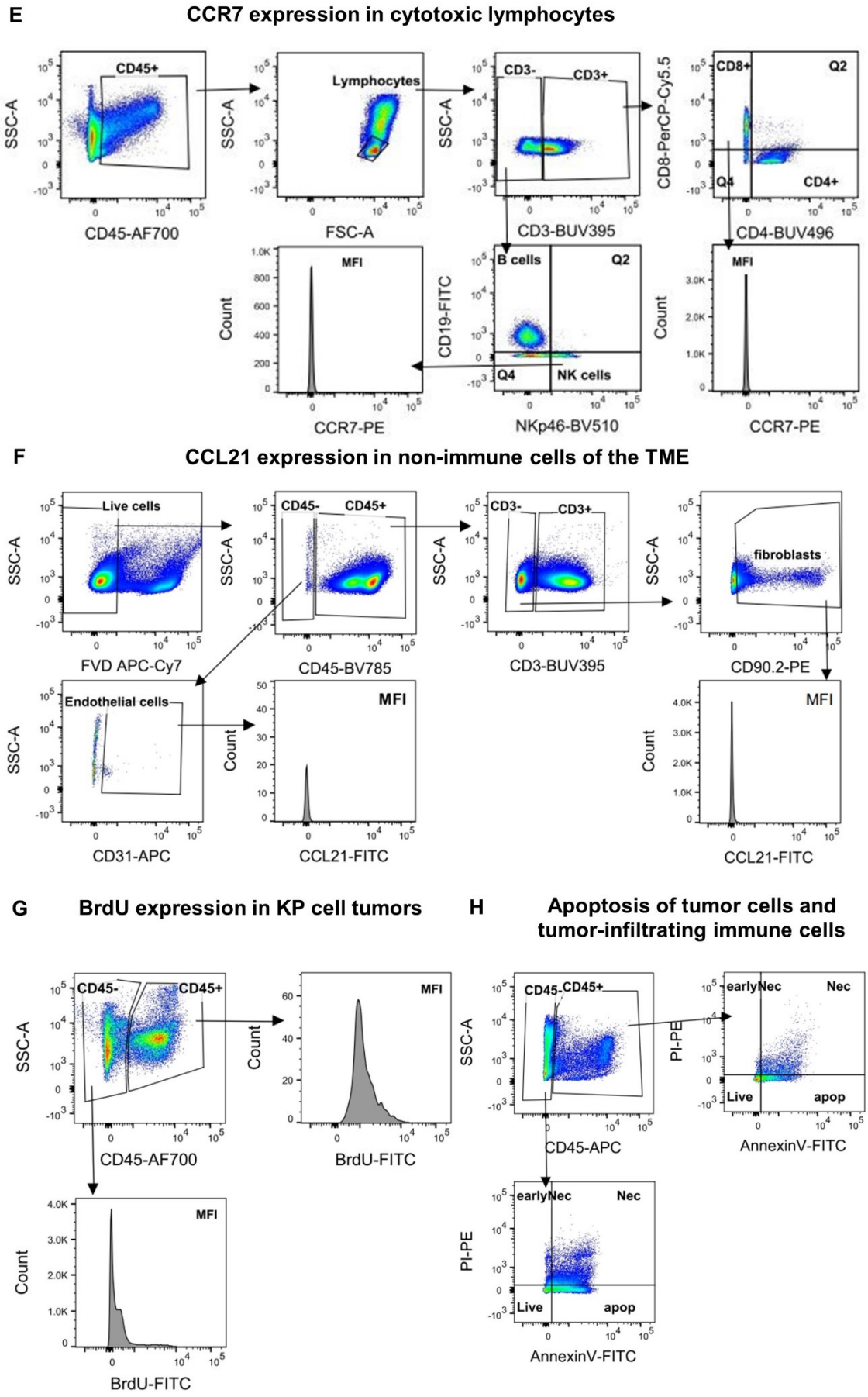
E
CCR7 expression in cytotoxic lymphocytes
CD45+
SSC-A
CD45-AF700
Lymphocytes
FSC-A
CD3-
CD3+
CD3-BUV395
CD8+
Q2
Q4
CD4+
CD8-PerCP-Cy5.5
CD4-BUV496
MFI
Count
CCR7-PE
B cells
Q2
Q4
NK cells
CD19-FITC
NKp46-BV510
F
CCL21 expression in non-immune cells of the TME
Live cells
FVD APC-Cy7
CD45-
CD45+
CD45-BV785
fibroblasts
CD90.2-PE
Endothelial cells
CD31-APC
CCL21-FITC
G
BrdU expression in KP cell tumors
BrdU-FITC
H
Apoptosis of tumor cells and tumor-infiltrating immune cells
earlyNec
Nec
Live
apop
PI-PE
AnnexinV-FITC
CD45-APC

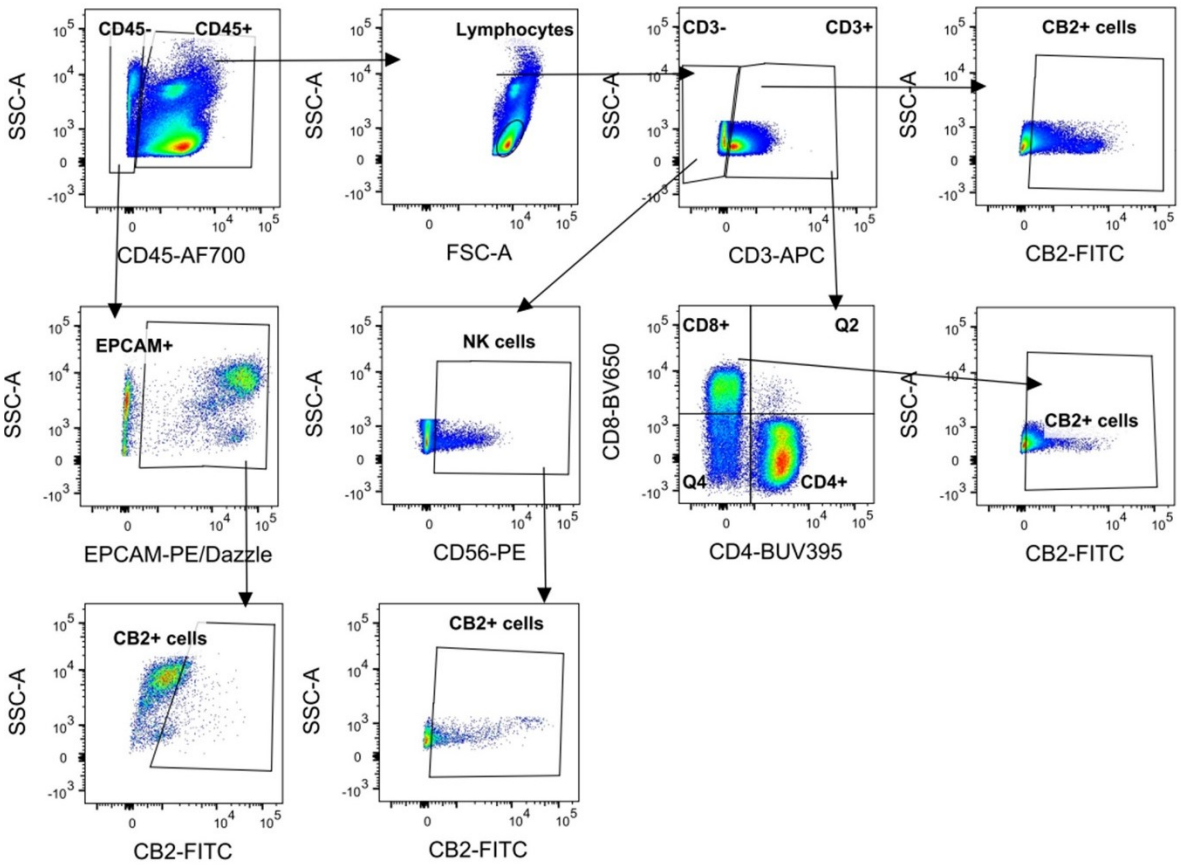

Figure 21. *Flow cytometry gating strategies.*

Schematic representation of the flow cytometric gating strategies to analyze single cell suspensions of KP cell tumors, murine spleen and lung tissues as well as human lung tumors. Infiltrating $CD45^+$ were pre-gated for time and single cells. Dead cells were excluded using FVD stain. To exclude myeloid cells from the lymphoid panel an additional lymphocyte gate was used.

(A) T cells were gated as $CD45^+/CD3^+$; NK cells as $CD45^+/CD3^-/NKp46^+$; B cells as $CD45^+/CD3^-/CD19^+$; $CD8^+$ T cells as $CD45^+/CD3^+/CD8^+$; $CD4^+$ T cells as $CD45^+/CD3^+/CD4^+$; Regulatory T cells (Tregs) as $CD45^+/CD3^+/CD4^+/FoxP3^+$; $CD8^+$ T effector (T eff) cells as $CD45^+/CD3^+/CD8^+/CD44^+$; $CD8^+$ T naïve cells as $CD45^+/CD3^+/CD8^+/CD62L^+$; $CD8^+$ T memory cells as $CD45^+/CD3^+/CD8^+/CD44^+/CD62L^+$; and NKT cells as $CD45^+/CD3^+/NKp46^+$. PD-1 expression was identified measuring median fluorescence intensity (MFI) of $CD8^+$ T and NK cells in the APC channel.

(B) Eosinophils were gated as $CD45^+/CD11b^+/CD11c^-/Siglec\text{-}F^+$; neutrophils as $CD45^+/CD11b^+/CD11c^-/Siglec\text{-}F^-/Ly6G^+$; monocytes as $CD45^+/CD11b^+/CD11c^-/Siglec\text{-}F^-/Ly6G^-/Ly6C^+$ and macrophages as $CD45^+/CD11b^+/CD11c^{-/+}/Siglec\text{-}F^-/Ly6G^-/Ly6C^-$

/F4/80$^+$. PD-L1 expression was determined measuring MFI of M1, M2 macrophages, pDCs and cDC1s in the PE-Cy7 channel.

(C) IFN-γ$^+$ CD8$^+$ T cells were gated as CD45$^+$/CD3$^+$/CD8$^+$/IFN-γ$^+$. CD107a expression was obtained measuring MFI of NK cells in the BV421 channel.

(D) CTLA-4 expression was determined measuring MFI of CD8$^+$ T and NK cells in the PE channel; TIGIT MFI of CD8$^+$ T and NK cells in the BV421 channel; TIM-3 MFI of CD8$^+$ T and NK cells in the BV785 channel; LAG-3 MFI of CD8$^+$ T and NK cells in the BV650 channel.

(E) CCR7 expression was determined measuring MFI of CD8$^+$ T and NK cells in the PE channel.

(F) CCL21 expression was determined measuring MFI of endothelial cells and fibroblasts as in the FITC channel.

(G) BrdU$^+$ CD45$^+$ cells were gated as CD45$^+$/ BrdU$^+$; BrdU$^-$ CD45$^-$ cells as CD45$^-$/ BrdU$^-$. BrdU expression was identified measuring MFI of CD45$^+$ and CD45$^-$ cells in the FITC channel.

(H) Apoptotic CD45$^+$ cells were gated as CD45$^+$/Annexin V$^+$; apoptotic CD45$^-$ cells as CD45$^-$/Annexin V$^+$.

(I) CB_2^+EPCAM$^+$ cells were gated as CD45$^-$/EPCAM$^+$/CB_2^+; CB_2^+CD3$^+$ T cells as CD45$^+$/CD3$^+$/CB_2^+; CB_2^+CD8$^+$ T cells as CD45$^+$/CD3$^+$/CD8$^+$/CB_2^+; CB_2^+NK cells as CD45$^+$/CD3$^-$/CD56$^+$/CB_2^+.

6.2 ISH and Immunofluorescence

Table 4. *20 ZZ probes used for in situ hybridization.*

Probe	Targeting bases
Murine CB_1	701-1792 of NM_007726.3
Murine CB_2	291-719 of NM_009924.3
Human CB_1	2504-3609 of NM_033181.3
Human CB_2	141-1193 of NM_001841.2

Table 5. *List of primary antibodies used in immunofluorescence.*

Antibody	Species	Dilution/ Concentration	Company	Catalogue #
Cytokeratin	Rabbit	1:200	Dako	ZO0622
CD3	Rabbit	1:200	Novus Biologicals	NB600-1441
CD8	Rabbit	1:100	Abcam	ab203035
Mouse NKp46/NCR1	Goat	10µg/mL	R&D systems	AF2225
CD163	Rabbit	1:200	Abcam	ab182422
F4/80	Rabbit	1:500	Cell Signaling Technology	70076
CD11b	Rabbit	1:200	Novus Biologicals	NB110-89474SS
Human NKp46/NCR1	Goat	15µg/mL	R&D systems	AF1850
Mouse PD-L1	Goat	7µg/mL	R&D systems	AF1019
Mouse PD-1	Rabbit	1:250	Cell Signaling Technology	D7D5W
Human PD-L1	Goat	15 µg/mL	R&D systems	MAB1561
Human PD-1	Rabbit	1:250	Cell Signaling Technology	D4W2J